From Intermolecular Potentials to the Spectra of van der Waals Molecules, and Vice Versa

Ad van der Avoird,* Paul E. S. Wormer, and Robert Moszynski†

Institute of Theoretical Chemistry, University of Nijmegen, Toernooiveld, 6525 ED Nijmegen, The Netherlands

Received March 7, 1994 (Revised Manuscript Received August 8, 1994)

Contents

I. Introduction: The Vibration–Rotation–Tunneling (VRT) States of van der Waals Molecules and Their Spectra

Several papers in this issue describe the *ab initio* calculation of intermolecular potentials, and other papers are concerned with the experimental spectra of van der Waals molecules. It is well known that these spectra, especially if the low-frequency intermolecular modes are resolved, are very sensitive probes of the intermolecular potentials. In the present paper we explain and illustrate the theoretical and computational methods used to obtain the spectrum from a given intermolecular potential. Comparison of the measured and computed spectrum can be used to check the quality of an *ab initio* potential or, after the introduction of some empirical parameters, to fit the experimental spectrum and thus to improve the potential. Given a potential energy surface, the calculation of the spectra involves two steps: first, one has to calculate the bound states (and sometimes resonances) of the van der Waals complex; next one has to compute the intensities of the transitions between these states from their wave functions and dipole (for emission or absorption spectra) or polarizability function (for Raman spectra). We concentrate on the calculation of the vibration–rotation–tunneling (VRT) states from a given potential surface, *i.e.* on the nuclear motion problem, the second step in the Born–Oppenheimer approximation.

In van der Waals complexes there is, by definition, a hierarchy in the nuclear motions. Within the stable, chemically bound molecules that constitute such a complex, the atoms (nuclei) vibrate fast. The motions of the molecules in the complex, against the weak van der Waals forces (or the somewhat stronger hydrogen bonding) that hold it together, are much slower. This allows another Born–Oppenheimer-like separation between the intramolecular vibrations and the intermolecular motions. The latter usually have large amplitudes and, since there are often multiple minima in the potential surface with only low barriers between them, the intermolecular "vibrations" may look more like hindered rotations or tunneling motions. In practically all cases there is a strong coupling between the different intermolecular degrees of freedom. Sometimes, the stable molecules that constitute the complex are flexible. In that case, some of the intramolecular modes may have low frequencies and large amplitudes as well, and will couple strongly to the intermolecular or van der Waals modes. In the Born–Oppenheimer-like separation of the intra- and intermolecular modes they may have to be included with the latter. It will be clear from this description that the more or less standard methods, based on the harmonic oscillator/rigid rotor model with (perturbation) corrections, which are used to study the rovibrational spectra of nearly rigid molecules[1–3] are not applicable to the intermolecular modes in van der Waals complexes. A new set of methods especially designed to compute the VRT states of van der Waals molecules is, and is still being, developed. These methods have much in common with the quantum theory of molecule scattering. This is natural since the scattering states of a pair of molecules are in fact the continuum states of a van der Waals molecule. In the present paper we describe these methods and illustrate their application on several examples.

† Permanent address: Department of Chemistry, University of Warsaw, Poland.

0009-2665/94/0794-1931$14.00/0

Ad van der Avoird studied chemical engineering at the Technical University in Eindhoven, The Netherlands, from 1959 to 1964. From 1964 to 1967 he was a member of the physics/mathematics group (director Laurens Jansen) at the Battelle Institute in Geneva, Switzerland. From 1967 to 1971 he worked at the Unilever Research Laboratory in Vlaardingen, where in 1968 he became head of the Molecular Physics section. In 1968 he obtained his Ph.D. degree at the Technical University in Eindhoven (supervisor G. C. A. Schuit). In 1968 he also became parttime professor at the University of Nijmegen; in 1971 he became full professor of Theoretical Chemistry at this university. In 1979 he was appointed member of the Netherlands Royal Academy of Sciences (KNAW). In October 1992 he worked in the spectroscopy group of Richard Saykally at the University of California at Berkeley as a Visiting Miller Research Professor.

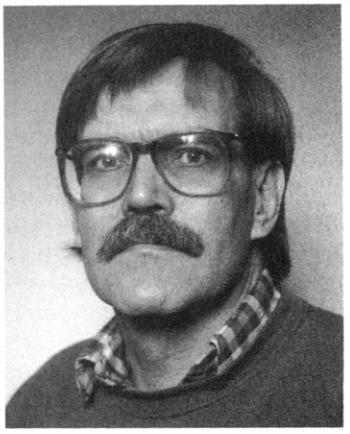

Paul E. S. Wormer was born in Amsterdam, The Netherlands, in 1942. He did his undergraduate work in Chemistry at the Technical University Delft, where he got his degree (with honors) in 1969. Immediately after graduation he spent a year as a research assistant at Duke University with D. B. Chesnut. After returning to The Netherlands he got a doctorate in Theoretical Chemistry from the University of Nijmegen in 1975 (with honors); A. van der Avoird was his promoter. Since that year he has held a permanent position in Nijmegen. He spent a sabbatical year and a few summers with J. Paldus in the Department of Applied Maths of the University of Waterloo, Canada, and was a Visiting Fellow of the Royal Society in 1986 as a guest of J. Gerratt, University of Bristol, UK. His main research interests are the topics covered in the present review and in addition the electronic correlation problem and the group theory of many-particle systems.

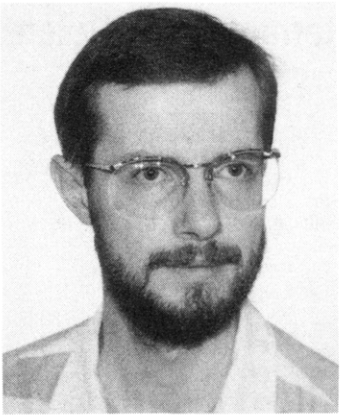

Robert Moszynski was born in Warsaw, Poland, in 1964. He received his M.S. degree in chemistry from the University of Warsaw in 1986. In 1987 he joined the Quantum Chemistry Laboratory at the University of Warsaw. He earned his Ph.D. degree in quantum chemistry from the University of Warsaw on intramonomer correlation effects in intermolecular interactions. In his research on perturbation theory of intermolecular forces he collaborated closely with Bogumil Jeziorski and Krzysztof Szalewicz. Recently, he joined the group of Ad van der Avoird at the Department of Chemistry, University of Nijmegen in the Netherlands. His research interests include *ab initio* studies of intermolecular forces, and spectra and dynamics of van der Waals molecules.

This paper is organized as follows. First we discuss the different choices of coordinate systems that are being used in the study of van der Waals molecules and give the corresponding kinetic energy expressions. The derivations of these expressions are outlined in Appendix A. We then discuss the analytic forms of the intermolecular potential energy surfaces. Since heavy emphasis will be on fits in terms of Legendre functions and their more-dimensional generalizations, we summarize the more important facts of the spherical functions in Appendix B. Given the Hamiltonians, we go on to discuss how to obtain their eigenstates. From the eigenstates we may obtain dimer properties and transition intensities. This is the topic of the next section. Permutation-inversion symmetry plays an important role in van der Waals molecules, which are highly nonrigid. We touch briefly on this subject, and in Appendix C we go deeper into this aspect of the theory. The next section is devoted to concrete results of calculations and their comparison with experiment. As examples we discuss the argon atom in interaction with H_2, NH_3, H_2O, and benzene. We look at He−HF and finally at the strange case of the ammonia dimer.

II. The Calculation of VRT States and Spectra

A. Choice of Coordinates

The development of an optimum strategy for the calculation of the bound (and scattering) states of a van der Waals molecule begins with the choice of coordinates. The nature of the motions in such a complex implies that one has to use mostly curvilinear coordinates. If the monomers in the weakly bound complex are considered to be rigid, then this follows immediately from this constraint. But, even if the monomers are not frozen, it is better to use curvilinear coordinates, in order to achieve the best separability between the internal motions of the monomers and the van der Waals motions. For the fast vibrations of the nearly rigid monomers it is customary to use the standard (harmonic) normal coordinates. These are linear combinations of the (mass weighted) atomic displacements that satisfy the Eckart conditions. Their coefficients might be determined by the standard Wilson GF-matrix method.[1−3] A natural choice of van der Waals coordinates in a dimer is given by the distance R between the centers of mass of the monomers A and

B and the Euler angles $\zeta_A = (\phi_A,\theta_A,\psi_A)$ and $\zeta_B = (\phi_B,\theta_B,\psi_B)$ that define the orientations of the Eckart frames on the monomers. These Euler angles may be defined with respect to a laboratory (or space-fixed) frame or with respect to a frame that is somehow embedded in the dimer. The latter has advantages if one tries to separate the "vibrations" of the dimer, *i.e.* its internal (van der Waals) motions, from its overall rotations. This separation of vibrations and rotations always involves an approximation, even in the case of nearly rigid molecules. For a highly nonrigid van der Waals complex there will be strong vibration−rotation coupling. Still, in calculations it may be advantageous to introduce this separation in first instance, and then to include the coupling terms in the second step. We will return to this point later, when we discuss the dimer Hamiltonians. It will be explained that the optimum choice of the angular coordinates is in fact determined by some characteristic properties of the system at hand, such as the rotational constants of the monomers and the anisotropy of the intermolecular potential. These properties determine already to some extent the kind of VRT motions in the complex, the approximate constants of the motion and, thereby, the coordinates that achieve the best separability.

It may occur that the rotations of the monomers are strongly hindered in some directions and less in others, so that the van der Waals motions follow certain (curved) pathways. In such a case one can introduce special curvilinear coordinates that describe the motions along these pathways and the motions orthogonal to them. Examples are given by the semirigid bender coordinates in the HF dimer[4] and the specific tunneling pathways in the H_2O dimer.[5,6] Also it may happen that certain intramolecular motions are relatively easy so that they lead to observable tunneling splittings and coupling to the van der Waals motions. An example of this is the umbrella inversion tunneling in NH_3, which occurs also (but more or less hindered) in van der Waals complexes such as $Ar-NH_3$[7−9] and NH_3-NH_3.[10−12] These examples will be treated in section III. An additional curvilinear coordinate in that case is the NH_3 umbrella angle; in the calculations[9] this coordinate is treated along with the intermolecular coordinates.

B. The Hamiltonian, Kinetic Energy Expressions

Even when we choose a set of intramolecular and intermolecular coordinates as described in section II.A, the nuclear motion Hamiltonian in a van der Waals complex depends on both. In this review we will not explicitly write its dependence on the intramolecular (normal) coordinates of the nearly rigid monomers. If one assumes the standard Eckart or Watson forms[3,13] of the Hamiltonians for these monomers, then it is easy, if necessary, to reintroduce the intramonomer coordinates into the Hamiltonian of the complex. Often one may get rid of the intramonomer coordinates by averaging the Hamiltonian of the complex over a given vibrational state of each monomer, as the monomer vibrations are usually faster by 1 or 2 orders of magnitude than the van der Waals motions. The simplest way to avoid the dependence on the intramonomer coordinates is to assume that the monomers are rigid, and even this seemingly crude model works well in many cases, especially if one adopts the vibrationally averaged geometries of the nearly rigid monomers, instead of their equilibrium geometries. And, in the treatment of the example $Ar-NH_3$ in section III, we will discuss how to reintroduce a monomer coordinate that corresponds to a large amplitude motion.

The kinetic energy expression for a set of general curvilinear coordinates q_i has been given by Podolsky,[14] see also ref 15,

$$T = {}^1/_2 g^{-1/2} \boldsymbol{p}_q^T g^{1/2} \mathbb{G}^{-1} \boldsymbol{p}_q \qquad (1)$$

where $p_i = -i\hbar(\partial/\partial q_i)$ are the momenta conjugate to q_i, $\mathbb{G}$ is the metric tensor and g is the determinant of $\mathbb{G}$, see Appendix A. In this appendix the Podolsky expression has been explicitly worked out for different sets of coordinates which are convenient to describe van der Waals dimers. The simplest Hamiltonian for a dimer consisting of two general, nonlinear, monomers is obtained by defining both the Euler angles $\zeta_A = (\phi_A,\theta_A,\psi_A)$ and $\zeta_B = (\phi_B,\theta_B,\psi_B)$ and the polar angles $\hat{\boldsymbol{R}} = (\beta,\alpha)$ of the vector $\vec{R} \equiv \overrightarrow{AB}$ with respect to a space-fixed (SF) frame. The kinetic energy expression in this Hamiltonian follows immediately from the diatom Hamiltonian in Appendix A.1, and the rigid rotor Hamiltonian in Appendix A.2. It simply reads

$$T = T_A + T_B + T_{AB} \qquad (2)$$

with T_X, $X = A$ or B, given by

$$T_X = A_X(j_{Xx}^{BF})^2 + B_X(j_{Xy}^{BF})^2 + C_X(j_{Xz}^{BF})^2 \qquad (3)$$

and

$$T_{AB} = \frac{1}{2\mu_{AB}R^2}\left[-\hbar^2 \frac{\partial}{\partial R} R^2 \frac{\partial}{\partial R} + (\boldsymbol{l}^{SF})^2\right] \qquad (4)$$

cf. eqs A54, A39, and A56. A_X, B_X, and C_X are the rotational constants of monomer X, the $\boldsymbol{j}_X^{BF}$ are the usual monomer angular momentum operators given in eq A52, μ_{AB} is the dimer reduced mass, and $\boldsymbol{l}^{SF}$ is the end-over-end angular momentum operator. Although this choice of SF coordinates leads to the simplest kinetic energy expression, the problem is that the intermolecular potential is not easily expressed in these coordinates. Instead, the potential is naturally dependent on the internal angles of the complex, *i.e* the angles that relate the monomer orientations to the dimer axis $\vec{R}$. These are the Euler angles in the embedded dimer frame of Appendix A.4. Still, it may be advantageous, when the end-over-end rotational constant $(2\mu_{AB}R^2)^{-1}$ of the dimer is large in comparison with the strength of the anisotropy in the intermolecular potential, to use the space-fixed coordinates that lead to eqs 2−4. This situation is called coupling case (*a*) in the early paper on van der Waals molecules by Bratoz and Martin[16] and case 1 in a review by Hutson.[17] It corresponds to the nearly free rotation of the monomers in the complex. In other words, the monomer rotational quantum num-

bers (*e.g.* j_A and j_B in the case of linear molecules) and the end-over-end angular momentum l are nearly good quantum numbers to describe the dimer states. The price one has to pay when using these SF coordinates is that the intermolecular potential has to be expressed in a specific analytic form, in terms of the Euler angles ζ_A^{BF} and ζ_B^{BF} of Appendix A.4, and then to be transformed to an expression in terms of the angles ζ_A^{SF} and ζ_B^{SF}. This will be discussed in section II.C. In practice this coupling case arises only for H_2, HD, or D_2 containing van der Waals complexes.

In most other cases it is convenient to use the dimer-embedded frame of Appendix A.4. The expression of the potential causes no problems then, and the kinetic energy operator reads

$$T = T_A + T_B + \frac{1}{2\mu_{AB}R^2}\left[-\hbar^2\frac{\partial}{\partial R}R^2\frac{\partial}{\partial R} + (J^{SF})^2 + (\boldsymbol{j}_A + \boldsymbol{j}_B)^2 - 2(\boldsymbol{j}_A + \boldsymbol{j}_B)\cdot\boldsymbol{J}\right] \quad (5)$$

where $\boldsymbol{J}$ is the total angular momentum of the dimer, $(J^{SF})^2$ is given by eq A80 and is related to J^2 via eq A79. This expression has been derived from eqs 2–4 by Brocks *et al.*[18] with the use of chain rules. An alternative derivation is given in Appendix A.4. At first sight it seems that one may simply obtain eq 5 by introducing the dimer (BF) frame and substituting $(\boldsymbol{l}^{BF})^2 = (\boldsymbol{J} - \boldsymbol{j}_A - \boldsymbol{j}_B)\cdot(\boldsymbol{J} - \boldsymbol{j}_A - \boldsymbol{j}_B)$ into eq 4. This is assumed in many expositions of the present theory, for instance refs 19–21. From the derivations in Appendix A.4 and in ref 18 it is evident, however, that this ignores the fact that $\boldsymbol{J}$ and $\boldsymbol{j}_X$ do not commute. Moreover, this procedure does not yield the explicit expressions (in terms of differential operators) for the components of $\boldsymbol{J}$, which are quite unusual and which do not obey the standard, eq A30, or even the so-called anomalous,[22] eq A37, commutation relations. It implies that one must accept without proof that $\boldsymbol{J}$ acts in the usual manner on rotation functions, but, as was shown by Brocks *et al.*[18] and in Appendix B this only holds for a specific choice of basis and is not true in general.

The dimer frame of Appendix A.4 is embedded by using only two external Euler angles: the polar angles of the vector $\vec{R}$. It is shown in the Appendix of ref 18 how to introduce the third external Euler angle as an embedding angle. The resulting kinetic energy expression becomes rather complicated, however, and it has the drawback that, in the case of identical monomers A and B, the interchange symmetry is no longer explicitly visible. Moreover, the resulting G tensor becomes singular for linear configurations of the dimer. Yet, in certain cases it may be useful to apply this form.

For dimers that consist of a rather large nonlinear molecule and an atom, such as benzene–Ar[23,24] it may be advantageous to use an Eckart frame which is embedded in the molecule. The corresponding van der Waals coordinates are $\zeta_A = (\phi_A,\theta_A,\psi_A)$, the Euler angles that describe the orientation of the molecule-embedded frame with respect to a space-fixed frame, and the Cartesian or polar components of the vector $\vec{R} \equiv \overrightarrow{AB}$ with respect to the molecule frame. The kinetic energy expression

$$T = \frac{1}{2}(\boldsymbol{J}^{BF} - \boldsymbol{l}^{BF})^T(\mathbb{I}^{BF})^{-1}(\boldsymbol{J}^{BF} - \boldsymbol{l}^{BF}) + \frac{|\boldsymbol{p}_R|^2}{2\mu_{AB}} \quad (6)$$

has been given in refs 23 and 24, $\mathbb{I}^{BF}$ is the inertia tensor of the molecule and $\boldsymbol{p}_R$ is the momentum conjugate to $\boldsymbol{R}$, which is the coordinate vector of $\vec{R}$ in the BF frame. An alternative derivation is given in Appendix A.3.

If one prefers to use still other coordinates to describe the motions in van der Waals complexes, one has to derive the metric tensor that corresponds to these coordinates and, according to the recipe of Appendix A, to substitute this tensor into the Podolsky formula for the kinetic energy. The same prescription can be followed if one wishes to include specific internal motions in flexible monomers, or if one considers van der Waals complexes consisting of more than two monomers.

C. (*Ab Initio*) Intermolecular Potentials, Representations

Since there are several papers[25–28] in this issue which deal with the *ab initio* calculation of intermolecular potentials, we will not discuss this problem in our contribution. Let us just mention that these computations can be divided in two categories: they are based on the supermolecule approach or on symmetry-adapted perturbation theory (SAPT). Both methods have already shown to be able to yield accurate potentials for (small) van der Waals dimers. We have some preference for the SAPT approach,[25,29–34] because it gives directly the individual contributions to the potential. Its accuracy is achieved by a well-balanced inclusion of the (intra- and intermonomer) electron correlation in these contributions. Moreover, the knowledge of the individual short-range and long-range terms makes it easier to obtain accurate analytical fits of the potential surface. This, in turn, greatly facilitates the calculation of the VRT states. It is relevant, in this respect, that, because of the occurrence of multiple minima in the potentials of most van der Waals molecules, and due to the floppiness of these systems, the calculation of the VRT states usually requires the knowledge of the complete potential surface. Later in this section we will make some comments on the various possible ways to represent the potential, which depend on the strategy that is chosen to calculate the VRT states.

First, we want to mention the spherical expansion of the intermolecular potential for a dimer.[35] This expansion is a generalization of the well-known Legendre expansion[17] for atom–diatom systems or the expansion in spherical harmonics[7] for atom–(nonlinear) molecule dimers. In its most general form it is expressed in the Euler angles ζ_A^{SF} and ζ_B^{SF} of the monomers and the polar angles $\hat{\boldsymbol{R}} = (\beta,\alpha)$ with respect to a space-fixed frame

$$V(R,\zeta_A,\zeta_B,\hat{\boldsymbol{R}}) = \sum_{\{\Lambda\}} v_{\{\Lambda\}}(R)A_{\{\Lambda\}}(\zeta_A,\zeta_B,\hat{\boldsymbol{R}}) \quad (7)$$

The orthogonal set of angular functions, labeled by

Table 1. Some Properties of Spherical Harmonics $C^l_m(\theta,\phi) = [4\pi/(2l+1)]^{1/2} Y^l_m(\theta,\phi)$ and Wigner D Matrices $D^l_{mk}(\alpha,\beta,\gamma)$ That Are Useful in the Symmetry Adaptation of Angular Basis Functions

$$C^l_m(\pi-\theta,\pi+\phi) = (-)^l C^l_m(\theta,\phi)$$

$$C^l_m(\theta,\pi-\phi) = C^l_{-m}(\theta,\phi)$$

$$C^l_m(\theta,\phi)^* = (-)^m C^l_{-m}(\theta,\phi)$$

$$D^l_{m0}(\alpha,\beta,\gamma) = (-)^m C^l_{-m}(\beta,\alpha)$$

$$D^l_{0m}(\alpha,\beta,\gamma) = C^l_{-m}(\beta,\gamma)$$

$$D^l_{mk}(\alpha,\pi-\beta,-\gamma) = (-)^{l+m} D^l_{mk}(\alpha,\beta,\gamma)$$

$$D^l_{mk}(\pi-\alpha,\beta,-\gamma) = (-)^m D^l_{-m,-k}(\alpha,\beta,\gamma)$$

$$D^l_{mk}(\alpha+\omega,\beta,\gamma) = e^{-im\omega} D^l_{mk}(\alpha,\beta,\gamma)$$

$$D^l_{mk}(\alpha,\beta,\gamma+\omega) = e^{-ik\omega} D^l_{mk}(\alpha,\beta,\gamma)$$

$\{\Lambda\} = \{L_A,K_A,L_B,K_B,L\}$, is given by

$$A_{\{\Lambda\}}(\zeta_A^{SF},\zeta_B^{SF},\hat{\boldsymbol{R}}) = \sum_{M_A M_B M} \begin{pmatrix} L_A & L_B & L \\ M_A & M_B & M \end{pmatrix} D^{(L_A)}_{M_A K_A}(\zeta_A^{SF})^* D^{(L_B)}_{M_B K_B}(\zeta_B^{SF})^* C^L_M(\hat{\boldsymbol{R}}) \quad (8)$$

where the functions $D^{(l)}_{mk}$ are Wigner rotation functions (see Appendix B), C^l_m are spherical harmonics in the Racah normalization and the expression in large brackets is a $3-j$ symbol.[36] Since the functions $A_{\{\Lambda\}}$ form a complete set, the expansion in eq 7 is exact, in principle. In practice, one may truncate the expansion when the coefficients $v_{\{\Lambda\}}(R)$ have become sufficiently small. These coefficients depend only on the distance R; if we include the dependence of the intermolecular potential on the molecular geometries they depend on the intramolecular (normal) coordinates too. One advantage of the spherical expansion is that it explicitly shows the anisotropy of the potential; the term with $\{L_A,K_A,L_B,K_B,L\} = \{0,0,0,0,0\}$ is the isotropic potential. Another advantage is that it can immediately be written in terms of the BF coordinates. One just has to realize that, by construction, the angular functions $A_{\{\Lambda\}}$ are invariant with respect to any frame rotation and to use the property that the polar angles $\hat{\boldsymbol{R}} = (\beta,\alpha)$ are (0,0) with respect to the dimer-embedded frame. Substitution of $C^L_M(0,0) = \delta_{M0}$ yields, then

$$A_{\{\Lambda\}}(\zeta_A^{BF},\zeta_B^{BF}) = \sum_{\substack{M_A \\ (M_B=-M_A)}} \begin{pmatrix} L_A & L_B & L \\ M_A & M_B & 0 \end{pmatrix} D^{(L_A)}_{M_A K_A}(\zeta_A^{BF})^* D^{(L_B)}_{M_B K_B}(\zeta_B^{BF})^* \quad (9)$$

For atom−molecule dimers $L_A = K_A = M_A = 0$. With the use of the properties of Wigner D functions and spherical harmonics given in Table 1, we find that the angular expansion functions become

$$A_{L_B K_B}(\zeta_B^{BF}) = (-1)^{L_B}(2L_B+1)^{-1/2} D^{(L_B)}_{0K_B}(\phi_B^{BF},\theta_B^{BF},\psi_B^{BF})^* = (-1)^{L_B-K_B}(2L_B+1)^{-1/2} C^{L_B}_{K_B}(\theta_B^{BF},\psi_B^{BF}) \quad (10)$$

The well-known Legendre expansion for atom−diatom systems, where $K_B = 0$, is obtained by the simple substitution of $C^L_0(\theta,\psi) = P_L(\cos\theta)$.

In *ab initio* calculations of the potential one always chooses a BF frame. The expansion coefficients can be written as

$$v_{\{\Lambda\}}(R) = \frac{(2L_A+1)(2L_B+1)(2L+1)}{64\pi^4} \int d\zeta_A^{BF} \int d\zeta_B^{BF} A_{\{\Lambda\}}(\zeta_A^{BF},\zeta_B^{BF})^* V(R,\zeta_A^{BF},\zeta_B^{BF}) \quad (11)$$

with $d\zeta_X = \sin\theta_X\, d\phi_X\, d\theta_X\, d\psi_X$. After the calculation of the potential V on a grid of angles ζ_A^{BF} and ζ_B^{BF}, the integration in eq 11 can be performed by numerical quadrature,[37] for each distance R. Actually, one may choose the BF frame such that one of the Euler angles, either ϕ_A^{BF} or ϕ_B^{BF}, is equal to zero and can be omitted from the integration. If we deal with simpler dimers, *e.g.* if A or B is an atom or a linear molecule, this procedure can be further simplified. Or, if A or B have some point group symmetry, we can reduce the integration intervals. The expansion coefficients $v_{\{\Lambda\}}(R)$ which are thus obtained define the potential, both with respect to the BF frame, via eqs 7 and 9, and with respect to the SF frame, via eqs 7 and 8. The transition from eq 9 to eq 8 is in fact the most general way to describe the transformation of a potential from BF coordinates to SF coordinates. For the Legendre expansion in atom−diatom systems this transformation is described in refs 17 and 20.

Also in practical calculations of the VRT states of a van der Waals dimer the spherical expansion of the potential may be very convenient. If the angular basis in such calculations is chosen as (coupled) products of monomer and overall rotor functions, all the angular integrals in the matrix elements of the potential are just $3n$-j symbols, see section II.D. For the same reason the spherical expansion is used in most scattering calculations. Only when the potential is too strongly anisotropic this procedure becomes inefficient, since one needs too many terms in the spherical expansion and too large a basis.

We can also explain now why in most cases the use of BF coordinates is the most convenient. As it follows from the relation $M_B = -M_A$ in eq 9 and from the definition of the Wigner D functions in eq B1, the intermolecular potential depends only on the difference angle $\phi_B - \phi_A$, not on ϕ_A itself. Hence, in the BF angular basis of eq B18, functions with different K are not mixed by the potential. Off-diagonal matrix elements between such functions are given only by the Coriolis terms $(\boldsymbol{j}_A + \boldsymbol{j}_B)\cdot\boldsymbol{J}/(\mu_{AB}R^2)$ in the BF kinetic energy operator, eq 5. In practically all cases (except for H_2 containing dimers or very high values of J), these terms are much smaller than the anisotropy of the potential. This anisotropy is dominated by the leading terms $v_{\{\Lambda\}}(R)$ with $\{\Lambda\} \neq$

{0,0,0,0,0}. In all these cases K, which is the eigenvalue of both J_z and j_z in Appendix A.4, is a nearly good quantum number in the dimer. These cases are treated as coupling case (b) by Bratoz and Martin[16] and as cases 2 and 3 by Hutson.[17] Even when the complex becomes nearly rigid, K is still a good quantum number in many van der Waals dimers, because such dimers are often prolate near-symmetric tops due to the relatively large van der Waals bonding distance R. Coupling case (c) of Bratoz and Martin[16] is not explicitly treated here, since this is the case where a van der Waals dimer is considered as a nearly rigid molecule to which the standard formalism for vibrations and rotations[1-3] can be applied. One must be careful, however, because the vibrations in van der Waals molecules have large amplitudes and rotation−vibration coupling is strong, so that the usual perturbation expansions for the effects of anharmonicity and rotation−vibration coupling may not converge. Still, in some cases like Ar−benzene (see section III.D) one may use the harmonic oscillator−rigid rotor quantum numbers to label the (lowest) VRT states.

At the end of this section, we make some observations regarding other, analytic or discrete, representations of the potential. These are closely connected to the method chosen to calculate the VRT states, so it is not so easy to make general remarks. If one chooses a discrete variable representation (DVR)[38] of the VRT states, for example, then it is only required to know the potential on a grid of quadrature points. But even then, if the potential has to be obtained from *ab initio* calculations, the DVR method may require too dense a grid to evaluate the potential in all points. Analytic fitting (global or using splines) or interpolation may solve this problem. A global fitting model which is applied widely is the atom−atom model:[39] $V_{AB} = \sum_{i\in A}\sum_{j\in B} v_{ij}(r_{ij})$ with Lennard-Jones $v_{ij}(r_{ij}) = A_{ij}r_{ij}^{-12} - B_{ij}r_{ij}^{-6}$ or exp-6 potentials $v_{ij}(r_{ij}) = A_{ij}\exp(-B_{ij}r_{ij}) - C_{ij}r_{ij}^{-6}$. A conceptual advantage of atom−atom potentials is that they also model the dependence of the intermolecular potential on the intramolecular degrees of freedom. In the standard applications of this model it is assumed that the atom−atom potentials are isotropic, which is a serious limit on its accuracy. In few cases, anisotropic atom−atom potentials have been introduced.[40]

Another manner to represent the anisotropy of the intermolecular potential is to choose a parametrized R-dependent form with parameters that depend on the orientations of the molecules. An example is the Lennard-Jones potential

$$V(R,\zeta_A,\zeta_B) = \epsilon(\zeta_A,\zeta_B)\left[\left(\frac{R_m(\zeta_A,\zeta_B)}{R}\right)^{12} - 2\left(\frac{R_m(\zeta_A,\zeta_B)}{R}\right)^{6}\right] \quad (12)$$

with the parameters ϵ and R_m depending on the Euler angles ζ_A and ζ_B.[41] In potentials that are used especially to fit the spectra of van der Waals molecules,[42-44] the short-range repulsion is modeled by

$$A(\zeta_A,\zeta_B)\exp[-\beta(\zeta_A,\zeta_B)R] \quad (13)$$

and the long-range electrostatic, induction, and dispersion terms by

$$-\sum_n C_n(\zeta_A,\zeta_B)D_n(R)R^{-n} \quad (14)$$

The damping functions $D_n(R)$ correct the long-range contributions for overlap effects.[45,46] The parameters in eqs 13 and 14 are not directly optimized, however. Instead, one adopts some reasonable (*ab initio*) values for all but the highest long-range coefficients C_n and then writes the highest $C_n(\zeta_A,\zeta_B)$ and the short-range coefficient $A(\zeta_A,\zeta_B)$ as functions of the (angular dependent) well depth $\epsilon(\zeta_A,\zeta_B)$ and position of the minimum $R_m(\zeta_A,\zeta_B)$ in the potential. The latter quantities and the exponent $\beta(\zeta_A,\zeta_B)$ are written as truncated expansions in the angular functions $A_{\{\Lambda\}}(\zeta_A,\zeta_B)$ of eq 9. The actual fitting parameters are the coefficients in these expansions. So these occur in the potential in a highly nonlinear way. This procedure is chosen to reduce the number of fitting parameters and to avoid a high correlation between them.

D. Methods for the Calculation of VRT States

The methods developed to calculate the VRT states in van der Waals molecules can be divided into two classes: variational and nonvariational. In variational methods one has to choose a basis, the form of which, of course, will depend on the choice of the (intermolecular) coordinates, see Section IIA. With the space-fixed coordinates, for instance, the basis for a dimer consisting of two arbitrary nonlinear molecules can be written as

$$|n,j_A,k_A,j_B,k_B,j_{AB},l;J,M\rangle = \Phi_n(R)\left[\frac{(2j_A+1)(2j_B+1)(2l+1)}{256\pi^5}\right]^{1/2} \times \sum_{m_A m_B}\sum_{Km} D^{(j_A)}_{m_A k_A}(\xi_A^{SF})^* D^{(j_B)}_{m_B k_B}(\xi_B^{SF})^* \times \langle j_A m_A; j_B m_B | j_{AB} K\rangle C^l_m(\hat{\boldsymbol{R}})\langle j_{AB}K; lm | JM\rangle \quad (15)$$

cf. eq B15. The angular momentum coupling in this basis, by means of the Clebsch−Gordan coefficients $\langle j_1 m_1; j_2 m_2 | jm\rangle$, takes already into account that the total angular momentum J and its space-fixed z component M are exact quantum numbers, see Appendix B. For the radial basis $\Phi_n(R)$ one uses analytic functions, such as the associated Laguerre functions[47] which resemble the eigenfunctions of a Morse oscillator, or distributed Gaussians,[48,49] or numerical functions defined on a grid of R points. If the intermolecular potential is just weakly anisotropic, a convenient numerical basis may be obtained by solving the one-dimensional Schrödinger equation with the isotropic potential and the radial terms in the kinetic energy. If, on the other hand, the dimer potential has a deep well at a certain orientation of the monomers, one may solve the one-dimensional equation with the R-dependent potential at fixed angles ζ_A and ζ_B. The solutions of the one-dimensional Schrödinger equation can be obtained by the Numerov−Cooley method,[50] for example. One has to

remember that it is necessary to generate also numerical basis functions that represent the continuum (for instance, by enclosing the system in a spherical box with finite or infinite walls), otherwise the set of functions $\Phi_n(R)$ is not complete. A similar procedure, *i.e.* the solution of an effective one-dimensional radial Schrödinger equation, has also been used[10] with the analytic radial basis sets. The eigenvectors from the secular equation for the one-dimensional problem can be used as contraction coefficients for the radial basis functions in the full problem.

In the case of somewhat stronger anisotropy it is more natural (because of the nearly conserved quantum number K, see section II.C), and also more convenient, to use the BF basis

$$|n j_A,k_A j_B,k_B j_{AB},K;J,M\rangle = \Phi_n(R)\left[\frac{(2j_A+1)(2j_B+1)(2J+1)}{256\pi^5}\right]^{1/2} \times \sum_{m_A m_B} D^{(j_A)}_{m_A k_A}(\zeta_A^{BF})^* D^{(j_B)}_{m_B k_B}(\zeta_B^{BF})^* \times \langle j_A m_A; j_B m_B | j_{AB} K\rangle D^{(J)}_{MK}(\alpha,\beta,0)^* \quad (16)$$

It is shown in Appendix B that, for fixed j_A, k_A, j_B, k_B, j_{AB}, J, M, and K running from $-\min(J,j_{AB})$ to $+\min(J,j_{AB})$ the BF basis in eq 16 spans the same space as the SF basis in eq 15 with l running from $|J - j_{AB}|$ to $J + j_{AB}$. So the final VRT states will be the same in both bases.

In the SF coordinate system one has to use the kinetic energy operator of eq 2. The monomer terms, T_A and T_B in eq 3, act on the functions $D^{(j_A)}_{m_A k_A}(\zeta_A^{SF})^*$ and $D^{(j_B)}_{m_B k_B}(\zeta_B^{SF})^*$ and they yield the standard rigid rotor expressions.[3,22] For example, for symmetric tops with $A_X = B_X$ the operator T_X is diagonal, with eigenvalues $A_X j_X(j_X+1) + (C_X - A_X)k_X^2$. Since the basis functions in eq 15 are eigenfunctions of $(l^{SF})^2$, with eigenvalue $l(l+1)$, the dimer term T_{AB} in eq 4 is diagonal in the angular basis. If the potential is expanded as in eqs 7 and 8, its matrix elements are

$$\langle n' j'_A,k'_A j'_B,k'_B j'_{AB},l';J,M|V|n j_A,k_A j_B,k_B,k_{AB},l;J,M\rangle = \sum_{\{\Lambda\}}\langle\Phi_{n'}(R)|v_{\{\Lambda\}}(R)|\Phi_n(R)\rangle\,(-1)^{j_A+j_B+j'_{AB}+L+J-k'_A-k'_B} \times [(2j'_A+1)(2j'_B+1)(2j_A+1)(2j_B+1)(2j'_{AB}+1) \times (2j_{AB}+1)(2l'+1)(2l+1)]^{1/2} \times \begin{pmatrix} j'_A & L_A & j_A \\ -k'_A & K_A & k_A\end{pmatrix}\begin{pmatrix} j'_B & L_B & j_B \\ -k'_B & K_B & k_B\end{pmatrix}\begin{pmatrix} l' & L & l \\ 0 & 0 & 0\end{pmatrix} \times \begin{Bmatrix} l & l' & L \\ j'_{AB} & j_{AB} & J\end{Bmatrix}\begin{Bmatrix} j'_A & L_A & j_A \\ j'_B & L_B & j_B \\ j'_{AB} & L & j_{AB}\end{Bmatrix} \quad (17)$$

where the expressions in large braces are $6-j$ and $9-j$ symbols,[36] respectively.

In the two-rotor BF coordinate system one should use the kinetic energy operator of eq 5. The monomer terms T_A and T_B yield the same standard rigid rotor expressions as in the SF case. The dimer term T_{AB} is different, however. In Appendix B it is explicitly shown how it acts on the angular basis of eq 16. Most of its terms are diagonal in this basis, but the terms $[(j_{Ax}+j_{Bx})J_x + (j_{Ay}+j_{By})J_y]/(\mu_{AB}R^2)$ connect the basis functions K with functions $K' = K \pm 1$. After expanding the potential as in eqs 7 and 9, the potential matrix elements over the BF basis in eq 16 are

$$\langle n' j'_A,k'_A j'_B,k'_B j'_{AB},K';J,M|V|n j_A,k_A j_B,k_B j_{AB},K;J,M\rangle = \delta_{KK}\sum_{\{\Lambda\}}\langle\Phi_{n'}(R)|v_{\{\Lambda\}}(R)|\Phi_n(R)\rangle\,(-1)^{j_A+j_B+j_{AB}+L-k'_A-k'_B-K} \times [(2j'_A+1)(2j'_B+1)(2j_A+1)(2j_B+1) \times (2j'_{AB}+1)(2j_{AB}+1)]^{1/2} \times \begin{pmatrix} j'_A & L_A & j_A \\ -k'_A & K_A & k_A\end{pmatrix}\begin{pmatrix} j'_B & L_B & j_B \\ -k'_B & K_B & k_B\end{pmatrix}\begin{pmatrix} j'_{AB} & L & j_{AB} \\ -K & 0 & K\end{pmatrix} \times \begin{Bmatrix} j'_A & L_A & j_A \\ j'_B & L_B & j_B \\ j'_{AB} & L & j_{AB}\end{Bmatrix} \quad (18)$$

The advantages of the BF basis become directly apparent now. The potential matrix elements are simpler than with the SF basis. This is especially advantageous for atom–molecule systems, where $j'_A = j_A = L_A = 0$, and the $9-j$ symbol in eqs 17 and 18 becomes simply $\delta_{j'_B j'_{AB}}\delta_{j_B j_{AB}}\delta_{L_B L}[(2j'_B+1)(2j_B+1)(2L_B+1)]^{-1/2}$. The remaining angular factors in eq 17 are called the Percival–Seaton coefficients.[17,20] By contrast with the corresponding expression in the BF coordinates, eq 18, these factors still contain the $6-j$ symbol. Moreover, it is obvious from eq 18 that the potential does not couple BF basis functions with different K. Although such functions are coupled by a Coriolis term in the kinetic energy, the corresponding off-diagonal matrix elements are small and they occur only for $K' = K \pm 1$. In calculations one may, in first instance, neglect these couplings and, thus, reduce the size of the Hamiltonian matrix by a factor $(2J+1)$. If one wishes to go beyond this "helicity decoupling" approximation, one may solve a (smaller) secular problem in a truncated basis of eigenstates of the simpler Hamiltonian while reintroducing these terms, or one may take them into account by perturbation theory.

Besides the fact that it gives a very simple kinetic energy expression and angular integrals over the potential which are just $3n-j$ coefficients, the use of the free rotor functions in the basis has another advantage. It does not introduce any bias for specific orientations of the monomers in the complex; these are free to find their most favorable orientational wave functions, depending on the barriers in the potential surface. Often, in van der Waals complexes, the orientations of the monomers are quite different in different VRT states.

When the monomers in a van der Waals complex are strongly aspherical (very long or flat) and are larger than the van der Waals bonding distance, the potential becomes too strongly anisotropic and the use of the free rotor basis is no longer appropriate. A border case is Ar–benzene,[51] where the spherical

expansion of the potential needs terms up to $L_B = 36$ and the convergence of the VRT states requires angular basis functions as high as $j_B = 27$. Other types of basis functions have to be applied in such cases, and it may be better to use other coordinates too. For atom–molecule systems, the BF frame may be embedded in the molecule, see Appendix A.3, which leads to the kinetic energy expression of eq 6. Instead of polar coordinates for the vector $\bar{R}$, it is advantageous to use its Cartesian components $\boldsymbol{R} = (x,y,z)$ and to apply a product basis of harmonic oscillator functions $H_k(x)H_l(y)H_m(z)$, centered at the equilibrium position $\boldsymbol{R}_e = (x_e,y_e,z_e)$. Or, if the atom is assumed to be less well localized, one could use a basis of distributed Gaussians.[52] The linear and angular momentum operators are simply

$$\boldsymbol{p}_R = -i\hbar\begin{pmatrix}\partial/\partial x\\ \partial/\partial y\\ \partial/\partial z\end{pmatrix} \quad \text{and} \quad \boldsymbol{l} = \boldsymbol{R} \times \boldsymbol{p}_R \tag{19}$$

If these are substituted into the kinetic energy of eq 6 and the coordinate and momentum operators are expressed in the ladder operators of the harmonic oscillator[53,54] (with frequency ω and mass m)

$$x = [\hbar/(2m\omega)]^{1/2}(a_x^\dagger + a_x)$$

$$p_x = i[(\hbar m\omega)/2]^{1/2}(a_x^\dagger - a_x) \tag{20}$$

which act on the basis as follows

$$a_x^\dagger H_k(x) = (k+1)^{1/2}H_{k+1}(x)$$

$$a_x H_k(x) = k^{1/2}H_{k-1}(x) \tag{21}$$

it is still possible to evaluate all the kinetic energy matrix elements analytically. For the matrix elements of the potential $V(x,y,z)$ over the harmonic oscillator basis it is appropriate to use Gauss–Hermite-type quadrature[37] with the same center and scaling as the basis functions $H_k(x)$, $H_l(y)$, and $H_m(z)$. This procedure works well, even if the molecule becomes as large as fluorene.[23] In other systems, *e.g.* the van der Waals trimer Ar–Ar–HCl,[21] one has proposed to combine the different types of analytical basis functions for the different intermolecular coordinates. This depends on the expected degree of localization in these coordinates.

Let us now discuss some nonvariational methods. The traditional nonvariational method to obtain the bound states of van der Waals dimers is the close-coupling method, as implemented for scattering calculations.[55,56] The angular basis functions used in such calculations are the same as in eq 15, for SF coordinates, and eq 16, for BF coordinates. The angular matrix elements are the same as in eqs 17 and 18, respectively. The radial functions are not expanded in a basis, however, but they are written as the R-dependent "coefficients" in the expansion of the exact wave function in the complete set of angular (channel) functions. When this expansion is substituted into the Schrödinger equation one obtains a set of coupled differential equations for the radial functions of the different channels.[17] In practice, this set is truncated, of course. The coupled differential equations are solved by the numerical propagator methods[57,58] developed for scattering calculations. For bound states, it is not possible to choose the energy, however. One has to find, by iteration, those energies that produce the radial wave functions which vanish at $R \to \infty$ and remain finite at $R = 0$.[59–62] Since this may be a rather time-consuming process, special methods for bound state calculations have been devised. In the SEPT (secular equation perturbation theory) method[63] one first calculates a (small) set of uncoupled channel functions, then solves a secular problem with these functions as a basis, and next, includes more channels by perturbation theory. The (first-order) perturbation equations are again a set of coupled differential equations in the radial coordinate, but these do not contain the unknown energy. Recent improvements of this method, such as the ISE (iterative secular equation) method[64] include the perturbed wave functions as additional basis functions in a (larger) secular problem. An advantage of these methods is that they are directly applicable to the resonances, vibrational and rotational predissociation states, which are often found in van der Waals complexes.

Nonvariational approaches which are based on discrete representations of the wave function are the DVR (discrete variable representation)[38,52,65] and the collocation method.[66–68] As we have seen, the use of an analytic basis, say $\varphi_n(x)$, leads to simple kinetic energy expressions, but to rather difficult multidimensional integrals over the potential. If, on the other hand, we would represent a wave function by the set of its values on a coordinate grid, $\Psi(x_i)$, the (diagonal) potential energy matrix is just given by the potential calculated at the grid points, but the kinetic energy would have to be evaluated by finite difference methods. This requires the use of high order difference formulas or dense multidimensional grids. Information on the (approximate) shape of the potential is not exploited. The "pseudospectral" methods (DVR and collocation) combine the best of both worlds. They are based on the property that the expansion of the wave function in the analytic basis $\varphi_n(x)$ with dimension N is equivalent to a discrete representation $\Psi(x_i)$ with N points x_i, provided that the potential energy matrix elements are approximated by the appropriate quadrature. For bases of orthogonal polynomials (of various kinds)[69,70] we must use the associated Gaussian quadratures with points x_i and weights w_i. Following Muckerman,[71] we show this by introducing the (analytic) grid basis

$$\psi_k(x) = \sum_n \varphi_n(x)T_{nk} \tag{22}$$

with the $N \times N$ transformation matrix $\mathbb{T}$ given by

$$T_{ni} = \varphi_n(x_i)w_i^{1/2} \tag{23}$$

The theory of orthogonal polynomials tells us that the integrals over products of these polynomials are evaluated exactly by the corresponding Gaussian quadrature. As a result we find that $\mathbb{T}$ is orthogonal

$$\delta_{nm} = \int \varphi_n(x)\varphi_m(x)\,dx = \sum_i w_i\varphi_n(x_i)\varphi_m(x_i) = \sum_i T_{ni}T_{mi} \quad (24)$$

From this property it follows easily that the functions ψ_k vanish at all grid points except x_k and have the value $w_k^{-1/2}$ at this point

$$\psi_k(x_i) = \sum_n \varphi_n(x_i)T_{nk} = w_i^{-1/2}\sum_n T_{ni}T_{nk} = w_i^{-1/2}\delta_{ik} \quad (25)$$

The essential assumption in the DVR method[38,52,65] is that the potential energy matrix elements can be approximated by the corresponding quadrature formula

$$\langle\varphi_n|V|\varphi_m\rangle = \sum_k w_k\varphi_n(x_k)V(x_k)\varphi_m(x_k) \quad (26)$$

Then, with the use of eq 25, it is easy to show that the potential becomes diagonal in the grid basis

$$\begin{aligned}\langle\psi_k|V|\psi_l\rangle &= \int \psi_k(x)V(x)\psi_l(x)\,dx \\ &= \sum_i w_i\psi_k(x_i)V(x_i)\psi_l(x_i) \\ &= \sum_i w_i w_i^{-1/2}\,\delta_{ik}w_i^{-1/2}\,\delta_{il}V(x_i) \\ &= \delta_{kl}V(x_k)\end{aligned} \quad (27)$$

It is readily demonstrated that the transformation to the analytic basis, see eq 22, would recover the normal quadrature formula, eq 26. In reality, it is more advantageous to keep the potential matrix diagonal, however. The kinetic energy matrix is calculated with the analytic basis $\varphi_n(x)$ (if this basis is conveniently chosen it may even be diagonal), transformed to the grid basis by multiplication with $\mathbb{T}^T$ from the left and with $\mathbb{T}$ from the right, and then added to the potential matrix. This route is preferable because, in multidimensional systems, the kinetic energy is better separable. In Cartesian coordinates it separates exactly; in curvilinear coordinates the kinetic energy matrix retains a relatively simple structure too. Moreover, it stays sparse.

In applying DVR to multidimensional systems it is most common to use a direct product basis, and a direct product of quadrature grids in the individual coordinates. Improvements of this scheme have been proposed recently.[72] Or, one may use discrete representations in some coordinates and analytic bases in others. For instance, in atom–diatom systems the DVR in the angular coordinate—with Legendre functions $P_l(\cos\theta)$ as the basis and Gauss–Legendre quadrature for $\cos\theta$—has been combined[65,73] with a basis of distributed Gaussians for the radial coordinate R. DVR is not a variational method: due to the approximation of the potential matrix elements by the quadrature formula the lowest DVR eigenvalue is not necessarily an upper bound to the exact ground state energy.

A closely related nonvariational method is the collocation method.[66–68] In this method the exact wave function is expanded in a finite (analytic) N-dimensional basis: $\Psi(x) = \sum_n \varphi_n(x)c_n$. The Schrödinger equation is required to be satisfied exactly, for N points x_i in the coordinate space. The resulting equation, in Dirac notation,

$$\sum_{n=1}^{N}[\langle x_i|H|\varphi_n\rangle - E\langle x_i|\varphi_n\rangle]c_n = 0 \quad \text{for} \quad i = 1, ..., N \quad (28)$$

is an $N \times N$ eigenvalue equation for a nonsymmetric matrix $H_{in} = \langle x_i|H|\varphi_n\rangle$ and "overlap' matrix $S_{in} = \langle x_i|\varphi_n\rangle = \varphi_n(x_i)$. The advantage of this method is that it is easy to program; one has just to compute at the grid points x_i the values of the potential, the basis functions φ_n, and their second derivatives (which occur in $H\varphi_n$). If the basis φ_n consists of orthogonal polynomials, it is advised to choose the associated quadrature points x_i. Formally, this method can be justified in the limit of a complete basis φ_n. Or, it can be derived variationally, by searching for a stationary point of the asymmetric functional $\langle\Psi'|H|\Psi\rangle$, while expanding Ψ in the analytic basis φ_n and Ψ' in a basis localized at the grid points x_i.[68] This stationary point is not required to be a minimum, however, and the collocation method is not variational in the sense that it gives an upper bound to the exact ground state energy. The eigenvalues of the nonsymmetric matrix H_{in} may even become complex. In practive, the collocation method seems to work well.[43,66–68,74]

For a basis φ_n of orthogonal polynomials with the associated quadrature points x_i, this method can be easily related to the DVR described earlier. In the DVR method, it is only the potential energy matrix which is assumed to be approximated by numerical quadrature. This matrix can then be evaluated in the grid basis. The kinetic energy is evaluated in the analytic basis φ_n and then transformed to the grid basis ψ_i by multiplication with $\mathbb{T}^T$ from the left and with $\mathbb{T}$ from the right. In the collocation method the complete Hamiltonian matrix H_{nm} is approximated by numerical quadrature. We define an alternative grid basis $\psi'_i = \psi_i w_i^{-1/2}$. Just as ψ_i, the ith element of this basis vanishes at all grid points except x_i, *cf.* eq 25, but its value at this grid point is w_i^{-1}. The basis ψ'_i is obtained from the analytic basis φ_n by transformation with $\mathbb{T}' = \mathbb{T}\mathbb{W}^{-1/2}$, where $\mathbb{W}$ is the diagonal matrix with elements equal to the weights w_i. The matrix $(\mathbb{T}')^T$ is just the "overlap" matrix in the collocation equation, eq 28, and it is not difficult to show now that eq 28 can be obtained from the "normal" secular equation by multiplication with the matrix $(\mathbb{T}')^T$, only from the left. This implies, in other words, that the matrix elements H_{in} in the collocation equations are constructed with the analytic basis φ_n, from the right, and with the grid basis ψ'_i, from the left. The kinetic energy matrix is kept simple by letting the differential operators act on the analytic basis, to the right. Also the potential energy matrix elements remain simple, however, since the basis functions ψ'_i vanish, except at one grid point x_i. The inverse weights, which are the function values at these points, reflect that, by contrast with DVR, no weights are involved in the collocation method. In spite of its simplicity, the collocation method may be

not the most efficient from the computational point of view. If the diagonalization of the H matrix is the most time-consuming step (as it is in most calculations, even with the variational methods), the time gained by the easier construction of the matrix is more than lost by the slower diagonalization of a nonsparse, nonsymmetric matrix.

A common property of all basis set and discrete representation methods is that, finally, one has to solve the (symmetric or nonsymmetric) matrix eigenvalue problem. Standard library routines are available for this purpose. If the basis becomes too large to store the Hamiltonian matrix in the computer memory, one may also use a different type of iterative procedure, such as the Lanczos[75,76] or Davidson[77] algorithm. If the system has many degrees of freedom, or if the construction and diagonalization of the H matrix has to be repeated many times in the process of improving the potential by fitting the experimental spectrum, it is desirable to reduce the size of the basis. Early work in this direction[78] used BOARS: the Born–Oppenheimer (or adiabatic) separation of the angular and radial motion. More recently, it has become common practice to use (sequential) adiabatic reduction methods:[38,52] one or more coordinates are clamped and the eigenvalue problem is solved for the remaining degrees of freedom. The eigenvalues, for different values of the clamped coordinates, form the effective potentials for the second step in the calculation. Adiabatic (or quasiadiabatic) reduction implies that in this second step, which yields the final wave function, one uses a truncated set of eigenfunctions from the first step. In multidimensional systems this procedure may be followed sequentially, in the different coordinates. It is easily implemented in DVR methods, which already use a finite grid representation for some of the coordinates. But, as we have been seen in the treatment of the off-diagonal Coriolis coupling in the scheme with the BF free rotor basis, similar simplifications can be achieved in other methods.

We end this discussion of methods for the calculation of the VRT states of van der Waals molecules by briefly mentioning the quantum Monte Carlo method. The variational Monte Carlo procedure,[79,80] in essence, is a method for the numerical computation of the multidimensional integrals of the Hamiltonian over a trial wave function. So, the accuracy of this method is limited by the trial function chosen. The Green's function or diffusional Monte Carlo method[80,81] is very powerful, however, and it will converge to the exact quantum states of the system. In its "standard" version, which converges to the ground state, it has been applied to several van der Waals complexes including even multiple monomers.[80,82] Also excited states can be studied, if they have a different symmetry from the ground state, so that their nodal planes are fixed, or if one applies the following adiabatic separation scheme:[81] A special coordinate in which the wave function is expected to have a node is clamped (at different values) and the Monte Carlo method is applied to the remaining degrees of freedom. The Schrödinger equation for the special coordinate is solved in the traditional manner (numerically or in a basis) with the effective potential given by the energies from the Monte Carlo calculations. This adiabatic separation involves an approximation, however, and it may be difficult to define the special (curvilinear) coordinate beforehand. A new, "correlation function" quantum Monte Carlo method which, by the use of the operator $\exp(-tH)$, will converge directly to vibrationally excited states (at the expense of a higher computational cost), has been devised also,[83] but not yet applied to van der Waals molecules. For a more detailed description of these Monte Carlo methods we refer to the papers mentioned in this paragraph.

E. Properties, Transitions, and Intensities

Most of the methods used for the calculation of the VRT states yield explicitly the wave functions of these states. It becomes relatively easy, then, to compute the different measurable properties and to evaluate the intensities of the transitions observed in spectra. The (infrared) absorption coefficient for the transition between two thermally populated VRT levels (i,J) and (i',J') is given by[84]

$$\frac{\pi N_A g_i}{3\hbar^2 \epsilon_0 c Z}(E_{i',J'} - E_{i,J})[\exp(-E_{i,J}/kT) - \exp(-E_{i',J'}/kT)]S(i,J\rightarrow i',J') \quad (29)$$

where $E_{i,J}$ is the energy of the VRT state (i,J) and Z is the partition function

$$Z = \sum_{i,J} g_i(2J+1)\exp(-E_{i,J}/kT) \quad (30)$$

It is assumed here that the distribution over the VRT levels is a Boltzmann distribution with temperature T; g_i is the nuclear spin statistical weight of the level i, N_A is Avogadro's number, and the other constants are fundamental constants. The (calculated) wave functions of the VRT states are the kets $|iJM\rangle$; in the absence of external fields these are degenerate for $M = -J, -J+1, \ldots, J$. The line strengths in eq 29 are defined as

$$S(i,J\rightarrow i',J') = \sum_{MM'm} |\langle i'J'M'|\mu_m^{SF}|iJM\rangle|^2 \quad (31)$$

If the wave functions $|iJM\rangle$ of the VRT states have been calculated in terms of the SF basis in eq 15, it is convenient to express the space-fixed (spherical) components μ_m^{SF} of the dipole moment operator in the same basis

$$\mu_m^{SF}(R,\zeta_A^{SF},\zeta_B^{SF},\hat{\boldsymbol{R}}) = \sum_{\{\Lambda\}\lambda} d^{SF}_{\{\Lambda\}\lambda}(R)\, B^{SF}_{\{\Lambda\}\lambda m}(\zeta_A^{SF},\zeta_B^{SF},\hat{\boldsymbol{R}}) \quad (32)$$

The angular functions $B_{\{\Lambda\}\lambda m}$ must transform as a vector quantity. In terms of the space-fixed orientation angles ζ_A^{SF} and ζ_B^{SF} and end-over-end angles $\hat{\boldsymbol{R}}$ they read

$$B^{SF}_{\{\Lambda\}\lambda m}(\zeta^{SF}_A,\zeta^{SF}_B,\hat{\boldsymbol{R}}) = \sum_{M_A M_B M_{AB} M} D^{(L_A)}_{M_A K_A}(\zeta^{SF}_A)^* D^{(L_B)}_{M_B K_B}(\zeta^{SF}_B)^* C^{\lambda}_{M}(\hat{\boldsymbol{R}}) \langle L_A M_A; L_B M_B | L M_{AB}\rangle \langle L M_{AB}; \lambda M | 1 m\rangle \quad (33)$$

with the composite index $\{\Lambda\} = \{L_A,K_A,L_B,K_B,L\}$. This might be compared with the functions in eq 8 for the angular expansion of the potential. Since the latter functions are scalars, the combination of the two Clebsch–Gordan coefficients becomes simply a $3-j$ symbol

$$\sum_{M_{AB}} \langle L_A M_A; L_B M_B | L M_{AB}\rangle \langle L M_{AB}; \lambda M | 00\rangle = \delta_{L\lambda}(-1)^{L_A-L_B+L} \begin{pmatrix} L_A & L_B & L \\ M_A & M_B & M \end{pmatrix} \quad (34)$$

If the dipole moment given by eq 32 and the wave functions $|iJM\rangle$ in terms of the basis in eq 15 are substituted into eq 31 for the line strength, all the occurring angular matrix elements are just $3n-j$ symbols. The result is similar to, but slightly more complicated than, the corresponding result for the potential, eq 17.

If the wave functions $|iJM\rangle$ have been calculated in terms of the BF basis, eq 16, it is preferable to express the dipole moment operator in that basis too. The dipole components relative to the BF frame are given by

$$\mu^{BF}_k(R,\zeta^{BF}_A,\zeta^{BF}_B) = \sum_{\{\Lambda\}} d^{BF}_{\{\Lambda\}k}(R)\, B^{BF}_{\{\Lambda\}k}(\zeta^{BF}_A,\zeta^{BF}_B) \quad (35)$$

and the angular functions are

$$B^{BF}_{\{\Lambda\}k}(\zeta^{BF}_A,\zeta^{BF}_B) = \sum_{M_A M_B} D^{(L_A)}_{M_A K_A}(\zeta^{BF}_A)^* D^{(L_B)}_{M_B K_B}(\zeta^{BF}_B)^* \langle L_A M_A; L_B M_B | L k\rangle \quad (36)$$

The relation between the SF and BF expansion coefficients is given by

$$d^{BF}_{\{\Lambda\}k}(R) = \sum_{\lambda} d^{SF}_{\{\Lambda\}\lambda}(R) \langle L k; \lambda 0 | 1 k\rangle \quad (37)$$

This relation follows directly, as a special case with $J = 1$, from eq B17 derived in Appendix B. The relation between the SF and BF dipole components is

$$\mu^{SF}_m(R,\zeta^{SF}_A,\zeta^{SF}_B,\hat{\boldsymbol{R}}) = \sum_k \mu^{BF}_k(R,\zeta^{BF}_A,\zeta^{BF}_B)\, D^{(1)}_{mk}(\alpha,\beta,0)^* \quad (38)$$

and the BF label k indicates whether a given transition has a parallel ($k = 0$) or a perpendicular ($k = \pm 1$) component.

If the monomers have large dipole moments, the infrared transitions are strongly determined by these, and the corresponding coefficients in eq 35 become simply

$$d^{BF}_{L_A,K_A,L_B,K_B,L,k}(R) = \delta_{L_B 0}\delta_{K_B 0}\delta_{L_A 1}\delta_{L_A L}\,\mu_{K_A} + \delta_{L_A 0}\delta_{K_A 0}\delta_{L_B 1}\delta_{L_B L}\,\mu_{K_B} \quad (39)$$

Table 2. Factors of $Q^{L_B}_{K_B}\alpha^{(1,1;L_A)}_{K_A}R^{-L_B-2}$ in the Induced Dipole Equation (Eq 40) with $k \geq 0$[a]

L_B	L_A	L	k	
0	0	0	0	$(1/3)\sqrt{3}$
0	2	2	0	$(-1/3)\sqrt{6}$
0	2	2	1	$(-1/2)\sqrt{2}$
1	0	1	0	$(-2/3)\sqrt{3}$
1	2	1	0	$(-1/15)\sqrt{15}$
1	2	3	0	$(3/5)\sqrt{10}$
1	0	1	1	$(1/3)\sqrt{3}$
1	2	1	1	$(1/30)\sqrt{15}$
1	2	2	1	$(1/2)\sqrt{3}$
1	2	3	1	$(2/5)\sqrt{15}$
2	0	2	0	$\sqrt{3}$
2	2	2	0	$(1/7)\sqrt{21}$
2	2	4	0	$(-2/7)\sqrt{105}$
2	0	2	1	-1
2	2	2	1	$(-1/7)\sqrt{7}$
2	2	3	1	$(-1/2)\sqrt{10}$
2	2	4	1	$(-5/14)\sqrt{42}$

[a] A coefficient with $k = -1$ is obtained from the coefficients in this table with the same L_B, L_A, L values by multiplication with $(-1)^{L+L_B}$. The factors of $Q^{L_A}_{K_A}\alpha^{(1,1;L_B)}_{K_B}R^{-L_A-2}$ are obtained from the corresponding coefficients in this table by multiplication with $-(-1)^{L+L_B}$.

where $\mu_{K_A} \equiv Q^1_{K_A}$ and $\mu_{K_B} \equiv Q^1_{K_B}$ are the components of the permanent dipoles on the monomers, expressed in the monomer frames. If we wish to include also the dipole moment induced on monomer A by the permanent multipole moments $Q^{L_B}_{K_B}$ on monomer B, we must add

$$d^{BF}_{L_A,K_A,L_B,K_B,L,k}(R) = \sum_{l_A}(-1)^{k+l_A}[(2L_A+1)(2l_A+2L_B+1)(2L+1)]^{1/2} \begin{pmatrix} 2l_A+2L_B \\ 2l_A \end{pmatrix}^{1/2} \begin{pmatrix} l_A+L_B & L & 1 \\ 0 & k & -k \end{pmatrix} \begin{Bmatrix} l_A+L_B & L_B & l_A \\ L_A & 1 & L \end{Bmatrix} Q^{L_B}_{K_B}\alpha^{(1,l_A;L_A)}_{K_A}R^{-l_A-L_B-1} \quad (40)$$

where $\alpha^{(1,l_A;L_A)}_{K_A}$ are the irreducible components of the (mixed) dipole–2^{l_A}-pole polarizability tensor of monomer A, with respect to the monomer frame. For $l_A = 1$ this is the normal dipole polarizability, with the isotropic value given by $\alpha^{(1,1;0)}_0 = -(\alpha_{xx}+\alpha_{yy}+\alpha_{zz})/\sqrt{3}$ and the axial anisotropic component by $\alpha^{(1,1;2)}_0 = (2\alpha_{zz}-\alpha_{xx}-\alpha_{yy})/\sqrt{6}$. The dipole induced on monomer B is obtained if we interchange A and B in this formula, and multiply by $(-1)^{L_B+L-l_B}$. For the most common cases of a dipole moment induced by a monopole (charge), dipole, or quadrupole through the normal dipole polarizability we have listed the numerical values of the coefficients in Table 2. For special cases, such as atom–polyatom,[8] atom–diatom,[85,86] and diatom–diatom complexes,[87,88] these formulas have been derived earlier. If monomer A is an atom, $l_A = 1$ and $L_A = 0$, and the $6-j$ coefficient in eq 40 becomes simply $\delta_{L_B L}[3(2L_B+1)]^{-1/2}$. The line strengths, eq 31, are calculated in the BF basis of eq 16 by the use of eqs 35 and 36 for the dipole moment, the computation of the radial integrals over eqs 39 and 40, and the evaluation of the angular integrals in terms of $3n-j$ symbols. Again, the result is similar to the expression, eq 18, for the potential

matrix elements, but slightly more complicated. For other (tensorial) properties, such as the polarizability function needed for the calculation of Raman intensities, it is easy now to write similar expressions.

As the van der Waals or hydrogen bonds are weak, the transitions between different VRT levels in a van der Waals complex are observed in the far-infrared, typically below 200 cm^{-1}. They may also be seen in the mid- or near-infrared, however, or even in visible or UV spectra, if they occur simultaneously with vibrational or electronic transitions in the monomers. van der Waals complexes are formed in relatively high concentrations during the expansion of a supersonic nozzle beam; the use of such beams for spectroscopy has two other important advantages. First, when the spectra are taken somewhat downstream from the expansion, they are practically free of collision and Doppler broadening. The spectral resolution can be enormously increased, so that the individual rotational $J \rightarrow J'$ transitions are resolved, even for rather large complexes. This yields a wealth of detailed and accurate information.[6,89-98] Second, the molecules have become very cold, typically a few degrees Kelvin. Only some J levels of the ground state are populated, which leads to simple spectra that can be (relatively) easily interpreted. Also the calculation of such spectra from the VRT states presents no special problems, once the wave functions of these states are known.[8,17,49] In gas phase spectra higher states are populated too, which causes a multitude of hot bands. In combination with the lower resolution this leads to very complex spectra, with composite, overlapping bands.[99-103] Also the computation of such spectra from the VRT states becomes a major task.[88,104,105]

F. Symmetry Aspects

In "normal" nearly rigid molecules it is customary to use the point group of the equilibrium structure to classify the vibrations and the electronic states. This is just an approximate symmetry, however. In van der Waals molecules with multiple minima in the potential surface and large amplitude vibrations it is no longer valid. The symmetry group of such molecules contains (i) permutations of identical nuclei, (ii) space inversion, and (iii) products of i and ii. Usually not all permutation inversions (PI's) are physically meaningful in the sense that they give rise to observable splittings; one only has to consider the so-called[106,107] feasible PI's. There are two kinds of these. The first kind is equivalent to a rotation of the (rigid) complex in isotropic space. In this case no energy barrier has to be surmounted. The second kind of feasible PI's requires the tunneling through some barrier, deforming the complex to another equivalent structure that is distinguished from the earlier structure by the change in one or more internal coordinates. It is very hard to predict *a priori* if an operation of the second kind is feasible. Detailed experiments or elaborate calculations are required to do so. Furthermore, whether or not an operation is considered to be feasible depends on the resolution of the measuring device.

The application of the molecular symmetry group, *i.e.* the group of all feasible PI's, is treated in several textbooks.[108,109] In Appendix C we have shown, for the various coordinate systems commonly used in van der Waals molecules, how to derive the action of the PI's on the coordinates. The action on the different basis functions then follows rather easily from the well-known analytic properties of these functions, see Table 1. In SF coordinates this derivation is rather trivial, and not much can be learned from it, since it is not possible in these coordinates to separate the overall rotations of the complex from its internal motions. With the use of BF coordinates such a separation is possible, although approximate. The action of the PI's becomes more complicated: each PI corresponds with an "equivalent rotation" of the BF frame[108] and a transformation of the internal coordinates of the complex. If the complex is nearly rigid and has a single equilibrium structure, the PI group contains just the operations of the first kind and it is isomorphic to the point group of the equilibrium structure. The action of the PI's on the internal coordinates is equivalent to that of the point group operations on the small vibrational displacements. It is the additional PI's, of the second kind, which make the VRT states of van der Waals molecules so interesting, however.

The PI group symmetry can be used for different purposes. In the calculation of the VRT states, the adaptation of the basis to the irreducible representation (irreps) of the PI group leads to a separation of the Hamiltonian matrix into smaller blocks. In some examples, such as $(NH_3)_2$,[10] this simplification was essential to make the calculations practically feasible. Also the VRT states are symmetry adapted and, since the dipole operator is invariant under all permutations of identical nuclei and antisymmetric under space inversion E^*, this causes the (exact) selection rules. Further, approximate selection rules may be derived as well, by considering the separate PI group adaptation of the overall rotation functions and of the internal VRT wave functions. For this purpose, the components of the dipole operator should be expressed with respect to the BF frame, as in eq 35. The PI group symmetry of the "parallel" and "perpendicular" dipole components follows easily from the transformation properties of the coordinates.

Finally, we note that also the nuclear spin eigenfunctions must be adapted to the permutations of (all) identical nuclei. The spin functions are invariant under space inversion. Since the nuclei are bosons (for integer I) or fermions (for half-integer I), it follows from the Pauli principle that the spatial wave functions of the VRT states are explicitly related, through their permutation symmetry, to the occurrence of specific nuclear spin quantum numbers. It is this relation that determines the nuclear spin statistical weight[108] of each VRT level. For the vibrational spectra of nearly rigid molecules this is not relevant, but for floppy van der Waals molecules the permutation symmetry of the VRT states will strongly affect the spectra. So, the spectra that pertain to the different nuclear spin species will be rather different. As, practically always, the various nuclear spin species occur simultaneously, the measured spectra in fact consist of a set of overlapping spectra for all the species. In high-resolution spectra

it is no problem to separate the individual species and to relate their spectra to the spectra calculated for the corresponding species.

III. Comparison with Experimental High-Resolution Spectra, Verification of ab Initio Potentials, Semiempirical Potential Fits, Examples

The route from the intermolecular potential to the spectra and vice versa, for which the map has been laid out in the preceding sections, will now be illustrated on several examples. These examples are mostly taken from our own work, as we have illustrative material available for these systems. First, we will describe two atom–diatom complexes, Ar–H_2 and He–HF, for which the route has been followed very precisely in both directions: recently calculated *ab initio* potentials reproduce the spectra with great precision, accurate semiempirical potentials were constructed already some time ago.

Next we discuss two atom–polyatom dimers, Ar–NH_3 and Ar–H_2O, where both directions were taken too, but the anisotropy of the *ab initio* potential still had to be scaled to get agreement with the spectra. The semiempirical potentials which were obtained from fits to the spectra are probably more accurate, but this is still being established by using them to calculate other observed data (such as state-to-state inelastic scattering cross sections). Higher quality *ab initio* potentials are now becoming available for these complexes. In the example of Ar–NH_3 an internal motion, the NH_3 umbrella vibration and inversion, was included in the calculations of the far- and mid-infrared spectra.

We then consider systems, some rare gas atom–aromatic molecule dimers, for which the use of "scattering" coordinates is better abandoned. This is because, for these large flat molecules, the distance to the rare gas atom is not too large at the van der Waals minimum, but at the same distance and other values of the angles, the atom feels a strong "steric" repulsion. The problem separates much better and is treated more naturally in Cartesian coordinates: z is the height of the rare gas atom above the molecular plane and x and y describe the lateral motions. For such systems, it proved to be convenient to embed the BF frame in the molecule and to use the kinetic energy operator in eq 6.

Finally, as an example of a dimer consisting of two nonlinear molecules, we discuss NH_3–NH_3. The question whether hydrogen bonding occurs in this complex, and whether the (average) structure found from microwave spectra is significantly different from the (calculated) equilibrium structure, has been subject to much debate. Far-infrared spectra became recently available, but it was not obvious which conclusions regarding the structure and the internal motions of this dimer had to be drawn from the various experimental data. Also the (incomplete) information about the potential surface from different *ab initio* calculations was partly contradictory. We will show that, with the use of the two-rotor BF coordinates and a sufficiently large basis of symmetrized free-rotor functions, this problem can be solved and these questions can be answered.

The examples given are by no means complete. We forgo a discussion of the simplest of all van der Waals molecules: the rare gas (Rg) pairs. The spectroscopy of those dimers is discussed in ref 110 (p 403). For a long time it was thought that the He–He potential did not support a single bound state, but bound He_2 was observed recently.[111] See ref 112 for a discussion of the Rg dimer potentials. Extensive work, which we will not explicitly review, has been performed also for Rg–HX dimers, with X = F, Cl, or Br. This work is summarized in ref 113. Further, we might mention the experimental and theoretical studies of the $(HF)_2$ dimer. This system is a typical example of a diatom–diatom complex, for which the whole trajectory from *ab initio* calculations of the potential surface to the spectra has been followed. We list only two papers,[81,114] which describe the calculation of the spectra from the potential and the comparison with the experimental data. For further information we refer to these papers and the references therein.

A. Ar–H_2

The Ar–H_2 van der Waals molecule is one of the most thoroughly investigated atom–diatom complexes, and the empirical potential energy surface for this system is probably the most accurately determined of any atom–diatom potentials. One of the earliest studies of the anisotropic interactions in Ar–H_2 was the work of Le Roy and van Kranendonk.[115] They derived an anisotropic potential energy surface for Ar–H_2 by fitting the potential to the near-infrared spectra of McKellar and Welsh.[116] Although these spectra were measured in the gas phase, with very long path cells, the rotational structure could still be resolved because H_2 is extremely light. Complementary work was later reported by Dunker and Gordon,[85] who also based their fits on the McKellar and Welsh data. In 1980 Le Roy and Carley[19] published further improved potentials based on these data. In the 1980s high-resolution near-infrared spectra,[117] hyperfine spectra,[118] and molecular beam differential cross sections[119] have been measured. Using these data Le Roy and Hutson[120] gave a new multiproperty fitted potential for Ar–H_2. Their final potential fit has been very successful. It reproduces the results of all the measurements to within the experimental error bars, including the data not utilized in the fit. The authors give the value of the potential at the minimum to an astonishing accuracy of four figures, and the free parameters of the potential have uncertainties of about 1%. Very recently McKellar[121,122] was able to measure also the far-infrared spectra which correspond to the pure van der Waals transitions, not accompanied by a vibrational excitation of the H_2 molecule.

Surprisingly, there is only one, very recent, full *ab initio* study of the potential and VRT states of this dimer. Williams *et al.*[31] performed symmetry-adapted perturbation theory (SAPT) calculations of the complete (*i.e.*, including variation of the H–H distance) potential energy surface for Ar–H_2. For a detailed discussion of the resulting potential we refer the reader to ref 31. Here, we only want to stress that high-level theory and large *spdfgh*-symmetry basis sets carefully optimized for intermolecular interac-

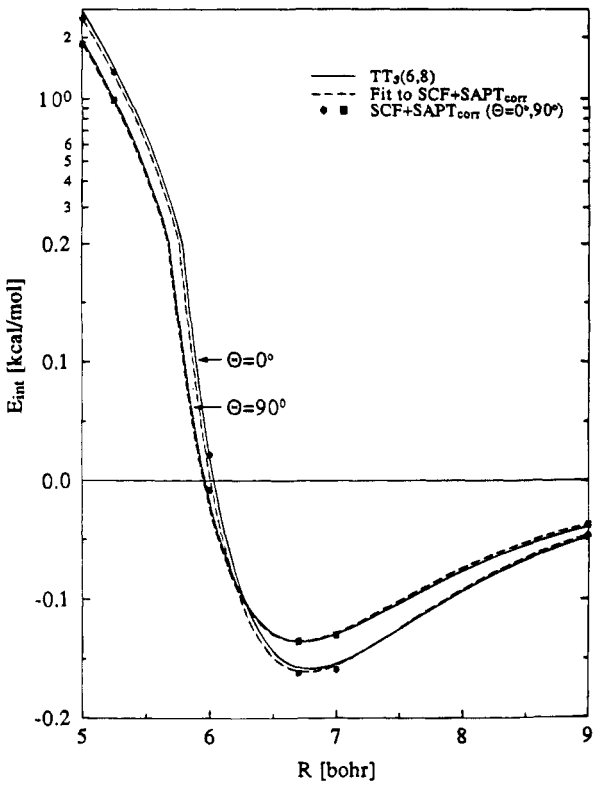

Figure 1. *Ab initio* SAPT[31] and empirical[120] indicated by $TT_3(6,8)$ interaction potentials of Ar−H_2.

tions have been used to achieve converged results. For a broad range of the configuration space the SAPT potential agrees to almost two significant digits with the empirical potential of Le Roy and Hutson[120] (see Figure 1). In particular, at the van der Waals minimum the two potentials agree within 3%.

Although the SAPT potential surface agrees very well with the empirical potentials, its accuracy is better judged by direct comparison with experiment. The quality of the *ab initio* SAPT potential[31] was checked[32] by exposing it to the severe test of computing the observed high-resolution near- and far-infrared spectra of McKellar.[117,121] Since for Ar−H_2 nearly exact calculations of the VRT states can be performed, any discrepancy between the observed and calculated transition frequencies can be attributed to possible deficiencies of the intermolecular potential.

Since the anisotropy in the potential for this system is very weak, relative to the large rotational constant of the H_2 subunit, we use the SF coordinates. The kinetic energy operator is given by eqs 2−4 with $T_A = 0$ and $T_B = C(r)j_B^2$, where $C(r)$ is the rotational constant of H_2 which depends on the H−H bond length r. The potential can be expanded as in eq 7; the expansion functions would simply be Legendre functions $P_L(\cos\theta_B)$ when expressed in BF coordinates, *cf.* eqs 9 and 10, but they must be transformed to the SF coordinates, *cf.* eq 8. The SF expansion functions are coupled products of two spherical harmonics[17,20] which are functions of $\zeta_B^{SF} = (\theta_B^{SF},\phi_B^{SB}) = \hat{r}$ and $\hat{R} = (\beta,\alpha)$. Also the SF angular basis functions for the VRT states, *cf.* eq 15, are coupled products of two spherical harmonics in $\hat{r}$ and $\hat{R}$. The expansion coefficients $v_L(R, r)$ in the potential depend on the length R of the van der Waals bond,

Table 3. Calculated Energy Levels (in cm^{-1}) of the Ar−H_2 ($v = 0, j = 0$) and Ar−D_2 ($v = 0, j = 0$) Complexes from the *ab Initio* SAPT Potential

J	l	Ar−H_2	Ar−D_2	
0	0	−21.883	−28.387	−4.134[a]
1	1	−20.756	−27.752	−3.734[a]
2	2	−18.516	−26.484	−2.942[a]
3	3	−15.188	−24.590	−1.776[a]
4	4	−10.821	−22.078	−0.260[a]
5	5	−5.487	−18.962	+1.571[a]
6	6	+0.685	−15.257	
7	7		−10.987	
8	8		−6.183	
9	9		−0.888	
10	10		+4.828	

[a] Excited Van der Waals stretch levels.

Table 4. Calculated Energy Levels (in cm^{-1}) of the Ar−H_2 ($v = 0, j = 1$) Complex from the *ab Initio* SAPT Potential

l	$J = l + 1$	$J = l$	$J = l - 1$
0	−22.352		
1	−21.206	−19.915	−22.437
2	−18.956	−17.677	−18.883
3	−15.662	−14.355	−15.572
4	−11.246	−9.998	−11.207
5	−5.894	−4.686	−5.868

as well as on r. Morse-type oscillator functions[47] were used as the basis in R, and since the potential in ref 31 was expanded as a Taylor series in r, the required integrals over the vibrational states of H_2 could be obtained from ref 19. The elements of the kinetic energy matrix become extremely simple with the SF angular basis, the potential matrix elements are more complex, *cf.* eq 17. For atom−molecule dimers one can avoid the calculation of the $9 - j$ symbols, however, by using the simplification indicated below eq 18. When the molecule is linear, as in this case, one can substitute $K_A = K_B = 0$ in the expansion of the potential and $k_A = k_B = 0$ in the basis. The angular factors thus appearing in these matrix elements are the Percival−Seaton coefficients.[17,20]

The only rigorously conserved quantum numbers are the total angular momentum J, its projection M on the space-fixed z axis, and the parity σ. Because of the very weak anisotropy of the potential, the H_2 rotational quantum number j and the quantum number l associated with the end-over-end rotation of the vector $\vec{R}$ are nearly conserved too (coupling case a of ref 16). These approximate quantum numbers can be used to label the VRT levels. In Tables 3 and 4 we report results of converged variational calculations for the bound states of Ar−H_2 ($j = 0$) and Ar−D_2 ($j = 0$), and for Ar−H_2 ($j = 1$), respectively. For details of the calculations we refer to ref 32. For the $j = 0$ states of Ar−H_2 the potential affords only one bound stretch state, with $J = l$ running from 0 to 5. By virtue of its larger mass, Ar−D_2 has two such bound states; the second state corresponds to the excited van der Waals stretch. In the $j = 1$ manifold of Ar−H_2 there are 16 bound states, see Table 4. The anisotropy of the potential splits each $(j=1,l)$-level into states with $J = l - 1$, l, and $l + 1$. In Table 4 we see illustrated that these splittings are very small. This is not surprising in view of the small anisotropy in the potential.

Table 5. Near-Infrared Transitions in Ar−D_2 (in cm^{-1}) Accompanying the Fundamental Band of *o*-D_2 [$Q_1(0)$ = 2993.614 cm^{-1}]

				$\Delta E(J'' \rightarrow J')$		
J''	l''	J'	l'	computed (ref 32)[a]	observed (ref 117)[b]	Δ[c]
1	1	2	2	2994.117	2994.042	+0.075
2	2	3	3	2994.728	2994.659	+0.069
3	3	4	4	2995.326	2995.287	+0.039
4	4	5	5	2995.908	2995.835	+0.073
5	5	6	6	2996.470	2996.402	+0.068
6	6	7	7	2997.009	2996.952	+0.051
7	7	8	8	2997.517	2997.475	+0.042
8	8	9	9	2997.986	2997.995	+0.031
9	9	10	10	2998.399	2998.375	+0.024
2	2	1	1	2991.592	2991.542	+0.050
3	3	2	2	2990.955	2990.904	+0.051
4	4	3	3	2990.322	2990.297	+0.025
5	5	4	4	2989.698	2989.690	+0.008
6	6	5	5	2989.087	2989.080	+0.007
7	7	6	6	2988.496	2988.549	−0.053
8	8	7	7	2987.935	2987.988	−0.053
9	9	8	8	2987.419	2987.485	−0.066
10	10	9	9	2986.976	2987.040	−0.064

[a] Computed near-infrared transitions from the *ab initio* SAPT potential (ref 31). [b] Measured near-infrared transitions (ref 117). [c] Absolute error of the transition frequency computed from the *ab initio* SAPT potential.

In the presentation of the computed transition frequencies we follow the spectroscopic notation which is common for the H_2 transitions. The symbols $Q(j)$ and $S(j)$ denote $\Delta j = 0$ and $\Delta j = 2$ transitions, respectively, that depart from a state j. The change in the vibrational quantum number is indicated by a subscript. For example, $Q_1(0)$ stands for a $v = 0 \rightarrow 1$ transition in *para* (even j) hydrogen in which the rotational state does not change. The $Q_v(0)$ transitions probe mainly the isotropic part of the potential and its dependence on the diatom stretching distance. The levels with higher j are also perturbed by the anisotropic part of the potential, so that the $Q_v(j)$ and $S_v(j)$ transitions contain information about the anisotropy in the interaction.

In Tables 5 and 6 we present the near-infrared transitions of the $Q_1(0)$ and $S_1(0)$ spectra of Ar−D_2. Note that both upper states are resonances that undergo vibrational predissociation and that the second upper state also decays via internal rotation predissociation. The lifetimes of these compound resonances are so long[123,124] that the associated line broadenings have not been observed experimentally and a bound state method can be safely applied. Table 7 gives the far-infrared transitions in the $S_0(0)$ spectrum of Ar−D_2. (Note that in ref 117 the assignments for the R branch of the $Q_1(0)$ spectrum of Ar−D_2 and the T branch of its $S_1(0)$ band contain some typographical errors.[125]) An inspection of Tables 5−7 shows that the SAPT potential[31] produces very accurately the transition frequencies for both the $Q_1(0)$ and $S_v(0)$ bands: typical errors are of the order of 0.1 cm^{-1}. This very good agreement between the results of *ab initio* calculations[32] and high-resolution measurements[117,121] suggests that not only the dominant isotropic part of the SAPT potential,[31] but also its dependence on the diatom stretching distance and the weak anisotropic term are very accurate.

Table 6. Near-Infrared Transitions in Ar−D_2 (in cm^{-1}) Accompanying the Fundamental Band of *o*-D_2 [$S_1(0)$ = 3166.359 cm^{-1}]

				$\Delta E(J'' \rightarrow J')$		
J''	l''	J'	l'	computed (ref 32)[a]	observed (ref 117)[b]	Δ[c]
1	1	2	4	3170.335	3170.290	+0.045
2	2	3	5	3172.221	3172.159	+0.062
3	3	4	6	3174.038	3173.986	+0.052
4	4	5	7	3175.790	3175.725	+0.065
5	5	6	8	3177.470	3177.387	+0.084
6	6	7	9	3179.059	3178.964	+0.095
7	7	8	10	3180.525	3180.418	+0.107
8	8	9	11	3181.797	3181.676	+0.121
9	9	10	12	3182.704	3182.640	+0.064
3	3	2	0	3161.352	3161.350	+0.002
4	4	3	1	3159.449	3159.472	−0.023
5	5	4	2	3157.612	3157.585	+0.027
6	6	5	3	3155.868	3155.768	+0.100
7	7	6	4	3153.806	3153.995	−0.186
8	8	7	5	3152.336	3152.290	+0.046
9	9	8	6	3150.829	3150.692	+0.137
10	10	9	7	3149.147	3149.246	−0.099

[a] Computed near-infrared transitions from the *ab initio* SAPT potential (ref 31). [b] Measured near-infrared transitions (ref 117). [c] Absolute error of the transition frequency computed from the *ab initio* SAPT potential.

Table 7. Far-Infrared Transitions in Ar−D_2 (in cm^{-1}) Accompanying the Δj = 2 Band of *o*-D_2 [$S_0(0)$ = 179.069 cm^{-1}]

				$\Delta E(J'' \rightarrow J')$		
J''	l''	J'	l'	computed (ref 32)[a]	observed (ref 121)[b]	Δ[c]
1	1	2	4	183.913	183.875	+0.038
2	2	3	5	185.822	185.749	+0.073
3	3	4	6	187.666	187.560	+0.106
4	4	5	7	189.447	189.331	+0.116
5	5	6	8	191.154	191.004	+0.150
6	6	7	9	192.765	192.598	+0.167
7	7	8	10	194.241	194.055	+0.186
8	8	9	11	195.491	195.257	+0.234
3	3	2	0	174.844	174.903	−0.059
4	4	3	1	172.911	172.995	−0.084
5	5	4	2	171.032	171.140	−0.108
6	6	5	3	169.202	169.323	−0.121
7	7	6	4	167.431	167.589	−0.158
8	8	7	5	165.734	165.900	−0.166
9	9	8	6	164.138	164.326	−0.188
10	10	9	7	162.688	162.895	−0.207

[a] Computed far-infrared transitions from the *ab initio* SAPT potential (ref 31). [b] Measured far-infrared transitions (ref 121). [c] Absolute error of the transition frequency computed from the *ab initio* SAPT potential.

B. He–HF

The He−HF complex is very weakly bound and until recently it was investigated only by scattering techniques.[126,127] In 1990 Lovejoy and Nesbitt[128] reported the first study of the high-resolution near-infrared vibration−rotation spectra, corresponding to the simultaneous excitation of the vibration and rotation of HF within the He−HF complex, and of the rotational predissociation.

The few dynamical calculations for this complex[128−130] were based on the *ab initio* potential of Rodwell *et al.*[131] The most advanced of these studies was reported by Lovejoy and Nesbitt.[128] Their calculations of bound and quasibound rovibrational

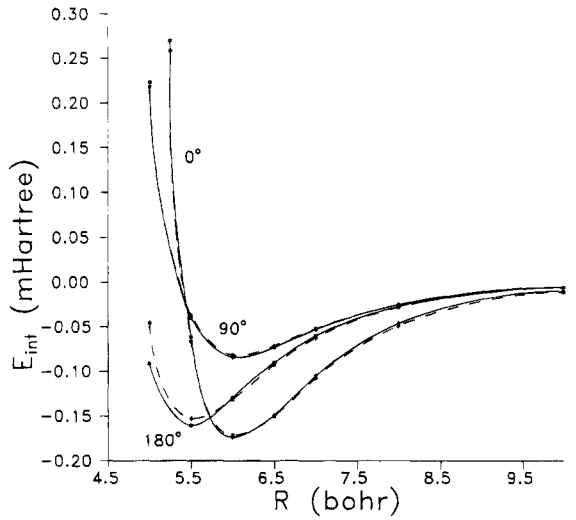

Figure 2. *Ab initio* interaction potential of He–HF computed by SAPT[33] (solid line) and semiempirical potential[128] (dashed line), for $\theta = 0°$, 90°, 180° and $r = 1.7328$ bohr.

levels and of the line widths revealed that the *ab initio* potential[131] does not correctly reproduce the near-infrared spectrum of the complex. Comparison of the experimental results with the *ab initio* predictions suggested that the van der Waals well in this potential is 11% too shallow and that its anisotropic terms are 30% too large in the repulsive region. This is not entirely surprising since the potential developed by Rodwell *et al.* follows the "Hartree–Fock plus dispersion" model[45] and neglects important intramonomer correlation effects. However, by a simple scaling of the long-range dispersion coefficients in this potential Lovejoy and Nesbitt[128] were able to obtain an anisotropic potential surface which reproduced all spectroscopic data available for He–HF.

Recently, Moszynski *et al.*[33] reported a SAPT calculation of the three-dimensional potential energy surface for the He–HF complex. This potential was represented by an expansion in Legendre polynomials $P_L(\cos\theta_B)$. The expansion coefficients $v_L(R,r)$, calculated for different values of the HF bond length r, were fitted by analytic functions of R which represent the various long-range R^{-n} and short-range (exponential) contributions. Further improvement of the important dispersion term was achieved by the computation of high-quality long-range dispersion coefficients at the same level of electron correlation[132–134] in a large *spdfg* basis set. The SAPT potential surface is in very good agreement with the semiempirical potential of Lovejoy and Nesbitt[128] (see Figure 2). In ref 34 the SAPT potential was checked by direct comparison with experiment,[128] after computation of the near-infrared spectrum and line widths. Here, we present a brief summary of the VRT states and spectrum of He–HF, as calculated with the SAPT[33] and semiempirical[128] interaction potentials.

Although the He–HF interaction potential in the region of the van der Waals minimum is only weakly anisotropic, it is most convenient to use the BF coordinates, with the kinetic energy operator given by eq 5 with $T_A = 0$ and $T_B = C(r)j_B^2$. The Legendre expansion of the potential can be directly used in these coordinates and the basis of eq 16, with $j_A = k_A = k_B = 0$ and after parity adaptation, is given by

$$|n,j,K;p,J,M\rangle = \Phi_n(R)\left[\frac{2J+1}{4\pi}\right]^{1/2}[Y^j_K(\hat{\mathbf{r}})D^{(J)}_{M,K}(\alpha,\beta,0)^* + pY^j_{-K}(\hat{\mathbf{r}})D^{(J)}_{M,-K}(\alpha,\beta,0)^*] \quad (41)$$

where $\hat{\mathbf{r}} = (\theta_B,\phi_B)$ and p is the spectroscopic parity. This parity is related to the conventional parity σ under space inversion E^* as $p = \sigma(-1)^J$.[135] The potential matrix elements are given by eq 18, with the $9-j$ symbol substituted as indicated below this equation and the labels k'_A, K_A, k_A and k'_B, K_B, k_B in the $3-j$ symbols equal to zero. The only rigorous quantum numbers are the total angular momentum J, M and the parity p. The HF rotational quantum number j, and the projection K of $\boldsymbol{J}$ (and $\boldsymbol{j}$) onto the body-fixed intermolecular axis, are nearly conserved (coupling case b of ref 16). Functions with different j are mixed by the anisotropic potential, functions with different K only by the off-diagonal Coriolis interactions. States with (approximately) $K = 0, \pm1$, etc. are denoted as Σ, Π, etc. Levels with $p = +1$ and $p = -1$ are designed by the superscripts e and f, respectively. For $K = 0$ only e parity states exist. The splitting of the states with $|K| > 0$ (the so-called l-doubling) into states with e and f parity is caused by the Coriolis interactions.

The allowed dipole transitions between the VRT states of the complex can be deduced from the expressions in section II.E. Also the simplified formulas for atom–diatom systems are indicated in this section, as well as in ref 86. They lead to the following rigorous selection rules

$$J'' = J', \quad p'' = -p', \quad \text{or} \quad J'' = J' \pm 1, \quad p'' = p' \quad (42)$$

Since the quantum number K is nearly conserved, an additional selection rule

$$K'' - K' = 0, \pm1 \quad (43)$$

holds to a good approximation. Thus, the observed bands in the cold He–HF near-infrared spectrum correspond to the transitions from the bound Σ states of He–HF ($v = 0$) to Σ^e, Π^e, and Π^f states of He–HF ($v = 1$). In view of eq 42, two branches (P and R) corresponding to $J'' = J' + 1$ and $J'' = J' - 1$, respectively, are observable for $\Sigma \rightarrow \Sigma^e$ and $\Sigma \rightarrow \Pi^e$ bands, for the $\Sigma \rightarrow \Pi^f$ transitions one should see only one (Q) branch. A schematic diagram of the energy levels and observed near-infrared transitions is depicted in Figure 3.

The only truly bound states in He–HF are those e levels which lie below the $j = 0$ states of the free HF, and since the parity must be conserved, the f levels which lie below the $j = 1$ state of HF. Other states are either so-called "shape" or "orbiting" resonances which dissociate directly by tunneling through the centrifugal barrier, or Feshbach or "compound" resonances[56] which decay via rotational predissociation. The latter mechanism implies that the energy of the rotational excitation to $j = 1$ is converted into translation energy of the dissociating fragments. Of

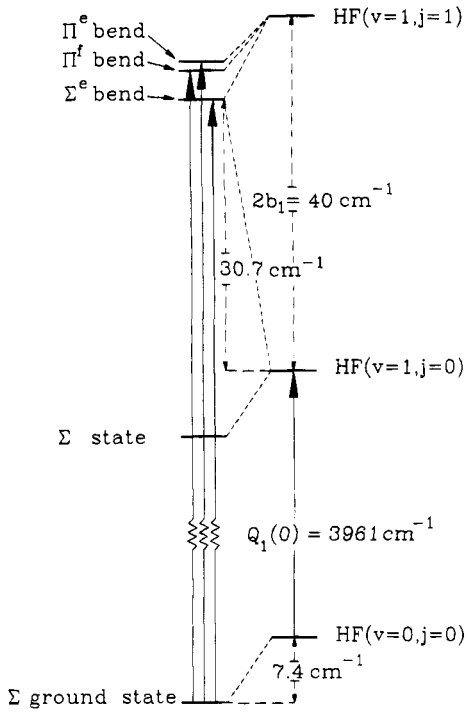

Figure 3. Schematic diagram of the rovibrational levels and nearinfrared transitions in He–HF, according to ref 34. $Q_1(0) = 3961.4229$ cm^{-1} corresponds to the stretch fundamental of HF. The Π^f state is located 33.9 cm^{-1} above the He–HF ($v = 1, j = 0$) threshold, while the l doubling (the splitting of the Π^e and Π^f energy levels) is 0.4 cm^{-1}.

course, all states of He–HF ($v = 1$) may undergo vibrational predissociation, which utilizes the HF vibrational energy to dissociate the He–HF ($v = 1$) complex into He and HF ($v = 0$) fragments. This process was found to be extremely slow,[128] however, and was ignored in ref 34.

By contrast with Ar–H_2, the lifetimes of metastable states of He–HF are not negligible, and the corresponding line broadenings have been measured.[128] In ref 34 the positions and widths of these upper states have been obtained from close-coupling scattering calculations. The resonance parameters can be extracted from the behavior of the S matrix as a function of the energy. In the vicinity of a resonance the energy dependence of the phase shift $\delta_J(E)$ is described by the Breit–Wigner function[56]

$$\delta_J(E) = \delta_J^d(E) + \tan^{-1}\left(\frac{\Gamma_J}{2(E_J - E)}\right) \qquad (44)$$

where $\delta_J^d(E)$ is the contribution from direct scattering and E_J and Γ_J are the position and the width of the resonance. Equation 44 is valid only in the one open channel case. For a generalization to situations with two or more open channels we refer to ref 136. Note that the parameters E_J and Γ_J are assumed to be independent of the energy, *i.e.*, that the isolated narrow resonance approximation[56] is valid. This is expected to hold since the resonances observed for van der Waals molecules are usually narrow and do not overlap with neighboring ones. In practice, the following procedure[136] can be applied to find the position and the width of a resonance. First, the phase shift must be computed as a function of energy

Table 8. Calculated Energy Levels (in cm^{-1}) of the He–HF ($v = 0$) and He–HF ($v = 1$) Complexes

		E_J	
	J	ref 34[a]	ref 128[b]
ground state[c]	0	−7.380	−7.347
	1	−6.608	−6.572
	2	−5.085	−5.043
	3	−2.861	−2.812
	4	−0.040	+0.011
Σ^e bend[d,e]	0	+30.684	+30.725
	1	+31.056	+31.124
	2	+32.013	+32.109
	3	+33.656	+33.776
	4	+35.982	+36.124
	5	+38.915	+39.071
Π^e bend[d,e]	1	+34.298	+34.508
	2	+36.371	+36.565
	3	+39.120	+39.294
Π^f bend[d,f]	1	+33.885	+34.112
	2	+35.364	+35.592
	3	+37.512	+37.736
	4	+40.206[g]	+40.371

[a] Energy levels computed using the *ab initio* SAPT potential (ref 33). [b] Energy levels computed using the empirical potential (ref 128). [c] Energies relative to HF ($v = 0, j = 0$). [d] Energies relative to HF ($v = 1, j = 0$). [e] Resonance states determined from close-coupling scattering calculations. [f] Bound states relative to HF ($v = 1, j = 1$). [g] Obtained from a variational calculation without the $j = 1$ function in the basis.

by solving the close-coupling scattering equations at a closely spaced grid of energies E_i around the location estimated *e.g.* from bound state calculations, subject to standard S-matrix boundary conditions. The position E_J and the width Γ_J can then be obtained by fitting the computed phase shifts $\delta_J(E_i)$ to the Breit–Wigner function.[44] The direct scattering term $\delta_J^d(E)$, which depends very weakly on the energy, may be approximated as a linear or quadratic function of the energy.[136]

In Table 8 we report the results of bound state and close-coupling calculations[34] of the energy levels in He–HF obtained from the *ab initio* potential energy surface.[33] As expected, the He–HF complex is very weakly bound. The potential energy surface for $v = 0$ supports only five bound states: the ground rovibrational state ($J = 0$) and four rotationally excited levels. The energy levels computed[128] from the semiempirical potential are also included in Table 8. The agreement is very good: the energies of bound states agree within 0.05 cm^{-1} or better, the positions of the Σ^e resonances within 0.1 cm^{-1}, and the positions of the Π^e resonances and the energies of the Π^f states within 0.2 cm^{-1}. The theoretical dissociation energy, $D_0 = 7.38$ cm^{-1}, compares very well with the result obtained from the semiempirical potential, $D_0 = 7.35$ cm^{-1}.

The computed transition frequencies[34] corresponding to the experimentally observed[128] $\Sigma \rightarrow \Sigma^e$, $\Sigma \rightarrow \Pi^e$, and $\Sigma \rightarrow \Pi^f$ bands are presented in Table 9. The SAPT potential surface[33] predicts all infrared transitions with errors smaller than 0.1 cm^{-1}. For comparison we also report in Table 9 the transition frequencies computed from the semiempirical potential.[128] In general, the *ab initio* SAPT potential reproduces the experimental data with similar accuracy as the semiempirical potential, which is fitted

Table 9. Near-Infrared Transitions in He–HF (in cm^{-1}) Accompanying the Fundamental Band of HF[a]

			$\Delta E(J'' \rightarrow J')$				
transition	J''	J'	computed (ref 34)[b]	observed (ref 128)[c]	computed (ref 128)[d]	Δ^e	Δ^f
$\Sigma \rightarrow \Sigma^e$	0	1	3999.860	3999.953	3999.894	−0.094	−0.059
	1	2	4000.044	4000.137	4000.104	−0.093	−0.033
	2	3	4000.164	4000.251	4000.242	−0.087	−0.009
	3	4	4000.266	4000.345	4000.359	−0.079	+0.014
	4	5	4000.378	4000.449	4000.483	−0.071	+0.034
$\Sigma \rightarrow \Pi^e$	0	1	4003.102	4003.161	4003.278	−0.059	+0.117
	1	2	4004.402	4004.418	4004.560	−0.016	+0.142
	2	1	4000.806	4000.904	4000.974	−0.098	+0.070
	3	2	4000.655	4000.735	4000.800	−0.080	+0.065
	4	3	4000.583	4000.639	4000.706	−0.056	+0.067
$\Sigma \rightarrow \Pi^f$	1	1	4001.916	4002.005	4002.107	−0.089	+0.102
	2	2	4001.871	4001.952	4002.058	−0.081	+0.106
	3	3	4001.796	4001.859	4001.971	−0.063	+0.112
	4	4	4001.669	4001.680	4001.783	−0.011	+0.103

[a] The frequency corresponding to the HF stretch fundamental is $Q_1(0) = 3961.4229$ cm^{-1}. [b] Computed transitions from the *ab initio* SAPT potential (ref 33). [c] Measured transitions (ref 128). [d] Computed transitions from the empirical potential (ref 128). [e] Absolute error of the transition frequency computed from the *ab initio* potential. [f] Absolute error of the transition frequency computed from the empirical potential.

to these data. Some transition frequencies are predicted even more accurately by the SAPT potential.

For dimers consisting of linear molecules, and in particular for an atom–diatom system (with $L_A = j_A = j'_A = 0$) as we have here, the labels K_A and K_B in the angular expansion of the potential and the labels k_A and k_B in the basis functions are zero. From eq 18 it follows then that the diagonal potential matrix elements vanish for odd values of $L = L_B$. This suggests that the energy levels and transition frequencies are mainly sensitive to the terms with even L in the Legendre expansion of the intermolecular potential. The results reported in Table 9 confirm that these terms in the *ab initio* potential[33] are indeed very accurate. The correctness of the (much smaller) terms with odd L can be checked by computing the widths of resonances which decay via rotational predissociation. Rotational predissociation lifetimes can be defined via the Fermi golden rule expression[137] which, indeed, mixes states with $j = 0$ and $j = 1$ via the $L = 1$ term in the Legendre expansion of the potential. Since Lovejoy and Nesbitt[128] measured the line widths of all $\Sigma \rightarrow \Sigma^e$ and $\Sigma \rightarrow \Pi^e$ transitions in He–HF, a direct comparison of the computed and measured widths serves as a further test of the accuracy of the *ab initio* potential.

In Table 10 we report the widths of the Σ^e and Π^e resonances computed on the *ab initio* potential. The agreement here is less satisfactory: all computed widths are too large by a factor of 2. This suggests that the small $L = 1$ anisotropy in the *ab initio* potential is not correct. To confirm this assumption, the short-range contribution to the $L = 1$ angular component of the potential was scaled by a factor of 0.95 and the widths of the Σ^e and Π^e resonances were recomputed. The results are given in parentheses in Table 10. The agreement with the measured line widths[128] is very good now: almost all widths computed from the scaled potential agree with the experimental data within the error bars. Also the agreement with the widths computed from the semiempirical potential[128] is very satisfactory. It should be noted that this scaling introduces a very small change in the interaction potential (see Figure 4). In the repulsive region the scaled potential is ~4% smaller than the original *ab initio* potential,[33] while the depth of the van der Waals well is only 2% lower. These results clearly show that the widths of

Table 10. Calculated Widths (MHz) of the He–HF Resonance States[a]

		Γ_J		
	J	computed (ref 34)[b]	observed (ref 128)[c]	computed (ref 128)[d]
Σ^e bend	1	7203 (3452)	3020 ± 500	3550
	2	5731 (2673)	2830 ± 200	2730
	3	4453 (2001)	1640 ± 150	1999
	4	3280 (1397)	1260 ± 100	1349
	5	2158 (848)	770 ± 100	780
Π^e bend	1	1080 (575)	530 ± 100	532
	2	1773 (928)	890 ± 150	900
	3	1930 (993)	1000 ± 400	990

[a] The widths corresponding to the scaled potential are given in parentheses. [b] Line widths computed using the *ab initio* SAPT potential (ref 33). [c] Measured line widths (ref 128). [d] Line widths computed using the empirical potential (ref 128).

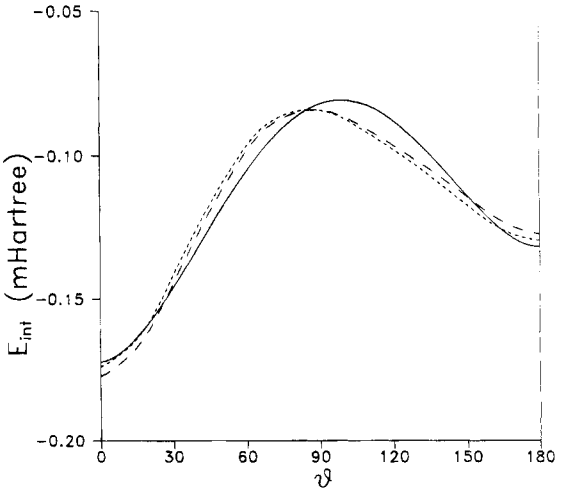

Figure 4. Anisotropies of the *ab initio* (- - -), scaled (———),[34] and semi-empirical (solid line)[128] potentials of He–HF in the region of the van der Waals minimum (R = 6 bohr and r = 1.7328 bohr).

resonances are extremely sensitive to the accuracy of the small odd terms. The quantitative prediction of the rotational predissociation lifetimes is a challenge for *ab initio* calculations.

C. Ar–NH_3 and Ar–H_2O

A considerable amount of high-resolution spectral data is available for both Ar–NH_3[138–146] and Ar–H_2O[43,44,146–150] in the infrared, far-infrared, and microwave regions. Also the isotopomers Ar–D_2O and Ar–HDO have been investigated. *Ab initio* potentials have been calculated for both dimers by the supermolecule MBPT2 method (second-order many-body perturbation theory),[151,152] as well as by an approximate SAPT approach.[153,154] The supermolecule results[151,152] can only be used for comparison with other *ab initio* or semiempirical potentials. They cannot be tested in calculations of the VRT states and spectra, since they did not represent complete potential surfaces, but only some specific cuts. The perturbational approach[153,154] used large (*spdfg*) basis sets and it did produce complete intermolecular potential surfaces. For Ar–NH_3 the NH_3 umbrella angle was varied too. The potential was represented as the sum of electrostatic, first-order exchange, induction, and dispersion interactions. The electrostatic and first-order exchange interaction was defined by the well-known Heitler–London formula (neglecting intramonomer correlation effects), while the second-order induction and dispersion interactions were calculated as damped multipole expansions. Tang–Toennies-type[46] damping functions were used to correct the second-order interactions for overlap effects; the damping parameters in these functions were derived from the exponential fits of the first-order exchange repulsion in the Heitler–London energy. The permanent multipole moments of the monomers were obtained from SCF calculations, while their static- and frequency-dependent polarizabilities were computed by the time-dependent coupled Hartree–Fock (TDCHF) method, followed by second-order many-body perturbation theory (MBPT) to account for the effects of (true) electron correlation.[155] Alternative calculations[156] were performed for Ar–H_2O by the "Hartree–Fock plus damped dispersion" approach, with the same basis. The resulting potential differed only slightly from the perturbational result. The calculations were performed on a Gauss–Legendre quadrature grid[37] of angles θ_B and Gauss–Chebyshev grid of angles ψ_B, so that the anisotropy of the potential could be expanded in spherical harmonics, *cf.* eq 10, and the coefficients $v_{L_BK_B}(R)$ in the expansion could be directly obtained by numerical integration, *cf.* eq 11. Analytic fits were made of the short-range (exponential) contributions to these coefficients. The different long-range R^{-n} terms were given automatically in the spherical expansion.[35] The results for Ar–NH_3 are shown in Figure 5.

In the paper on Ar–H_2O[154] it was shown how to transform the anisotropic potential to Ar–D_2O, *i.e.* how to correct for the shift of the monomer center of mass. The long-range contributions can be transformed analytically, a numerical transformation procedure was described for the short-range terms. If also the principal inertia axes of a monomer are

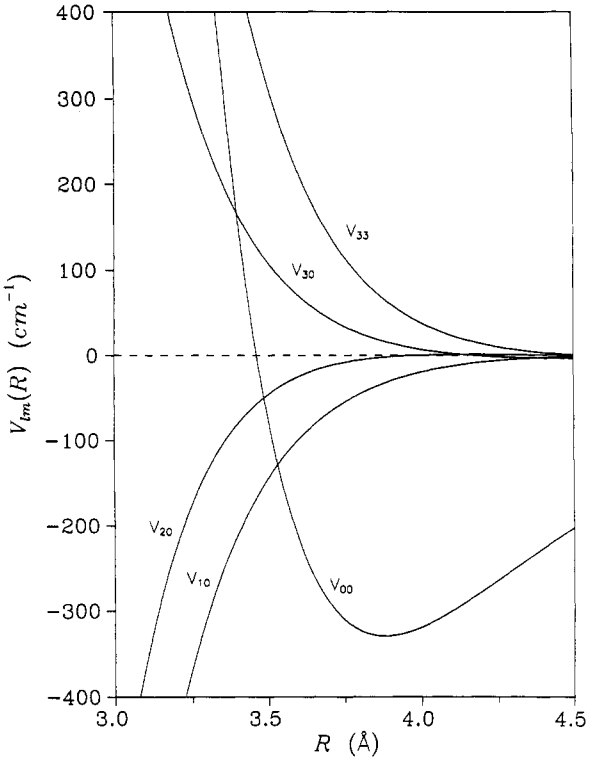

Figure 5. Coefficients $v_{lm}(R)$ in the expansion (without the scaling in $v_{3,3}$) of the *ab initio* Ar–NH_3 interaction potential[153] in functions $S_{lm}(\theta,\psi)$. These functions are normalized real combinations of spherical harmonics $Y^l_m(\theta,\psi)$, which differ from the angular functions in eq 10 only by normalization.

rotated by isotope substitution, as in Ar–HDO, it is possible to transform the potential by the use of the well-known rotation properties of spherical harmonics.[36] Or, alternatively, one may retain the off-diagonal components of the inertia tensor in the kinetic energy expression.

The calculation of the VRT states and spectra for Ar–NH_3 from the *ab initio* potential[153] was described in refs 7–9. Similar calculations were performed for Ar–H_2O, Ar–D_2O, and Ar–HDO.[158] It was most convenient to use the BF coordinates with the kinetic energy expressed as in eq 5 with $T_A = 0$, the potential expanded as in eq 10 and the basis of eq 16 with $j_A = m_A = k_A = 0$. The inclusion of the monomer umbrella angle $0 \le \varrho \le \pi$ as a dynamical variable in Ar–NH_3 can be based on the existing theory for NH_3.[3] The principal moments of inertia, which are the inverse of the rotational constants (times $\hbar^2/2$) in the kinetic energy T_B of the NH_3 monomer are given by

$$I_{xx}(\varrho) = I_{yy}(\varrho) = 3m_H r_0^2(^1/_2\sin^2\varrho + \zeta\cos^2\varrho)$$

$$I_{zz}(\varrho) = 3m_H r_0^2 \sin^2\varrho \qquad (45)$$

where m_H and m_N are the masses of hydrogen and nitrogen, $\zeta = m_N/(3m_H + m_N)$, and r_0 is the (fixed) N–H bond length. The kinetic energy associated with the curvilinear umbrella motion is given by the Podolsky[14] expression

$$T_{\text{umb}}(\varrho) = -\frac{1}{2}\hbar^2 g(\varrho)^{-1/2}\frac{\partial}{\partial\varrho}I_{\varrho\varrho}(\varrho)^{-1}g(\varrho)^{1/2}\frac{\partial}{\partial\varrho} \qquad (46)$$

with

$$I_{\varrho\varrho}(\varrho) = 3m_H r_0^2(\cos^2 \varrho + \zeta \sin^2 \varrho) \quad (47)$$

and, since the $\mathbb{G}(= \mathbb{I})$ tensor is diagonal (there is no Coriolis coupling, because the 3-fold symmetry is conserved[159])

$$g(\varrho) = I_{xx}I_{yy}I_{zz}I_{\varrho\varrho} \quad (48)$$

Also the well-known[3] double-well potential $V_{\text{umb}}(\varrho)$ for the umbrella motion in the NH_3 monomer has to be included in the Hamiltonian, and the expansion coefficients $v_{L_BK_B}(R)$ of the intermolecular potential become dependent on ϱ. A convenient numerical basis or contracted basis of analytic functions $\sin(m\varrho)$ can be obtained by first diagonalizing the monomer Hamiltonian $H_{\text{umb}}(\varrho) = T_{\text{umb}}(\varrho) + V_{\text{umb}}(\varrho)$. The ν_2 vibrational ground state $0^{\pm}$ is split by 23.8 GHz = 0.793 cm^{-1} by tunneling through the NH_3 inversion barrier,[160] and the first excited $1^{\pm}$ state splits by 35.8 cm^{-1}. Since the ν_2 fundamental frequency is about 950 cm^{-1}, the inclusion of other than the $0^{\pm}$ basis functions in the calculation of the VRT states has very little effect.[9] In the calculation of the mid-infrared spectrum[140,143] of Ar–NH_3, which corresponds to excitation of the ν_2 mode, the $1^{\pm}$ functions must be taken into account. Note, incidentally, that the simple basis functions $\sin(m\varrho)$ are not orthogonal, since the volume element is $g(\varrho)^{1/2}\, d\varrho$.

The consideration of permutation inversion symmetry is important in these dimers. For Ar–H_2O the feasible symmetry operations are (12), the interchange of the two protons, and space inversion, E^*. The PI group is isomorphic with the point group C_{2v} and it may be designated as $PI(C_{2v})$. The VRT states of Ar–H_2O with A_1 and A_2 symmetry correspond to p-H_2O, states with B_1 and B_2 symmetry to o-H_2O. Transitions within each dimer species are observed in the spectrum in the weight ratio *para:ortho* = 1:3. Since deuterons are bosons, while protons are fermions, the *ortho–para* classification of the VRT states is reversed in Ar–D_2O; the weight ratio is *ortho:para* = 6:3. For Ar–NH_3 the symmetry group is $PI(C_{3v})$ if the NH_3 umbrella is considered to be frozen and $PI(D_{3h})$ if the umbrella inversion is included; see Appendix C. VRT states with A'_1 and A''_1 symmetry are Pauli–forbidden; states with A'_2 and A''_2 symmetry correspond to o-NH_3 and states with E' and E'' symmetry to p-NH_3. The observed spectra are superpositions in the ratio *ortho:para* = 4:2.

In Figures 6 and 7 we illustrate how the rotor states of NH_3, with energies $Aj(j + 1) + (C - A)k^2$, which are $(2j + 1)$-fold degenerate in the free monomer, are split by the anisotropic potential in Ar–NH_3. We observe that the terms with $(L_B,K_B) = (1,0)$ and (3,3) are the dominant anisotropic interaction terms. States with different j and k are mixed by these interactions, but the symmetry restrictions tell us that the *ortho* states with $k = 0$ (mod 3) must remain separate from the *para* states with $k = \pm 1$ (mod 3). It is typical for a van der Waals complex that the states with different *ortho/para* symmetry display a completely different VRT level scheme, although they feel the same interaction potential. For normal, nearly rigid molecules such differences are usually not visible in vibrational spectra, only in rotational

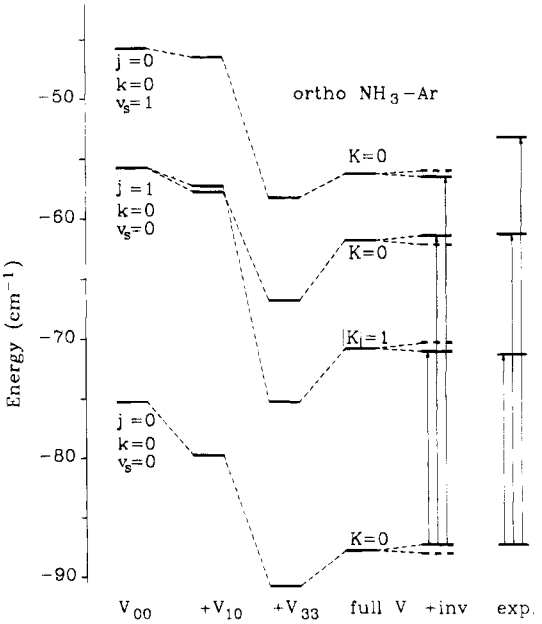

Figure 6. Calculated and experimental VRT levels (band origins) of o-Ar–NH_3. The leftmost column is obtained from the isotropic potential $v_{0,0}(R)$; j and k are exact quantum numbers at this level, v_s is the R stretch quantum number. The second column shows the effect of the $v_{1,0}(R)$ term; the third column, the cumulative effect of the (scaled) $v_{3,3}(R)$ term; the fourth column, the effect of the remaining anisotropic interactions. The quantum number $|K|$ is approximate. The fifth column includes the inversion–tunneling splittings, and the last column contains the experimental frequencies from refs 141, 142, 144, and 146. The dashed levels in the inversion doublets are Pauli forbidden. The arrows indicate the calculated and measured transitions, with the ground level adjusted.

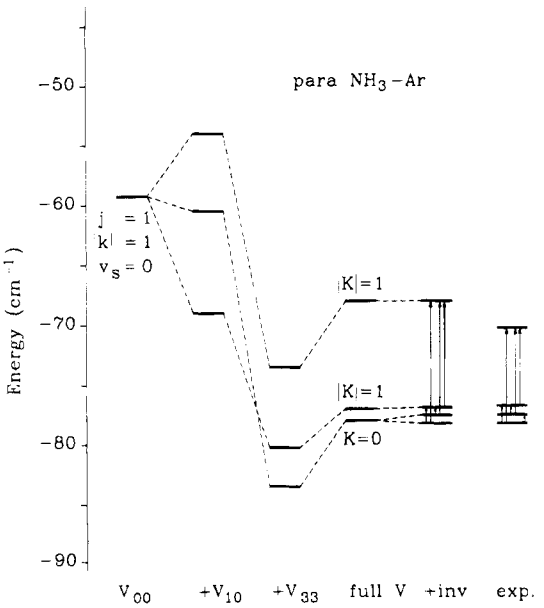

Figure 7. Calculated and experimental VRT levels of p-Ar–NH_3. See the caption of Figure 6 for the explanation. The inversion splitting of the $|K| = 1$ levels is so small that it is not visible here.

ones. We also observe in these figures that the K label in the BF basis (*i.e.* the projection of $\boldsymbol{j}$ and $\boldsymbol{J}$ on the dimer axis) remains a nearly good quantum number. Although this is formally justified only for atom–linear molecule dimers, states with $K = 0$ are

often called Σ states, and states with $|K| = 1$ are Π states. The Σ states in Ar−NH_3 are split by the NH_3 inversion tunneling by almost the same amount as in free NH_3. The Π states are split only by minute amounts; if they were not mixed with the Σ states through the weak Coriolis coupling they would not split at all. This can be understood from the model in ref 8, which treats the effect of the NH_3 umbrella inversion as a (first-order) perturbation on the VRT states.

The VRT levels in Ar−NH_3 have been calculated for $J = 0, 1, ..., 15$ and, with the aid of the theory in section II.E, also the intensities of all the allowed transitions from the ground state in the *ortho* and *para* species have been computed.[8] The applied dipole surface contains the permanent dipole of NH_3 and the dipole induced on Ar by the NH_3 permanent dipole and quadrupole, *cf.* eq 40 and Table 2. The induced dipole contributes only about 10% to the intensities, however. Also the ^{14}N nuclear quadrupole splittings have been computed for the different VRT states. Some generated spectra[8] are shown in Figure 8, parts A−C. The intensity ratios between the *P*, *Q*, and *R* branches in Figure 8, parts A and B, are mostly determined by the Hönl−London factors,[157] but in Figure 8C they show a typical deviation from these factors. This was found in the experiment[142] also. It turned out, however, that the frequencies of the bands resulting from the *ab initio* potential[153] deviate rather strongly from the measured frequencies.[138−146] The van der Waals stretch frequency which probes the *R* dependence of (mainly) the isotropic potential was quite realistic, but the "bending" frequencies which correspond to the level splittings by the anisotropic potential, *cf.* Figures 6 and 7, were completely wrong. Even the order of these hindered rotor levels was incorrect. A simple scaling by a factor of 1.43 of the short-range contribution to the anisotropic expansion coefficient $v_{3,3}(R)$ produced nearly correct splittings; see Figures 6 and 7. Also the calculated intensities (which could only be measured rather crudely[142]) and quadrupole splittings agree well with experiment then.

Something similar was experienced for Ar−H_2O and Ar−D_2O: the order of the hindered rotor levels from the *ab initio* potential[154] was incorrect.[158] Here, it was not so easy to obtain the correct splittings, however, since many different anisotropic terms in the potential appeared to contribute to these splittings. Several anisotropic coefficients $v_{L_BK_B}(R)$ change sign, just in the range of *R* where they are probed, *i.e.* in the well of the isotropic potential $v_{0,0}(R)$. We may conclude that, indeed, the spectra probe the anisotropy of the potential surface very sensitively. The accurate *ab initio* prediction of this anisotropy, especially for Ar−H_2O, is a great challenge. Neither the supermolecule MBPT2 method,[151,152] nor the approximate SAPT,[153,154] nor the "Hartree−Fock plus damped dispersion" model[156] can meet this challenge. We have seen in sections III.A and III.B, however, that considerably more accurate *ab initio* potentials are now becoming available for atom−diatom systems, both from a more rigorous version of SAPT[31,33] and from supermolecule MBPT4 calculations.[161] It will not take much longer before we will see full *ab initio* potentials of similar accuracy for atom−polyatom systems such as Ar−H_2O and Ar−NH_3.

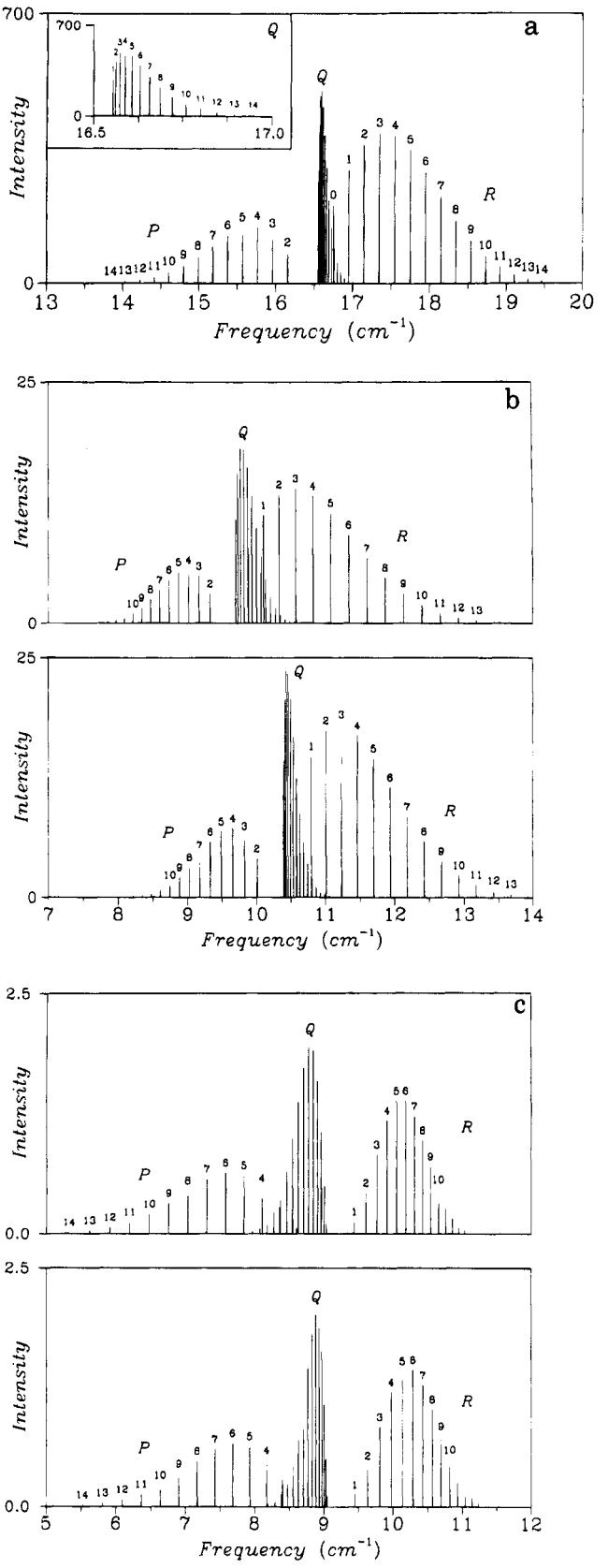

Figure 8. Rovibrational spectra calculated for (A) the lowest Σ → Π transition in *o*-Ar−NH_3 and (B) the lowest Σ → Π and (C) Π → Π transitions in *p*-Ar−NH_3 from ref 8. Intensities in 10^{10} m^2 s^{-1} mol^{-1}; temperature 5 K. The two windows in the last two figures contain the spectra for the allowed $E' \leftrightarrow E''$ transitions between inversion doublets.

Table 11. State-to-State Cross Sections $\sigma(0_0^+ \rightarrow j_k^\epsilon)$ for *o*-Ar–NH_3 (in Å^2) at a Collision Energy of 280 cm^{-1} [a]

j_k^ϵ	scaled *ab initio* potential (ref 8)	experiment	semi-empirical potential (ref 145)	experiment
1_0^+	9.14 (5.83)	4.51	10.21 (5.94)	5.55
2_0^+	9.65 (9.63)	5.01	4.59 (5.28)	6.16
3_0^+	3.21 (3.26)	1.63	2.14 (2.05)	2.01
4_0^+	0.33 (0.47)	0.36	0.13 (0.19)	0.44
3_3^+	1.18 (1.67)	2.56	0.22 (1.06)	3.15
3_3^-	6.78 (6.50)	9.10	13.79 (13.24)	11.19
4_3^-	0.80 (0.81)	4.29	7.19 (6.75)	5.28
4_3^+	0.17 (0.26)	0.97	0.09 (0.46)	1.19
5_3^+	0.08 (0.09)		0.04 (0.06)	
5_3^-	0.10 (0.14)		0.30 (0.29)	
Q [b]	54%		23%	

[a] The values given in parentheses are corrected for the imperfect initial state preparation; the 0_0^+ ground state is contaminated with 8% of the 1_0^+ state. Since the measurement provides only relative cross sections, the sum of the experimental values has been "normalized" to the sum of the corresponding calculated values. The error is defined as $Q = [\sum_i(\sigma_{\mathrm{calc},i} - \sigma_{\mathrm{exper},i})^2/\sum_i\sigma^2_{\mathrm{exper},i}]^{1/2}$, where the values of σ_{calc} are those given in parentheses. [b] For a collision energy of 485 cm^{-1} the error is 55% for the scaled *ab initio* potential and 31% for the semiempirical potential.

Table 12. State-to-State Cross Sections $\sigma(1_1^- \rightarrow j_k^\epsilon)$ for *p*-Ar–NH_3 (in Å^2) at a Collision Energy of 280 cm^{-1} [a]

j_k^ϵ	scaled *ab initio* potential (ref 8)	experiment	semiempirical potential (ref 145)	experiment
2_1^-	4.71 (4.83)	4.51	8.13 (7.95)	5.14
2_1^+	7.02 (6.91)	6.06	4.47 (4.65)	6.91
3_1^+	1.82 (1.84)	0.85	1.69 (1.64)	0.97
3_1^-	2.19 (2.17)	1.30	0.76 (0.80)	1.48
4_1^-	0.63 (0.60)		0.30 (0.29)	
4_1^+	0.09 (0.12)		0.01 (0.03)	
2_2^-	0.96 (1.51)	1.14	0.07 (0.71)	1.30
2_2^+	11.97 (11.42)	12.40	12.88 (12.24)	14.13
3_2^+	3.01 (2.96)	3.10	7.22 (6.91)	3.53
3_2^-	2.03 (2.08)	2.45	1.12 (1.43)	2.79
4_2^-	0.60 (0.58)	0.93	0.78 (0.77)	1.06
4_2^+	0.35 (0.36)		0.69 (0.69)	
5_2^+	0.12 (0.11)		0.04 (0.04)	
5_2^-	0.01 (0.02)		0.04 (0.04)	
4_4^-	0.74 (0.75)	0.77	1.08 (1.14)	0.88
4_4^+	0.91 (0.90)	2.33	2.24 (2.18)	2.66
5_4^+	0.33 (0.32)	0.43	0.96 (0.92)	0.49
5_4^-	0.10 (0.11)		0.07 (0.12)	
5_5^+	0.20 (0.20)		0.08 (0.10)	
5_5^-	0.21 (0.21)		0.56 (0.53)	
Q [b]	16%		32%	

[a] The values given in parentheses are corrected for the imperfect initial state preparation; the 1_1^- state is contaminated with 5% of the 1_1^+ state. The normalization of the experimental values and the error Q are defined in Table 11. [b] For a collision energy of 485 cm^{-1} the error is 36% for the scaled *ab initio* potential and 19% for the semiempirical potential.

Rather soon after the measurement of the high-resolution spectra, one tried to extract intermolecular potentials directly from these spectra. At first, this was restricted to an effective angular potential surface (see refs 150 and 162 for Ar–H_2O and refs 142 and 144 for Ar–NH_3) which yields information about the anisotropy of the potential, without specifying at which (in fact, variable) value of R this anisotropy was probed. Cohen and Saykally[43] were the first to obtain a full three-dimensional intermolecular surface for Ar–H_2O. This surface was improved[44] when more spectral data became available. A similar semiempirical potential surface was recently constructed[145] for Ar–NH_3. The potentials used are of the form of eqs 13 and 14; the long-range coefficients C_n were partly fixed at the *ab initio* values,[133,153,154] and typically, about 10 nonlinear parameters were varied. The VRT levels were calculated by the collocation method (see section II.D) and the parameters were optimized by a nonlinear least-squares fit to the observed transition frequencies.

For Ar–NH_3 a very effective, independent test of the accuracy of the intermolecular potential was applied. A state-selected crossed-beam experiment[163] has provided the cross sections for the inelastic collisions in which the rotational (j,k) and the umbrella inversion $\epsilon = \pm$ states of NH_3 are changed by the anisotropic interaction with the Ar atoms. These scattering cross sections $\sigma(j_k^\epsilon \rightarrow j'^{\epsilon'}_{k'})$ could be calculated in a full close-coupling calculation.[164] Both the experiments and the scattering calculations were performed for *o*- and *p*-NH_3, at two different collision energies (280 and 485 cm^{-1}). The results obtained from the scaled *ab initio* potential[8] and from the semiempirical potential of Schmuttenmaer *et al.*[145] are given in Tables 11 and 12, for *o*- and *p*-NH_3. We observe that the scaled *ab initio* potential, as well as the semiempirical potential yield very realistic values of the inelastic scattering cross sections. Without the scaling of the anisotropic $v_{3,3}(R)$ term, the cross sections from the *ab initio* potential were considerably worse. Especially in the case of the semiempirical potential obtained from the spectra, the agreement with the measured scattering cross sections begins to approach the (estimated) experimental accuracy. Hence, we are justified to believe that the semiempirical potential for Ar–NH_3[145] and also the one for Ar–H_2O,[44] are rather accurate.

D. Ar–Benzene

Although the VRT states of Ar–benzene and Ar–tetrazine have been calculated[51] by the same approach as described for Ar–H_2O and Ar–NH_3 in the preceding section, this approach proved to be rather inefficient. The expansion of the (empirical) intermolecular potential in spherical harmonics required very high values of L (up to 36) and the angular basis had to contain Wigner D functions with values of j up to 27. A different embedding of the BF frame (in the molecule rather than along the intermolecular axis, see Appendix A.3) and a different choice of coordinates (the Cartesian components of the vector $\vec{R}$, rather than the polar coordinates R,θ,ϕ) have been proposed.[23] The kinetic energy for these coordinates is given by eqs 6 and 19. This approach can be easily applied to even larger atom–aromatic molecule dimers, such as Ar–fluorene[23] and Ar–naphthalene.[52] Different basis sets, harmonic oscillator functions,[23,24] distributed Gaussians,[165] and discrete variable representations (DVR),[52] have been implemented

Table 13. van der Waals Vibrational Energies and Properties of Ar−C_6H_6 Calculated with the "Global" Fit of the *ab initio* Potential (ref 175) for $J = 0$[a]

$PI(C_{6v})$ irrep	band origin (cm^{-1})	$\langle z \rangle$ (Å)	Δx (Å)		Δy (Å)	Δz (Å)	$\langle l_z \rangle$ ($\hbar$)	mode[d] character
A_1	0.00[b]	3.608	0.348		0.348	0.121	0.0	ground state
E_1	25.52	3.622	0.364	↔	0.631[c]	0.123	±0.999997	b^1
A_1	37.51	3.655	0.515		0.515	0.179	0.0	s^1(43% b^2)
E_2	49.12	3.632	0.662	↔	0.659[c]	0.126	±1.999936	b^2
A_1	54.89	3.660	0.564		0.564	0.173	0.0	b^2(48% s)
E_1	58.27	3.654	0.493	↔	0.855[c]	0.168	±0.999945	s^1b^1
B_1	70.72	3.637	0.799		0.799	0.130	0.0	b^3
B_2	71.08	3.638	0.794		0.794	0.129	0.0	b^3
A_1	71.20	3.686	0.687		0.687	0.212	0.0	s^2(57% b^2)

[a] Equilibrium distance $R_e = 3.560$ Å, well depth $D_e = 393.44$ cm^{-1}. The root mean square displacements are defined as $\Delta x = [\langle x^2 \rangle - \langle x \rangle^2]^{1/2}$, etc. [b] $D_0 = 342.47$ cm^{-1}. [c] These numbers are interchanged for the other substate in the degenerate pair. [d] s^{n_s} and b^{n_b} indicate the excitation level in stretch and bend, as determined from the eigenvectors.

in computer programs. Other dimers for which experimental spectra needed interpretation, such as Ar−aniline,[166] Ar−styrene and Ar−4-fluorostyrene,[167] and Ar−2,3-dimethylnaphthalene[168] have been studied too, but we will further concentrate on the prototype system Ar−benzene.

The UV spectrum of Ar−benzene has been recorded in such high resolution[169−171] that the rotational structure in this spectrum could be well resolved. It corresponds to the excitation of the benzene monomer to its lowest excited electronic singlet S_1 state. The pure $S_0 \rightarrow S_1$ transition is dipole forbidden, however. The (strong) transition which is actually observed is the vibronic 6_0^1 transition from the ground S_0 state to the S_1 state with the ν_6 vibration excited simultaneously. For Ar−benzene, formed in a cold molecular beam, three different van der Waals transitions were observed, in combination with the 6_0^1 transition. Two of these bands, at relative frequencies of 40.1 and 62.9 cm^{-1}, had essentially the same rotational structure as the pure 6_0^1 transition. So, the excited VRT states should have A_1 symmetry, just as the ground state, and these transitions were assigned[170] to the R stretch fundamental, s^1, and overtone, s^2. This implies a very strong anharmonicity. The third band, at 31.2 cm^{-1}, has a different rotational structure and was tentatively assigned to the bending overtone b^2, which has components of A_1 and E_2 symmetry. The observed rotational structure of this band could not be understood, though. Further information is available from the microwave spectrum,[172] which yields the ground state rotational constants, and from stimulated Raman scattering[173] which shows an unresolved band at about 33 cm^{-1}. It followed from the experimental setup that this band corresponds to the same transition, in the S_0 ground state, as the transition at 31.2 cm^{-1} in the excited 6^1 state.

An *ab initio* potential surface for Ar−benzene was available from supermolecule MBPT2 calculations.[174] Another unsolved problem was that the well depth in this potential was 429 cm^{-1}, while the anharmonicity in the assigned s^1 and s^2 frequencies would not allow a well depth greater than about 150 cm^{-1}. Two different analytic representations were made of this *ab initio* potential.[175] The first is a "global" fit by an atom−atom potential of generalized Lennard-Jones type

$$V(\boldsymbol{R}) = \sum_{i=1}^{6}\left[\left(\frac{C_1}{r_{\mathrm{ArC}_i}}\right)^N - \left(\frac{C_2}{r_{\mathrm{ArC}_i}}\right)^6\right] + \sum_{i=1}^{6}\left[\left(\frac{C_3}{r_{\mathrm{ArH}_i}}\right)^N - \left(\frac{C_4}{r_{\mathrm{ArH}_i}}\right)^6\left(1 - \frac{C_5}{r_{\mathrm{ArH}_i}}\right)\right] \quad (49)$$

the second is an expansion in displacements d_x, d_y, d_z about the minimum at $\boldsymbol{R}_e = (x_e,y_e,z_e) = (0,0,R_e)$

$$V(\boldsymbol{d}) = k_{xx}(d_x^2 + d_y^2) + k_{zz}w^2 + k_{xxz}w(d_x^2 + d_y^2) - D_e \quad (50)$$

with a "Morse-type" scaling applied to the z coordinate: $w = 1 - \exp(-ad_z)$. Given these *ab initio* potentials and the unsolved questions regarding the interpretation of the experimental high-resolution spectrum, it was worthwhile to undertake a calculation of the VRT states of Ar−benzene and to study the symmetry-allowed transitions. Such calculations were made by Bludsky *et al.*,[175] by van der Avoird,[24] and by Faeder.[165] Different numerical and analytic bases were used, and the results of Faeder agree very well with those of van der Avoird. The results of Bludsky *et al.* are different, however, although they used the same potential and kinetic energy expression. The energies and some characteristics of the VRT states are listed in Tables 13 and 14. The two different analytic fits of the same *ab initio* potential produce somewhat different results. Especially those from the "Morse-type" expansion agree well with the experimental frequencies, if one makes the assignment[24] that the band observed at 40.1 cm^{-1} indeed corresponds to the A_1 stretch fundamental s^1, but that the band at 62.9 cm^{-1} corresponds to the A_1 component of the bending overtone b^2 and the band at 31.2 cm^{-1} to the bending fundamental b^1 of E_1 symmetry. Although the s^1 and b^2 frequencies are rather different, there is strong mixing (Fermi resonance) between these modes; see also Figures 9 and 10. It must be noted here that the calculations were performed on the ground state potential, whereas the experimental spectra probe the intermolecular potential of the vibronically excited 6^1 state. It can be inferred from the observed rotational constants and from the relatively small red shift of the 6_0^1 band in Ar−benzene (with respect to the benzene monomer) that the intermolecular potential is not strongly altered upon 6_0^1 excitation.

Table 14. van der Waals Vibrational Energies and Properties of Ar–C_6H_6 Calculated with the "Morse-type" Fit of the *ab Initio* Potential (ref 175) for $J = 0$ (Equilibrium Distance $R_e = 3.553$ Å; Well Depth $D_e = 425.00$ cm^{-1})

$PI(C_{6v})$ irrep	band origin (cm^{-1})	$\langle z \rangle$ (Å)	Δx (Å)		Δy (Å)	Δz (Å)	$\langle l_z \rangle$ ($\hbar$)	mode[c] character
A_1	0.00[a]	3.594	0.320		0.320	0.121	0.0	ground state
E_1	30.17	3.605	0.321	↔	0.557[b]	0.123	±1.0	b^1
A_1	41.03	3.651	0.385		0.385	0.197	0.0	s^1 (18% b^2)
E_2	60.35	3.617	0.560	↔	0.560[b]	0.125	±2.0	b^2
A_1	64.39	3.627	0.519		0.519	0.147	0.0	b^2 (22% s)
E_1	68.45	3.660	0.370	↔	0.642[b]	0.194	±1.0	s^1b^1
A_1	79.35	3.710	0.451		0.451	0.254	0.0	s^2 (21% b^2)
B_1	90.50	3.629	0.651		0.651	0.127	0.0	b^3
B_2	90.50	3.629	0.651		0.651	0.127	0.0	b^3

[a] $D_0 = 371.48$ cm^{-1}. [b] These numbers are interchanged for the other substate in the degenerate pair. [c] s^{n_s} and b^{n_b} indicate the excitation level in stretch and bend, as determined from the eigenvectors.

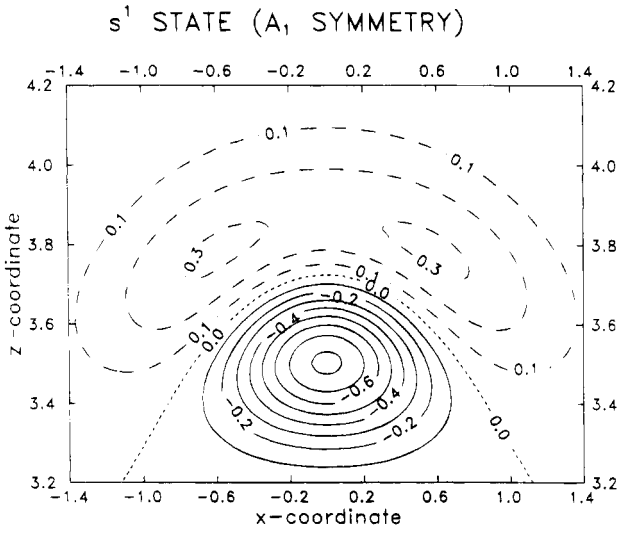

Figure 9. Fundamental stretch excited wave function of Ar–benzene calculated[24] from the "global" fit of the *ab initio* potential[175] for $J = 0$ (coordinates in Å). Observe that the nodal plane is not horizontal, because of the Fermi resonance with the wave function in Figure 10.

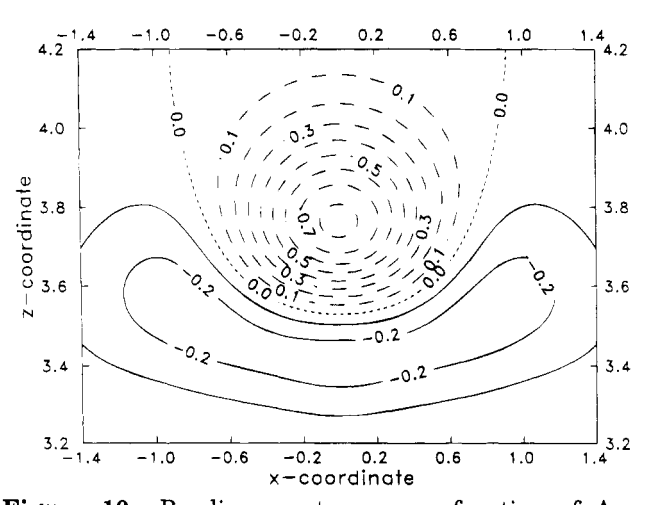

Figure 10. Bending overtone wave function of Ar–benzene calculated[24] from the "global" fit of the *ab initio* potential[175] for $J = 0$ (coordinates in Å).

For an analysis of the experimental spectrum it is very important to use the symmetry and to include the vibronic 6_0^1 excitation in the selection rules. The symmetry group of the nearly rigid benzene monomer is isomorphic to the point group D_{6h}. If the Ar atom would be delocalized to both sides of this planar molecule, the PI group of Ar–benzene would also be $PI(D_{6h})$. Since it appears to be localized on one side, with no observable tunneling to the other side, the feasible symmetry group is $PI(C_{6v})$. The symmetry of the VRT states for $J = 0$ is indicated already in Tables 13 and 14. It can easily be derived if one realizes that the relative motions of the Ar atom are nearly isotropic in x and y (the first anisotropic terms are of order 6). The states of a two-dimensional isotropic (harmonic) oscillator can be characterized by the label l, which is the eigenvalue of the vibrational angular momentum operator l_z. As we observe in Tables 13 and 14, this vibrational angular momentum is nearly unquenched in Ar–benzene, and the symmetry of the VRT states follows directly from Table 15. Also the symmetry of the rotational wave functions is given in this table. One should realize that Ar–benzene is a prolate symmetric top, with the quantum number K broken only by weak Coriolis coupling. Further, it is important to observe that the vibronically excited 6^1 state has E_1 symmetry, while the ground S_0 state has A_1 symmetry, of course. The dipole moment operator has A_2 symmetry, when expressed with respect to the SF frame (it is invariant under all permutations and antisymmetric under space inversion). With the use of eq 38 it can be expressed with respect to the BF frame. Its "internal" components have A_1 symmetry (the parallel component with $k = 0$) and E_1 symmetry (the perpendicular components with $k = \pm 1$) and the corresponding rotation functions (the Wigner D functions) have A_2 and E_1 symmetry, respectively.

All the appropriate selection rules can be derived then, and it follows that the assigned transitions are indeed allowed. Still, it was expected that the transition to the b^1 state of E_1 symmetry would be extremely weak, since it is forbidden by the Frank–Condon principle (ref 176, p 149). This principle is based on the assumption that the electronic transition dipole moment does not depend on the nuclear displacements and, hence, that simultaneous vibrational excitations are allowed only when the excited vibrational state has A_1 symmetry. We shall return to this point below. First, we note that it was possible to explain the complete rotational structure of the band at 31.2 cm^{-1} based on the assignment of ref 24. Apart from the selection rules, one has to take into account that the VRT levels are split by first and higher order Coriolis coupling between the vibronic angular momentum of the monomer 6^1 state (remember that this state is degenerate with E_1 symmetry),

Table 15. Symmetry-Adapted Rotational and Vibrational States of Ar–Benzene

$PI(C_{6v})$ irrep	statistical weight[a]	rotor state	K (mod 6)	vibrational state $\|n_s,n_b,l\rangle$	l (mod 6)
A_1	10	$\|J,K,M\rangle + (-)^J\|J,-K,M\rangle$	0	$\|l\rangle + \|-l\rangle$	0
A_2	10	$\|J,K,M\rangle - (-)^J\|J,-K,M\rangle$	0	$\|l\rangle - \|-l\rangle$	0
E_1	22	$\|J,K,M\rangle$	±1	$\|l\rangle$	±1
E_2	18	$\|J,K,M\rangle$	±2	$\|l\rangle$	±2
B_1	14	$\|J,K,M\rangle - (-)^J\|J,-K,M\rangle$	3	$\|l\rangle + \|-l\rangle$	3
B_2	14	$\|J,K,M\rangle + (-)^J\|J,-K,M\rangle$	3	$\|l\rangle - \|-l\rangle$	3

[a] For the complete rovibrational states.

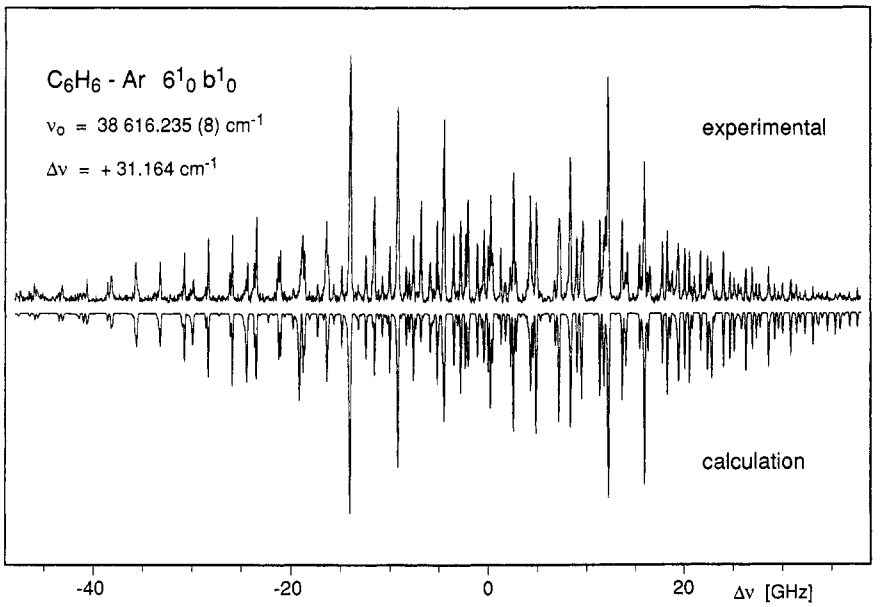

Figure 11. Measured[170] and calculated[177] rotational structure of the Ar–benzene band at (relative) frequency 31.2 cm^{-1}, assigned[24] to the bending fundamental. The ground-state rotational constants $A'' = 0.0948\ 809\ cm^{-1}$ and $B'' = 0.0394\ 025\ 76\ cm^{-1}$ were taken from microwave measurements,[172] and the b^1 excited state rotational constants $A' = 0.091\ 583\ cm^{-1}$, $B' = 0.039\ 222\ cm^{-1}$, and the Coriolis splitting constant $\zeta' = 0.7987$ were fitted to the experimental spectrum, with the *ab initio* value $\zeta' = 0.797$[24] taken as starting value.

the vibrational angular momentum of the b^1 state of E_1 symmetry and the overall rotations (labeled by J,K,M). Calculations of the VRT states have recently been performed[177] for different J, in which the coupling to the vibronic angular momentum of the benzene 6^1 state was explicitly included. The perfect agreement with the observed rotational structure of the band at 31.2 cm^{-1} (see Figure 11) confirms without doubt that the assignment of this band to the (parallel) $6^1_0b^1$ transition must be correct. The fact that this band, in spite of the Frank–Condon principle, has an appreciable intensity, shows that the vibronic 6^1_0 transition dipole moment in benzene is influenced rather strongly by the interaction with the Ar atom. More generally, it might be learned from this conclusion that the applicability of such principles, which are usually based on the experience with "normal" nearly rigid molecules, must be reconsidered in van der Waals molecules with their large amplitude motions.

Additional calculations were performed[177] for the fully deuterated species Ar–C_6D_6. These calculations reproduce the observed isotope shifts in the van der Waals frequencies.[170] The observed change in the relative intensities of the s^1 and b^2 bands can be understood from the calculated change in the extent of Fermi resonance between these modes. Note that the b^2 overtone steals intensity from the s^1 fundamental through this resonance. This is a further confirmation of the assignment proposed in ref 24. Finally, let us mention that, also via calculations of the VRT levels, an empirical potential has been fitted[178] to the spectra. This potential is, rather crudely, represented by a simplified atom–atom model which omits the hydrogens, but the parameters in this model have been optimized such that the measured vibrational frequencies are reproduced. The well depth in the optimized empirical potential is about 400 cm^{-1}, just as in the *ab initio* potential. Collecting all these experiences, we think that the latter is of fairly good quality. The local "Morse -type" expansion is better in representing the vibrational frequencies, but it lacks some of the anharmonicity, which in the "global" fit gives rise to additional splittings and shifts and to a slight breaking of the cylindrical symmetry in the (x,y) directions.

E. NH_3–NH_3

It is a fact, well-established theoretically[4,179–187] and experimentally,[6,188–192] that the dimers $(HF)_2$ and $(H_2O)_2$ have a hydrogen-bonded structure. Until 1985 it was generally believed that the ammonia dimer, too, had a "classical" hydrogen-bonded structure with a proton of one monomer pointing to the nitrogen lone pair of the other. In that year Nelson, Fraser, and Klemperer[193] interpreted their microwave spectra by assuming that the dimer has a nearly cyclic structure in which the two umbrellas

are almost antiparallel. This finding was surprising in view of the fact that most *ab initio* calculations[194,195] predicted the classical, nearly linear, hydrogen-bonded structure. Although the calculations by Sagarik, Ahlrichs, and Brode[196] seemed to support the nearly cyclic structure, it was convincingly argued later[197] that a slight bending of the linear hydrogen bond in these calculations would have favored the classical hydrogen-bonded structure. And, in fact, it was shown in ref 10 that the analytical model potential which Sagarik *et al.* fitted to their *ab initio* data indeed supports a slightly bent hydrogen-bonded structure as the most stable one. Two of the most recent calculations differ in the prediction of the equilibrium structure: Hassett, Marsden, and Smith[197] found a hydrogen-bonded structure, whereas Tao and Klemperer[198] found a cyclic structure thanks to the addition of bond functions.

An obvious explanation of the discrepancy between the outcome of most calculations and the microwave data might be found in the effect of vibrational averaging. Whereas the electronic structure calculations focus mainly on finding the minimum of the intermolecular potential, the experiment gave a vibrationally averaged structure. This question was addressed experimentally by Nelson *et al*[89,199] by means of various isotope substitutions. From the fact that the relevant intermolecular bond angles hardly change with isotope substitution they conclude that $(NH_3)_2$ is fairly rigid and that also its equilibrium structure must be (nearly) cyclic. They supported this latter conclusion by the observation that the dipole moment of $(ND_3)_2$—in which the vibrational averaging effects are expected to be less than in $(NH_3)_2$—is 0.17 D smaller than the value of 0.74 D found for the $(NH_3)_2$ dimer. Nelson and co-workers took this as an indication that, indeed, the equilibrium structure is nearly cyclic. Note, parenthetically, that the dipole of the free ammonia is 1.47 D, which means that the sum of the components of the permanent dipoles along the dimer axis in the linear hydrogen-bonded structure is about 2.0 D.

The effects of vibrational averaging have been assessed theoretically in our group by van Bladel *et al.*[10] With the use of the model potential of Sagarik *et al.*,[196] which was the only full potential surface available from *ab initio* calculations at the time, the six-dimensional Schrödinger equation for the intermolecular motions was solved in a basis of coupled internal rotor functions and Morse-type stretch functions. Although it was found that the vibrationally averaged structure was shifted from the equilibrium hydrogen-bonded structure toward the cyclic geometry, the work did not produce complete reconciliation with the microwave geometry. Further van Bladel *et al.* obtained indirect evidence that the umbrella inversion of the two monomers is not completely quenched, as was assumed by Nelson *et al.*[193]

The latter conclusion was also reached by Loeser *et al.*,[11] who reported an extensive set of new far-infrared and microwave measurements and gave a very detailed analysis of these—as well as previous[200]—experimental data. They conclude that the group of feasible operations (permutations, inversion and their products, see Appendix C) is of the order 144, which implies that they observed the tunneling splittings associated with the two umbrella inversions and the interchange tunneling in which the role of the two monomers is reversed. The same conclusion was reached by the Nijmegen/Bonn group,[12] on the basis of infrared/far-infrared double-resonance experiments. The latter authors also measured the dipole moment in the $|K| = 1$ state of G symmetry.[201] Thus, the various experimental approaches present evidence that seems conflicting regarding the rigidity of $(NH_3)_2$ and its equilibrium structure. Also the different *ab initio* calculations lead to different pictures. Multiple discussions[89,94,202] have been devoted to this problem.

Recently Olthof *et al.*[203-206] presented a more complete theoretical approach. They constructed a family of model potentials with different barriers in the interchange motion and in the hindered rotations of the two NH_3 monomers around their C_3 axes. For each of these potentials they calculated the six-dimensional vibration−rotation−tunneling (VRT) states and the various transition frequencies that have been observed. For various states they computed the expectation values of the dipole moment and the nuclear quadrupole splittings, which are indicative of the orientations of the NH_3 monomers in the complex. By improving the parameters they arrived at a model potential that was able to reproduce all observed splittings with deviations of less than 0.5 cm^{-1}. Also the dipole and the nuclear quadrupole splittings were in good agreement with the observed values, both for $(NH_3)_2$ and $(ND_3)_2$.

The potentials used by Olthof *et al.* contain the permanent dipole, quadrupole, and octopole moments (calculated at the MBPT2 level[133]) on the NH_3 monomers to model the electrostatic interactions. In Figure 12A a cut through the electrostatic potential energy surface is shown. The angles θ_X are the angles of the respective symmetry axes with the vector connecting the mass centers of the monomers. We observe two equivalent minima, both corresponding to a slightly bent hydrogen bridge, separated by an energy barrier. To this the exp-6 site−site potential

$$V_{AB} = \sum_{i\in A}\sum_{j\in B}\left[A_i A_j \exp[-(b_i + b_j)R_{ij}] - \frac{c_i c_j}{R_{ij}^6}\right] \quad (51)$$

was added to account for the exchange repulsion and dispersion interactions. The parameters A_i were tuned to give agreement with the observed quantities. By changing these parameters in the exchange repulsion one is able to alter the shape of the potential surface and, in particular, to vary the barriers to internal rotation and to interchange of the monomers. Since induction effects are not explicitly included and the parameters are adapted to reproduce the experimental data, the potential must be considered as largely empirical. The presence of an octopole is essential, because the dipole and quadrupole of NH_3 have only axial components and the octopole yields the first contributions to the electrostatic interactions that depend on the directions of the individual N−H bonds. In addition to the

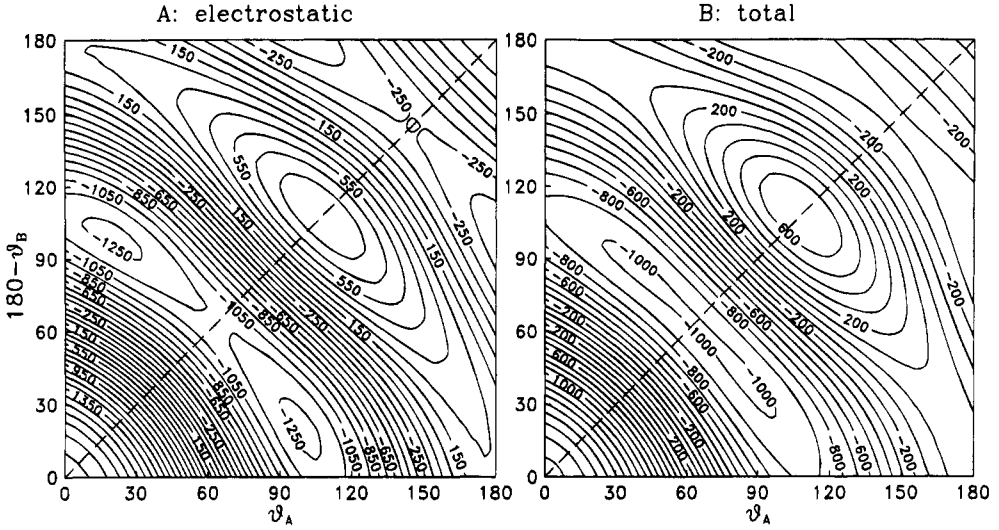

Figure 12. NH_3–NH_3 interaction potential (in cm^{-1}) as a function of θ_A and θ_B, with all other angles at their equilibrium values. Part A shows the electrostatic dipole–quadrupole–octopole interaction at R = 3.23 Å. Part B shows the total potential, with R = 3.373 Å; observe the same valley for interchange tunneling as in the purely electrostatic case.

nitrogen nuclei and protons also the nitrogen lone pairs were considered as centers of force, following the work of Dykstra and Andrews.[207] Olthof *et al.* took the parameters c_i simply from ref 207. The parameters b_i were determined from the (6–12) Lennard-Jones (LJ) potential of ref 207 by requiring that the depth and the position of the minimum in the N–N and H–H terms of eq 51 coincide with the minimum in the corresponding term of the LJ potential. See ref 204 for the reason why Olthof *et al.* did not use the LJ potential itself. This potential is shown in Figure 12B, where we see the considerable lowering of the barrier to 7.5 cm^{-1}. Further the minima are shifted somewhat to a cyclic structure (the saddle point of the barrier) by the addition of the site–site potential, but the equilibrium structures can still rightly be called "hydrogen bonded".

Before use in the calculation of the VRT states the potentials were expanded in the complete set of angular functions of eq 9. The R-dependent coefficients were computed by numerical quadrature, *cf.* eq 11. Olthof *et al.* carefully checked that the truncation of these expansions at $L_A^{max} = L_B^{max} = 5$ did not significantly affect the shape of the potential surfaces. The Hamiltonian, which has to be diagonalized in order to obtain the VRT states, is given by eqs 5, 7, and 9. The body-fixed basis and the calculation of the matrix elements are described in section II.D. In the exploratory calculations, in which the potential parameters were varied in order to get agreement with the experiments, the bases were truncated at $j_A = j_B = 5$, *cf.* eq 16. The final calculations, employing the optimum parameters, were performed in a much larger basis truncated at $j_A = j_B = 7$.

Because of the size of the basis, the full symmetry of the system had to be taken into account. The molecular symmetry group is of order 36, provided the umbrella inversions are frozen. Otherwise it is of order 144. These groups are denoted by G_{36} and G_{144}, respectively. Olthof *et al.* mainly focused on G_{36}, which has four one-dimensional irreducible representations (irreps), designated A_i, i = 1, ..., 4, four two-dimensional irreps (E_i, i = 1, ..., 4), and one four-dimensional irrep G. Recall that the three proton spins of NH_3 can couple either to a quartet (*o*-ammonia) or to a doublet (*p*-ammonia). The kets of A_i symmetry belong to two *ortho* monomers, those of E_i symmetry belong to two *para* monomers and G kets describe a mixed *ortho–para* dimer. For more details on symmetry adaptation we refer to Appendix C. See Table 16 for the behavior of the coordinates under the symmetry operations.

Table 16. Transformation Properties of the Coordinates in $(NH_3)_2$ under the Generators of G_{36} (the First Five Columns) and G_{144} (Here $\omega \equiv 2\pi/3$)

E	(123)	(456)	(14)(25)(36)(78)	(23)(56)*	(23)	(56)
R	R	R	R	R	R	R
α	α	α	$\alpha+\pi$	$\alpha+\pi$	α	α
β	β	β	$\pi-\beta$	$\pi-\beta$	β	β
ϕ_A	ϕ_A	ϕ_A	$-\phi_B$	$\pi-\phi_A$	$\pi+\phi_A$	ϕ_A
θ_A	θ_A	θ_A	$\pi-\theta_B$	θ_A	$\pi-\theta_A$	θ_A
ψ_A	$\psi_A-\omega$	ψ_A	$\pi+\psi_B$	$-\psi_A$	$-\psi_A$	ψ_A
ϕ_B	ϕ_B	ϕ_B	$-\phi_A$	$\pi-\phi_B$	ϕ_B	$\pi+\phi_B$
θ_B	θ_B	θ_B	$\pi-\theta_A$	θ_B	θ_B	$\pi-\theta_B$
ψ_B	ψ_B	$\psi_B-\omega$	$\pi+\psi_A$	$-\psi_B$	ψ_B	$-\psi_B$
ϱ_A	ϱ_A	ϱ_A	ϱ_B	ϱ_A	$\pi-\varrho_A$	ϱ_A
ϱ_B	ϱ_B	ϱ_B	ϱ_A	ϱ_B	ϱ_B	$\pi-\varrho_B$

Table 17. Comparison of Calculated and Measured Properties of $(NH_3)_2$ (All Values Pertain to K = 0 States, Unless Indicated Otherwise)

property	calculation (ref 205)	experiment
equilibrium dipole	1.08 D	
equilibrium θ_A	40.47°	
equilibrium 180° − θ_B	84.49°	
dipole G	0.66 D	0.74 D (ref 199)
dipole G ($\|K\|$ = 1)	0.19 D	0.10 D (ref 201)
$\theta_A{}^a$	48.5°	48.6° (ref 199)
180° − $\theta_B{}^b$	64.7°	64.5° (ref 199)
$E_{A_4} - E_{A_1}$	15.85 cm^{-1}	16.12 cm^{-1} (ref 11)
$E_{E_2} - E_{E_1}$	19.14 cm^{-1}	19.36 cm^{-1} (ref 11)
$E'_G - E_G$	20.25 cm^{-1}	20.50 cm^{-1} (ref 11)
$E_{G_{\bar{2}}} - E_{G_2^+}$	2.05 GHz	3.31 GHz (ref 11)
$E'_{G_{\bar{2}}} - E'_{G_2^+}$	1.24 GHz	2.39 GHz (ref 11)

[a] From $\langle P_2(\cos\theta_A)\rangle$. [b] From $\langle P_2(\cos\theta_B)\rangle$.

The results from the calculations on $(NH_3)_2$ are summarized in Table 17 for K = 0 and $|K|$ = 1. Note

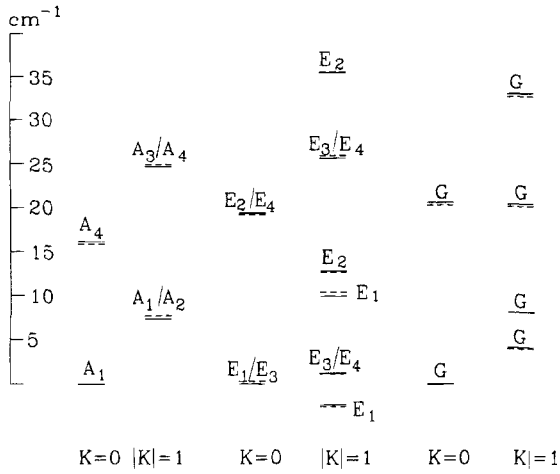

Figure 13. Comparison of computed and observed levels of NH_3–NH_3: dashed lines, computed; solid lines, observed.[11] The $K = 0$ ground level of each species A, E, and G is adjusted. In several cases the difference between computed and observed values is within the width of the lines.

that K, which is the projection of the total angular momentum J on the dimer bond axis, is not an exact quantum number. Since the off-diagonal Coriolis coupling is small, the observed states can be well characterized by K and therefore the Coriolis coupling was neglected. The energy differences $E_{A_4} - E_{A_1}$ and $E_{E_2} - E_{E_1}$ in Table 17 are due to the interchange tunneling. Note that these differences are large, in the order of 20 cm^{-1}, which confirms that the interchange between the donor and the acceptor molecule in the hydrogen bond takes place rapidly. Also the splitting $E'_G - E_G$ between the lowest G states is partly due to this interchange tunneling and partly to the difference between the *ortho* and the *para* monomers that form these G states. We present values of $180° - \theta_B$ in Table 17, rather than of θ_B, because whenever $\theta_A \approx 180° - \theta_B$, we have a cyclic structure. The observed and calculated energy levels are visualized in Figure 13, which clearly shows their surprisingly good agreement.

Owing to the fact that the G states belong to two nonidentical molecules, *viz. ortho* and *para*, they are localized to some extent on one side of the interchange barrier. This is in contrast with the A_i and E_i states, which are either symmetric or antisymmetric with respect to interchange. See Figure 14 for contour plots of the G symmetry wave functions. These plots show clearly that the dimer is highly nonrigid, a fact which is confirmed by the difference between the equilibrium dipole and the G state dipoles, see Table 17. Another important observation is that the partial localization, which manifests itself in the G state expectation values of the dipole moment, depends also on the barriers to rotation around the symmetry axes over ψ_A and ψ_B. It was found that addition of octopole moments to the potential gave a substantial increase in the dipole moment; recall that the first ψ_X-dependent electrostatic term is due to the octopole on monomer X.

The final two splittings in Table 17 are due to monomer umbrella inversion. An exact calculation would require the solution of an eight-dimensional dynamics problem: six intermolecular coordinates plus the two umbrella angles ϱ_A and ϱ_B. The group of this system is G_{144} and the labels $G_2^{\pm}$ refer to irreps of this group. These irreps correlate with the irrep G of $G_{36} \subset G_{144}$. A dynamics problem of this size cannot be handled at present, so Olthof *et al.*[206] employed an approximate model, which is an extension of a model proposed earlier for Ar–NH_3.[8] In order to explain this model, we recall that in section III.C the inversion part of the monomer Hamiltonian was designated by $H_{umb}(\varrho)$. The model entails the computation of the expectation value of $H_{umb}(\varrho_A) + H_{umb}(\varrho_B)$, with respect to the functions $[E - (56)][E \mp (56)^*]\Psi_{vdW} f(\varrho_A) f(\varrho_B)$, where $(56)^*$ is the operator inverting monomer A and (56) inverts B. The wave function Ψ_{vdW} is the lowest, or the one but lowest, eigenstate of the body-fixed Hamiltonian of G symmetry, $f(\varrho_A)$ and $f(\varrho_B)$ are ground umbrella (ν_2) states of A and B localized in one of the wells of their respective monomers. Assuming that $\langle f(\varrho_A)|(56)^*|f(\varrho_A)\rangle \approx 0$ and an equivalent relation on B, we obtain for the splitting

$$E_{G_2^-} - E_{G_2^+} = \Delta\langle\Psi_{vdW}|(56)^*|\Psi_{vdW}\rangle \qquad (52)$$

where $\Delta = 0.793$ cm^{-1}, the tunneling splitting of the free monomer.[160] This splitting corresponds to the inversion of the *para* partner in the dimer.

Let us end this section by discussing the decrease of the G state dipole moment observed when going from $(NH_3)_2$ to $(ND_3)_2$. Since the value of the dipole at the equilibrium geometry is 1.08 D, much larger than the average value of 0.66 D, and since one would expect $(ND_3)_2$ to stay closer to equilibrium than $(NH_3)_2$, it is not *a priori* clear that this decrease will also come out of the calculations. However, the rovibrationally averaged computed dipole moment does decrease, from 0.66 D for $(NH_3)_2$ to 0.38 D for $(ND_3)_2$. This decrease follows nicely the experimentally observed[199] decrease from 0.74 D for $(NH_3)_2$ to 0.57 D for $(ND_3)_2$. And, also the accompanying changes in the angles θ_A and θ_B obtained from the expectation values $\langle P_2(\cos\theta_A)\rangle$ and $\langle P_2(\cos\theta_B)\rangle$ agree well with the changes observed by measuring the nuclear quadrupole splittings in $(NH_3)_2$ and $(ND_3)_2$: $(\theta_A, 180°-\theta_B)$ change from (48.5°,64.7°) to (51.2°,61.7°), experimentally they change from (48.6°,64.5°) to (49.6°,62.6°). So it appears that $(ND_3)_2$ is more nearly cyclic than $(NH_3)_2$. In ref 204 this rather unexpected observation is explained by analysis of the wave functions (see Figure 14). When the wave function of the lowest G state of $(ND_3)_2$ is compared with the corresponding wave function of $(NH_3)_2$, we clearly observe two effects. First, as expected, the wave function of $(ND_3)_2$ has a larger amplitude near the equilibrium position around which it is localized. This leads to an increase of the average dipole moment. Secondly, a substantially larger amplitude of the wave function of $(ND_3)_2$ on the side of the *other*, equivalent, minimum is observed. In order to understand the latter effect one has to remember that, in spite of the equivalence of the two minima in the potential, the G-state wave functions are mainly localized on one side because of the *ortho–para* differences. This difference in the behavior of *ortho* and *para* monomers will be less for ND_3 than for NH_3, because its rotational constant A_z

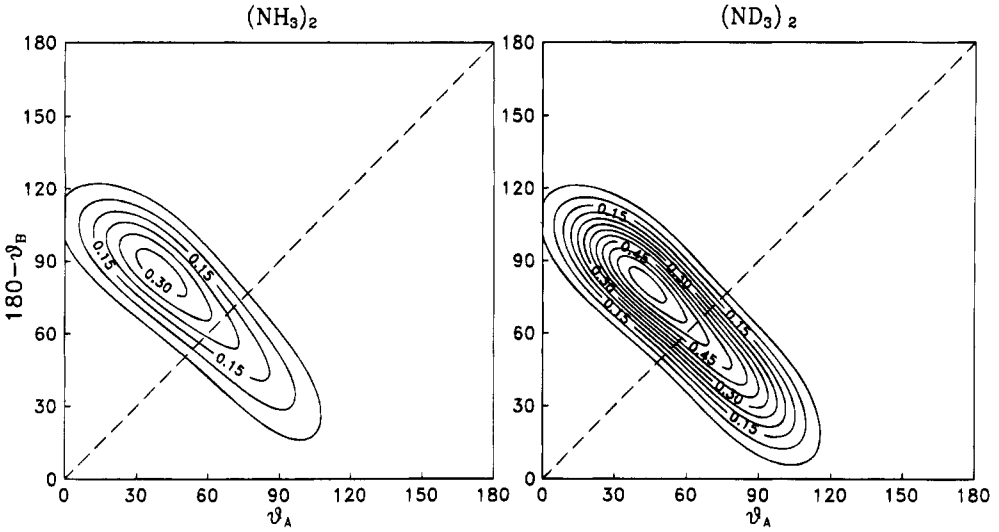

Figure 14. The lowest G state wave functions (absolute squared) of NH_3-NH_3 and ND_3-ND_3 in the $\theta_A-\theta_B$ plane. All other angles are fixed at their equilibrium values and $R = 3.373$ Å. Note that the wave functions are not symmetric with respect to reflection in the diagonal, unlike the potential in Figure 12 from which they are obtained.

Table 18. Comparison of Calculated and Measured Properties of $(ND_3)_2$ (All Values Pertain to $K = 0$)

property	calculation (ref 205)	experiment (ref 199)
dipole G	0.38 D	0.57 D
$\theta_A{}^a$	51.2°	49.6°
$180° - \theta_B{}^b$	61.7°	62.6°
$E_{A_4} - E_{A_1}$	11.03 cm^{-1}	
$E_{E_2} - E_{E_1}$	13.78 cm^{-1}	
$E'_G - E_G$	13.06 cm^{-1}	

[a] From $\langle P_2(\cos\theta_A)\rangle$. [b] From $\langle P_2(\cos\theta_B)\rangle$.

is smaller by a factor of 2. And, consequently, the asymmetry in the G state wave functions which is caused by these *ortho–para* differences, will be smaller in $(ND_3)_2$. In other words, $(ND_3)_2$ is more nearly cyclic (in its G state) because of the smaller *ortho–para* differences. This leads to a smaller average dipole moment. Apparently, for the final potential used in the calculations with its low interchange barrier of 7.5 cm^{-1} the latter effect dominates the first and explains the observed decrease of the dipole moment.

Other results from the calculations on $(ND_3)_2$ which are most relevant for comparison with the quantities observed by Nelson *et al.*[199] are collected in Table 18. We note that the interchange tunneling frequencies, which have not been measured yet, are about 30% smaller than in $(NH_3)_2$.

So, within one consistent computational model and by the use of a single parametrized potential, Olthof *et al.* were able to reproduce the observed level splittings, the observed dimer geometry, and the fact that the deuterated dimer has a smaller dipole than the protonated one. In the explanation of these features there was no need to invoke near-rigidity or a nearly cyclic equilibrium structure.

IV. Summary, Related Work

In the first part of this paper we have given an overview of the methods used to obtain the bound states and the spectra of van der Waals molecules from a given intermolecular potential. The basic theory is outlined in sections II.A–F, derivations are given in the appendixes. In the second part we have illustrated that the spectra of van der Waals molecules are very sensitive, but indirect, gauges of intermolecular potentials. Indirect, because one has to use the methods of section II with (sometimes extensive) computational efforts to extract the information from this gauge.

In $Ar-H_2$ and He–HF we have seen examples where recent *ab initio* potentials[31,33] perfectly reproduce[32,34] the spectra. Still, a minor improvement in the anisotropy of the *ab initio* potential could be achieved for He–HF by considering the rotational predissociation line width. Accurate semiempirical potentials are available for these systems too.[120,128] For $Ar-NH_3$ and $Ar-H_2O$ it was found[7-9,158] that the available *ab initio* potentials[153,154] were not yet sufficiently accurate to reproduce the high-resolution spectra. A fairly accurate spectrum could be calculated[8,9] for $Ar-NH_3$ by scaling one parameter in the short-range anisotropy of the *ab initio* potential. For $Ar-H_2O$ this was not possible.[158] Taking parametrized model potentials and optimizing the parameters in a fit of the spectrum was more successful for these systems.[44,145] Yet, it might be said in favor of the electronic structure calculations that the analytic form of these model potentials, as well as a number of their parameters, is fixed in advance on the basis of *ab initio* calculations. Full close-coupling calculations[164] of the measured[163] inelastic scattering cross sections have confirmed for $Ar-NH_3$ that the semiempirical potential[145] thus obtained is rather accurate. We expect, however, that for these and similar systems with three or four intermolecular degrees of freedom high-quality *ab initio* potentials will very soon be available also.

For Ar–benzene the *ab initio* potential[174,175] is probably of about the same quality as the *ab initio* potentials for $Ar-NH_3$ and $Ar-H_2O$, but the requirements to get a correct description of the bound states are less subtle. The reason for this is the much stronger anisotropy in Ar–benzene, which restrains the Ar atom to stay fairly close to its equilibrium

position, above the center of the benzene ring. The frequencies of the van der Waals vibrations which were calculated[24,165] from this *ab initio* potential agreed sufficiently well with the measured values to assign the experimental spectrum. To interpret also the rotational structure in this UV spectrum,[169-171] it was necessary[177] to include all Coriolis coupling between the (partly degenerate) van der Waals vibrations, the vibronic excitation on the benzene monomer which accompanies these van der Waals vibrations, and the overall rotations of the dimer. Further, it was essential to look in detail at the selection rules based on the permutation inversion symmetry. Another conclusion from this study on van der Waals vibrations in combination with a vibronic transition on the monomer is that the Frank–Condon principle, which determines the intensities of vibronic transitions in normal molecules, is less applicable in van der Waals complexes.

In NH_3–NH_3 the *ab initio* calculations[196-198] covered only a small fraction of the potential surface, *viz.* that part which is critical for the question whether hydrogen bonding occurs in this complex. The calculation of bound states requires a full surface, however, or at least a full scan of the regions with lower energy. A model potential was found[203-205] which gives an accurate reproduction of the measured far-infrared and microwave spectra. Questions regarding the deviation between the vibrationally averaged structure and the equilibrium structure and regarding the rigidity of this dimer, in relation with isotope substitution studies, could thus be answered. It appeared that the far-infrared frequencies, as well as the dipole moment and nuclear quadrupole splittings derived from the microwave spectrum, are particularly sensitive to the height of the interchange barrier. This barrier separates one hydrogen-bonded structure from the equivalent structure in which the proton donor and acceptor are reversed. The ammonia dimer is one of the cases where it will be hard to get accurate *ab initio* results, since it was found[205] that the height of this barrier is only about 7.5 cm^{-1}, less than 1% of the binding energy (D_e) of NH_3–NH_3, which is about 1000 cm^{-1}. Another interesting aspect of this study on NH_3–NH_3 is that it was necessary to use the full permutation inversion symmetry, in order to make the calculations feasible, but also to get even a qualitative understanding of the measured properties. The fact that the dipole moment, nuclear quadrupole splittings, etc., depend so much on the symmetry of the different rovibrational states which feel the same potential, and on the associated nuclear (*ortho–para*) spin species, is typical for a van der Waals molecule.

Finally, we wish to give some references to work on van der Waals molecules which was not covered in this review. We have concentrated on dimers, consisting of stable, although sometimes flexible, closed-shell molecules. The angular momentum coupling techniques which are extensively described in this paper are also applicable to open-shell monomers. The coupling scheme has to be extended, however, in order to include the electronic orbital and spin momenta of such monomers. Examples are given by the theoretical studies on Ar–OH,[208] Ar–O_2,[209-211] Ar–NH,[212] and O_2–O_2.[213] A general discussion of the possible coupling cases for atom–diatom systems with open shells is given in ref 214.

Trimers can also be treated by the dimer methods described in section II if two of the monomers are considered as a single subunit. Thus, it was possible, for instance, to describe Ar_3 as an atom–diatom system[215] and Ar_2HCl as a diatom–diatom complex.[21,216,217] The internal vibration of the Ar_2 diatom must be explicitly included, of course, and the basis provided has to be adequate to take into account that the amplitude of this vibration is as large as that of other motions in the trimer. Alternatively, one may use the quantum Monte Carlo method which was briefly mentioned in section II.D. This method was applied to $(HF)_3$,[82] but also to van der Waals complexes with more than three monomers.[79,80,218] Still larger clusters were used to study the onset of macroscopic processes such as melting, evaporation, wetting, etc. The spectra can be used to monitor these processes.[219] The interpretation of these spectra may be supported by classical molecular dynamics of (MD) or Monte Carlo calculations[220-225] or by thermodynamical considerations.[226]

Another topic which was mentioned only in passing is the vibrational (or electronic) predissociation of van der Waals complexes. If one of the monomers is vibrationally or electronically excited, the excitation energy will be redistributed among the various intra- and intermolecular modes of the complex, in a rather specific manner.[227] When the excitation energy is higher than the binding energy of the complex and sufficient energy enters into the intermolecular stretch mode, the complex dissociates. In high-resolution spectra this manifests itself by a broadening of the spectral lines, which is inversely proportional to the time that it takes for the excited state to dissociate. More detailed information can be obtained[98] by analyzing the velocities and the vibrational and rotational state distributions of the fragments. In time-resolved experiments[228] these dynamical processes can be probed directly. In calculations of such processes, especially the angular aspects of the theory presented in this review can still be used. At least one relevant intramolecular degree of freedom must be included, however, and the description of the photodissociation process requires a special treatment of the R stretch coordinate.[208,229-235]

An interesting option is the use of van der Waals complexes to study chemical reactions. Thus, one can prepare the impact geometry of the reactants, and by photoexcitation, one can select specific initial states. Also the final state distributions of the reaction products can be monitored through their spectra. Very detailed state-to-state knowledge about a chemical reaction is then becoming available, even more so than in crossed (oriented) beam experiments where the impact parameter cannot be controlled. Interesting experimental work is going on already,[236-238] but the theory to describe the dynamics of these van der Waals molecule reactions in equally great detail is still lagging behind.

In closing, we wish to mention the previous issue of *Chemical Reviews* (ref 239) which was devoted to van der Waals complexes, as well as some other

reviews (refs 17, 89, 91–94, and 98), conference proceedings and books (refs 240–244).

Acknowledgments. We thank Dr. G. C. Groenenboom for valuable discussions. This work was supported in part by the Netherlands Foundation for Chemical Research (SON) with financial aid from the Netherlands Organization for Scientific Research (NWO). One of us (R.M.) also thanks the Polish Scientific Research Council (grant KBN 2 0556 91 01).

Appendixes

A. Kinetic Energy

In this appendix we sketch the derivation of the kinetic energy in three different frames commonly used in calculations on van der Waals molecules. The first is a space- (or laboratory-) fixed frame, the second is the "two-angle embedded frame" discussed by Brocks *et al.*,[18] and the third is a frame fixed to one of the monomers. The derivations depart from a general expression—derived by Beltrami over 125 years ago—for the Laplace operator in general nonorthogonal curvilinear coordinates. In 1928 Podolsky[14] pointed out that the Beltrami form of the Laplacian (times $-{}^1/_2\hbar^2$) is the proper expression for the quantum mechanical kinetic energy. By its use one avoids tedious applications of the chain rule and is also able to take account of possible holonomic constraints that reduce the number of degrees of freedom. See the excellent review by Essén[15] for a discussion of the problems associated with this approach.

First we will review the case of a system of two atoms and point out some problems that appear in body-fixed frames. The diatom is the simplest example by which we can discuss this. Then we review the case of a rigid rotor, because the monomers constituting a van der Waals molecule are often assumed to be rigid. This is followed by a discussion of a rotor–atom system with the frame attached to the rotor. Finally we consider a dimer consisting of two rigid rotors described in the two-angle embedded frame.

We will indicate a geometric—frame independent—vector (an "arrow") by an arrow over the symbol. Usually such a vector points from one particle to another. The coordinate representation (three real numbers) of a vector with respect to a certain frame, is given in bold face. A frame is bold with an arrow on top of it. Thus, the vector pointing from A to B is written as

$$\overrightarrow{AB} = \vec{e}_1 x + \vec{e}_2 y + \vec{e}_3 z \equiv (\vec{e}_1, \vec{e}_2, \vec{e}_3)\begin{pmatrix} x \\ y \\ z \end{pmatrix} \equiv \vec{\boldsymbol{e}}\,\boldsymbol{r}$$

where $\vec{\boldsymbol{e}} \equiv (\vec{e}_1, \vec{e}_2, \vec{e}_3)$ is a certain frame.

In the case of time-independent constraints the classical kinetic energy of a system with n degrees of freedom can be written (see ref 245, p 25) in general curvilinear coordinates q_i, $i = 1, ..., n$, as

$$2T = \dot{\boldsymbol{q}}^T \mathbb{G} \dot{\boldsymbol{q}} \tag{A1}$$

which defines the metric tensor G. The determinant of G will be denoted by g; as is well known (ref 246, p 195) $\sqrt{g}\ dq_1 ... dq_n$ is the volume element of the coordinate system. The momentum $\boldsymbol{p}_q$ conjugate to $\boldsymbol{q}$ is defined by

$$\boldsymbol{p}_q = \mathbb{G}\dot{\boldsymbol{q}} \leftrightarrows p_i = \frac{\partial T}{\partial \dot{q}_i} \tag{A2}$$

so that the kinetic energy in Hamilton form is

$$2T = \boldsymbol{p}_q^T \mathbb{G}^{-1} \boldsymbol{p}_q \tag{A3}$$

Quantization is performed by substituting

$$p_i \rightarrow -i\hbar \frac{\partial}{\partial q_i} \qquad i = 1, ..., n \tag{A4}$$

not into eq A3, but into

$$2T = g^{-1/2} \boldsymbol{p}_q^T g^{1/2} \mathbb{G}^{-1} \boldsymbol{p}_q \tag{A5}$$

This is because the Laplace operator in general curvilinear coordinates has the form (ref 246, p 197)

$$\Delta = g^{-1/2} \sum_{ij} \frac{\partial}{\partial q_i} g^{1/2} (\mathbb{G}^{-1})_{ij} \frac{\partial}{\partial q_j} \tag{A6}$$

Podolsky[14] also discusses a more symmetric form of the operator obtained by renormalizing the wave function Ψ. That is, he substitutes $\Psi \rightarrow g^{-1/4}\Psi$ and takes an unweighted volume element. This gives

$$2T = -\hbar^2 g^{-1/4} \sum_{ij} \frac{\partial}{\partial q_i} g^{1/2} (\mathbb{G}^{-1})_{ij} \frac{\partial}{\partial q_j} g^{-1/4} \tag{A7}$$

1. Two Atoms

Let us apply formula A6 to a diatomic van der Waals molecule A–B with its mass center at rest. In a space fixed frame $\vec{\boldsymbol{e}} \equiv (\vec{e}_x, \vec{e}_y, \vec{e}_z)$, we have classically

$$\overrightarrow{AB} = \vec{\boldsymbol{e}} \begin{pmatrix} R(t) \cos\alpha(t) \sin\beta(t) \\ R(t) \sin\alpha(t) \sin\beta(t) \\ R(t) \cos\beta(t) \end{pmatrix} \equiv \vec{\boldsymbol{e}} \begin{pmatrix} x(t) \\ y(t) \\ z(t) \end{pmatrix} \tag{A8}$$

By the chain rule

$$\begin{pmatrix} \dot{x} \\ \dot{y} \\ \dot{z} \end{pmatrix} = \frac{\partial(x,y,z)}{\partial(\beta,\alpha,R)} \begin{pmatrix} \dot{\beta} \\ \dot{\alpha} \\ \dot{R} \end{pmatrix} \tag{A9}$$

It is easily verified that the Jacobi matrix arising in this expression is given by

$$\frac{\partial(x,y,z)}{\partial(\beta,\alpha,R)} = \mathrm{R}_z(\alpha)\mathrm{R}_y(\beta) \begin{pmatrix} R & 0 & 0 \\ 0 & R\sin\beta & 0 \\ 0 & 0 & 1 \end{pmatrix} \tag{A10}$$

where

$$\mathrm{R}_z(\alpha) = \begin{pmatrix} \cos\alpha & -\sin\alpha & 0 \\ \sin\alpha & \cos\alpha & 0 \\ 0 & 0 & 1 \end{pmatrix} \quad \text{and}$$

$$\mathrm{R}_y(\beta) = \begin{pmatrix} \cos\beta & 0 & \sin\beta \\ 0 & 1 & 0 \\ -\sin\beta & 0 & \cos\beta \end{pmatrix} \tag{A11}$$

Hence

$$2T = \mu_{AB}(\dot\beta,\dot\alpha,\dot R)\frac{\partial(x,y,z)^T}{\partial(\beta,\alpha,R)}\frac{\partial(x,y,z)}{\partial(\beta,\alpha,R)}\begin{pmatrix}\dot\beta\\ \dot\alpha\\ \dot R\end{pmatrix} \quad \text{(A12)}$$

with

$$\mu_{AB} = \frac{m_A m_B}{(m_A + m_B)}$$

so that

$$\mathbb{G} = \mu_{AB}\begin{pmatrix}R^2 & 0 & 0\\ 0 & R^2\sin^2\beta & 0\\ 0 & 0 & 1\end{pmatrix} \quad \text{(A13)}$$

and

$$\sqrt{g} = {\mu_{AB}}^{3/2}R^2\sin\beta$$

The momentum conjugate to the spherical polar coordinates is

$$\boldsymbol{p} = \mu_{AB}\begin{pmatrix}R^2\dot\beta\\ R^2\sin^2\beta\dot\alpha\\ \dot R\end{pmatrix} \equiv \begin{pmatrix}p_\beta\\ p_\alpha\\ p_R\end{pmatrix} \quad \text{(A14)}$$

The quantum mechanical kinetic energy is from eqs A13 and A6

$$2T = -\frac{\hbar^2}{\mu_{AB}R^2}\left[\frac{1}{\sin\beta}\frac{\partial}{\partial\beta}\sin\beta\frac{\partial}{\partial\beta} + \frac{1}{\sin^2\beta}\frac{\partial^2}{\partial\alpha^2} + \frac{\partial}{\partial R}R^2\frac{\partial}{\partial R}\right] \quad \text{(A15)}$$

which we recognize as the usual one-particle kinetic energy in spherical polar coordinates. In the absence of an external potential the Schrödinger equation can be separated and the angular solutions are the spherical harmonic functions $Y^l_m(\beta,\alpha)$. In this discussion we ignored the quantum mechanical translational motion, which we do everywhere in this paper.

The angular momentum defined classically as

$$\vec l = \mu_{AB}\overrightarrow{AB} \times \frac{\mathrm{d}\overrightarrow{AB}}{\mathrm{d}t} \quad \text{(A16)}$$

can be most easily evaluated in the following frame embedded in the molecule

$$\vec{\boldsymbol{f}} \equiv \vec{\boldsymbol{e}}\mathbb{R}(\alpha,\beta) \quad \text{with} \quad \mathbb{R}(\alpha,\beta) = \mathbb{R}_z(\alpha)\mathbb{R}_y(\beta) \quad \text{(A17)}$$

It is worth noting that the matrix $\mathbb{R}(\alpha,\beta)$ consists of direction cosines, since $[\mathbb{R}(\alpha,\beta)]_{ij} = \vec{e_i}\cdot\vec{f_j}$. By the use of eqs A17, A9, A10, and A14 we find that in this frame

$$\overrightarrow{AB} = \vec{\boldsymbol{f}}\begin{pmatrix}0\\ 0\\ R\end{pmatrix} \quad \text{and} \quad \frac{\mathrm{d}\overrightarrow{AB}}{\mathrm{d}t} = \vec{\boldsymbol{f}}\begin{pmatrix}p_\beta/R\\ p_\alpha/(R\sin\beta)\\ p_R\end{pmatrix} \quad \text{(A18)}$$

so that

$$\vec l = \vec{\boldsymbol{f}}\begin{pmatrix}-p_\alpha/\sin\beta\\ p_\beta\\ 0\end{pmatrix} \equiv \vec{\boldsymbol{f}}\,\boldsymbol{l}^{\mathrm{BF}} \quad \text{(A19)}$$

Quantization gives

$$\hat{\boldsymbol{l}}^{\mathrm{BF}} = -i\hbar\begin{pmatrix}-\frac{1}{\sin\beta}\frac{\partial}{\partial\alpha}\\ \frac{\partial}{\partial\beta}\\ 0\end{pmatrix} \quad \text{(A20)}$$

It is important to note that the components of $\hat{\boldsymbol{l}}^{\mathrm{BF}}$ do not satisfy the usual angular momentum commutation relations. Because of the presence of $\sin\beta$ in the volume element, the operator $\hat l_y^{\mathrm{BF}}$ is not even Hermitian. In the space-fixed frame we obtain the usual orbital angular momentum operators, which are Hermitian and do satisfy the normal commutation relations

$$\hat{\vec l} = \vec{\boldsymbol{e}}\mathbb{R}(\alpha,\beta)\hat{\boldsymbol{l}}^{\mathrm{BF}} = \vec{\boldsymbol{e}}\hat{\boldsymbol{l}}^{\mathrm{SF}} = -i\hbar\vec{\boldsymbol{e}}\begin{pmatrix}-\cot\beta\cos\alpha\frac{\partial}{\partial\alpha} - \sin\alpha\frac{\partial}{\partial\beta}\\ -\cot\beta\sin\alpha\frac{\partial}{\partial\alpha} + \cos\alpha\frac{\partial}{\partial\beta}\\ \frac{\partial}{\partial\alpha}\end{pmatrix} \quad \text{(A21)}$$

It is also important to note that the operators representing $|\vec l|^2$ in the space- and body-fixed frame are different

$$(\hat l^{\mathrm{SF}})^2 = (\hat l^{\mathrm{BF}})^2 - i\hbar\cot\beta\hat l_y^{\mathrm{BF}} = -\hbar^2\left[\frac{1}{\sin\beta}\frac{\partial}{\partial\beta}\sin\beta\frac{\partial}{\partial\beta} + \frac{1}{\sin^2\beta}\frac{\partial^2}{\partial\alpha^2}\right] \quad \text{(A22)}$$

The space-fixed operator is the proper representation of the observable $|\vec l|^2$.

2. The Rigid Rotor

We next turn to a rigid rotor consisting of N point masses m_i with space-fixed coordinate vectors $\boldsymbol{r}_i$. We take a frame $\vec{\boldsymbol{f}}$ attached to the rotor and define the Euler angles of the rotor by

$$\vec{\boldsymbol{f}} = \vec{\boldsymbol{e}}\mathbb{R}_z(\phi)\mathbb{R}_y(\theta)\mathbb{R}_z(\psi) \equiv \vec{\boldsymbol{e}}\mathbb{R}(\zeta), \quad \zeta \equiv (\phi, \theta, \psi) \quad \text{(A23)}$$

The matrices $\mathbb{R}_i$ are defined in eq A11. The classical kinetic energy of a rigid rotor is

$$2T = (\boldsymbol{\omega}^{\mathrm{SF}})^T\mathbb{I}^{\mathrm{SF}}\boldsymbol{\omega}^{\mathrm{SF}} \quad \text{(A24)}$$

The inertia tensor of the rotor is defined by (ref 245, p 195)

$$I^{\mathrm{SF}}_{ab} \equiv \sum_{i=1}^{N} m_i(\delta_{ab}{r_i}^2 - r_{ia}r_{ib}) \quad \text{(A25)}$$

The components of the angular velocity $\boldsymbol{\omega}^{\mathrm{SF}}$ are not the time derivatives of certain coordinates (ref 247, p 41), but they are related to the derivatives of the Euler angles by

$$\boldsymbol{\omega}^{\mathrm{SF}} = \mathbb{M}\dot\zeta \quad \text{where} \quad \mathbb{M} = \begin{pmatrix}0 & -\sin\phi & \cos\phi\sin\theta\\ 0 & \cos\phi & \sin\phi\sin\theta\\ 1 & 0 & \cos\theta\end{pmatrix} \quad \text{(A26)}$$

Hence

$$G = M^T I^{SF} M \tag{A27}$$

The derivation of eq A26 is along the lines given in ref 245, sections 4−9, but modified for our definition (eq A23) of Euler angles, which differs from the one in ref 245.

The determinant of G is the product of the inertia moments (the eigenvalues of I^{SF}) and the determinant squared of M; the latter factor is $\sin^2\theta$. The angular momentum of the rotor is

$$\vec{j} = \vec{e} I^{SF} \omega^{SF} = \vec{e} (M^{-1})^T p_\zeta \equiv \vec{e} j^{SF} \tag{A28}$$

where p_ζ is the momentum conjugate to ζ. By substituting $p_i \rightarrow -i\hbar\,\partial/\partial\zeta_i$ and inverting M we find the well-known expressions

$$\begin{cases} j_x^{SF} = i\hbar\left(\cos\phi\cot\theta\dfrac{\partial}{\partial\phi} + \sin\phi\dfrac{\partial}{\partial\theta} - \dfrac{\cos\phi}{\sin\theta}\dfrac{\partial}{\partial\psi}\right) \\ j_y^{SF} = i\hbar\left(\sin\phi\cot\theta\dfrac{\partial}{\partial\phi} - \cos\phi\dfrac{\partial}{\partial\theta} - \dfrac{\sin\phi}{\sin\theta}\dfrac{\partial}{\partial\psi}\right) \\ j_z^{SF} = -i\hbar\dfrac{\partial}{\partial\phi} \end{cases} \tag{A29}$$

It is not difficult to prove that these operators satisfy the usual commutation relations

$$[j_i^{SF}, j_j^{SF}] = i\hbar\sum_k \epsilon_{ijk} j_k^{SF} \tag{A30}$$

where ϵ_{ijk} is the antisymmetric (Levi−Civita) tensor. By virtue of the fact that

$$\sum_i \left[\frac{\partial}{\partial\zeta_i}, \sin\theta\,(M^{-1})_{ij}\right] = 0 \quad \text{for} \quad j = 1, 2, 3 \tag{A31}$$

the square roots of the determinant of G appearing in the Beltrami formula (eq A6) cancel and the kinetic energy of the rotor can be written in terms of the angular momenta

$$2T = (j^{SF})^T (I^{SF})^{-1} j^{SF} \tag{A32}$$

If we take the frame $\vec{f}$ to be a principal axes frame (*i.e.* it to consist of eigenvectors of the inertia tensor), then by definition

$$R(\zeta)^T I^{SF} R(\zeta) \equiv I^{BF} = \begin{pmatrix} I_a & 0 & 0 \\ 0 & I_b & 0 \\ 0 & 0 & I_c \end{pmatrix} \tag{A33}$$

If all three inertia moments I_a, I_b, I_c are equal, the rotor is a spherical top (example CH_4). If two are equal we have a symmetric top (example NH_3) and if none are equal we have an asymmetric top (example H_2O). Defining the matrix

$$N \equiv R(\zeta)^{-1} M \tag{A34}$$

we find

$$\vec{j} = \vec{f} (N^{-1})^T p_\zeta = \vec{f} j^{BF} \tag{A35}$$

with

$$j^{BF} = R(\zeta)^T j^{SF} \tag{A36}$$

This relation is analogous to the one between l^{SF} and l^{BF}, see eq A21. However, the components of j^{BF} are Hermitian (as are the components of j^{SF}), although they do not satisfy the usual commutation relations, but rather the so-called anomalous relations

$$[j_i^{BF}, j_j^{BF}] = -i\hbar\sum_k \epsilon_{ijk} j_k^{BF} \tag{A37}$$

The lengths are the same in the two frames

$$(j^{SF})^2 = (j^{BF})^2 = -\frac{\hbar^2}{\sin^2\theta}\left[\frac{\partial^2}{\partial\phi^2} + \frac{\partial^2}{\partial\psi^2} - 2\cos\theta\frac{\partial^2}{\partial\phi\partial\psi}\right] - \frac{\hbar^2}{\sin\theta}\frac{\partial}{\partial\theta}\sin\theta\frac{\partial}{\partial\theta} \tag{A38}$$

Since a relation analogous to eq A31 holds for N, the kinetic energy can be written as

$$T = A(j_x^{BF})^2 + B(j_y^{BF})^2 + C(j_z^{BF})^2 \tag{A39}$$

where the rotational constants A, B, and C are inversely proportional to the inertia moments of the rotor.

3. Rotor–Atom

We will now consider the case of a rigid rotor A and a freely moving point mass B. The kinetic energy operator will be expressed with respect to a frame $\vec{f}$ attached to A. The frame is for example a principal axes frame of the rotor. The kinetic energy expression, to be derived via the Podolsky route, was obtained earlier[24] by application of the chain rule.

The frame independent classical kinetic energy takes the form

$$2T = 2T_A + \mu_{AB}\left|\frac{d\vec{AB}}{dt}\right|^2 \tag{A40}$$

where μ_{AB} is the reduced mass of the dimer and A and B are the respective centers of mass. By the use of eqs A24, A33, and A34 we can write

$$2T_A = \omega^T I^{BF} \omega \quad \text{with} \quad \omega = N\dot{\zeta} \tag{A41}$$

where $\zeta = (\phi,\theta,\psi)$ are the Euler angles of the rotor. The vector $\vec{AB}$ has the coordinate $R(t) = [x(t),y(t),z(t)]$ with respect to the body-fixed frame, and so

$$\frac{d\vec{AB}}{dt} = \frac{d\vec{f}(t)}{dt}R(t) + \vec{f}(t)\frac{dR(t)}{dt} \tag{A42}$$

It is well-known, see for instance ref 245, sections 4−9, that

$$\frac{d\vec{f}(t)}{dt}R(t) = \vec{f}(t)\omega \times R(t) \tag{A43}$$

We will rewrite the vector product as follows, in order

to get an expression for T quadratic in $\dot{\zeta}$,

$$\boldsymbol{\omega} \times \boldsymbol{R}(t) = \mathbb{X}^T\boldsymbol{\omega} \equiv \begin{pmatrix} 0 & z(t) & -y(t) \\ -z(t) & 0 & x(t) \\ y(t) & -x(t) & 0 \end{pmatrix}\boldsymbol{\omega} \quad \text{(A44)}$$

From

$$\frac{\mathrm{d}\vec{AB}}{\mathrm{d}t} = \vec{f}[\mathbb{X}^T\boldsymbol{\omega} + \dot{\boldsymbol{R}}] \quad \text{(A45)}$$

we find

$$\left|\frac{\mathrm{d}\vec{AB}}{\mathrm{d}t}\right|^2 = \boldsymbol{\omega}^T\mathbb{X}\mathbb{X}^T\boldsymbol{\omega} + \dot{\boldsymbol{R}}(t)^T\mathbb{X}^T\boldsymbol{\omega} + \boldsymbol{\omega}^T\mathbb{X}\dot{\boldsymbol{R}}(t) + |\dot{\boldsymbol{R}}(t)|^2 \quad \text{(A46)}$$

By the use of eqs A41 and A46, we obtain the following expression for the rotor–atom system, from which we may extract the metric tensor $\mathbb{G}$:

$$2T = (\dot{\boldsymbol{\zeta}}^T, \dot{\boldsymbol{R}}^T)\begin{pmatrix} \mathbb{N}^T & \mathbb{O} \\ \mathbb{O} & \mathbb{E} \end{pmatrix}\begin{pmatrix} \mathbb{I}^{\mathrm{BF}} + \mu_{AB}\mathbb{X}\mathbb{X}^T & \mu_{AB}\mathbb{X} \\ \mu_{AB}\mathbb{X}^T & \mu_{AB}\mathbb{E} \end{pmatrix}\begin{pmatrix} \mathbb{N} & \mathbb{O} \\ \mathbb{O} & \mathbb{E} \end{pmatrix}\begin{pmatrix} \dot{\boldsymbol{\zeta}} \\ \dot{\boldsymbol{R}} \end{pmatrix} \quad \text{(A47)}$$

The inverse of $\mathbb{G}$ can easily be calculated by the Frobenius formula (ref 248, p 73) and gives (*cf.* eq A3) the classical Hamiltonian

$$2T = (\boldsymbol{p}_\zeta^T, \boldsymbol{p}_R^T)\begin{pmatrix} \mathbb{N}^{-1} & \mathbb{O} \\ \mathbb{O} & \mathbb{X}^T \end{pmatrix} \begin{pmatrix} (\mathbb{I}^{\mathrm{BF}})^{-1} & -(\mathbb{I}^{\mathrm{BF}})^{-1} \\ -(\mathbb{I}^{\mathrm{BF}})^{-1} & (\mathbb{I}^{\mathrm{BF}})^{-1} + (\mu_{AB}\mathbb{X}^T\mathbb{X})^{-1} \end{pmatrix}\begin{pmatrix} \mathbb{N}^{-1} & \mathbb{O} \\ \mathbb{O} & \mathbb{X}^T \end{pmatrix}^T\begin{pmatrix} \boldsymbol{p}_\zeta \\ \boldsymbol{p}_R \end{pmatrix} \quad \text{(A48)}$$

where $\boldsymbol{p}_R = \mu_{AB}\dot{\boldsymbol{R}} + \mu_{AB}\mathbb{X}^T\mathbb{N}\dot{\boldsymbol{\zeta}}$ is conjugate to $\boldsymbol{R}$ and $\boldsymbol{p}_\zeta$ to ζ, and

$$\boldsymbol{p}_\zeta = \mathbb{N}^T[(\mathbb{I}^{\mathrm{BF}} + \mu_{AB}\mathbb{X}\mathbb{X}^T)\mathbb{N}\dot{\boldsymbol{\zeta}} + \mu_{AB}\mathbb{X}\dot{\boldsymbol{R}}] \quad \text{(A49)}$$

Note that $\boldsymbol{p}_\zeta$ contains contributions due to the motion of the rotor (the terms linear in $\mathbb{I}^{\mathrm{BF}}$), and terms arising from the motion of the "relative particle" (linear in the reduced dimer mass μ_{AB}). After quantizing, *i.e.*, after replacing p_ϕ by $-i\hbar\,\partial/\partial\phi$, etc., the operator $\boldsymbol{p}_\zeta$ depends only on the Euler angles of the rotor. However, we must bear in mind that these angles are also the Euler angles of the frame in which the motion of the whole complex is described, so $\boldsymbol{p}_\zeta$ is (the angular part of) the generalized momentum of the *whole* complex.

In accordance with eq A35 we write $\boldsymbol{J}^{\mathrm{BF}} = (\mathbb{N}^{-1})^T\boldsymbol{p}_\zeta$, which is the total dimer angular momentum. We define the angular momentum of the relative particle by

$$\boldsymbol{l}^{\mathrm{BF}} \equiv \boldsymbol{R} \times \boldsymbol{p}_R = \mathbb{X}\boldsymbol{p}_R \quad \text{(A50)}$$

With these definitions the classical Hamiltonian A48 becomes

$$2T = (\boldsymbol{J}^{\mathrm{BF}} - \boldsymbol{l}^{\mathrm{BF}})^T(\mathbb{I}^{\mathrm{BF}})^{-1}(\boldsymbol{J}^{\mathrm{BF}} - \boldsymbol{l}^{\mathrm{BF}}) + \frac{|\boldsymbol{p}_R|^2}{\mu_{AB}} \quad \text{(A51)}$$

Equation A51 has a clear physical interpretation: since $\boldsymbol{J}^{\mathrm{BF}}-\boldsymbol{l}^{\mathrm{BF}}$ is the angular momentum of the rotor and $\mathbb{I}^{\mathrm{BF}}$ is its inertia tensor, the total kinetic energy is the sum of the kinetic energies of the rotor and the relative particle.

In order to obtain the quantum mechanical form we use again the Laplace-Beltrami expression, eq A6, for which we need the determinant $g \equiv \det(\mathbb{G})$. From eq A47 follows that $g = \mu_{AB}^3 \det(\mathbb{N})^2 \det(\mathbb{I}^{\mathrm{BF}})$. Furthermore, on account of eq A34 we have $\det(\mathbb{N}) = -\sin\theta$. By the analogue of eq A31, holding also for $\mathbb{N}$, it follows that $g^{1/2}$ drops out of the Laplace–Beltrami expression, so that the quantum mechanical kinetic energy obtains the same appearance as the classical expression A51, but with the total angular momenta defined as follows:

$$\begin{cases} J_x^{\mathrm{BF}} = i\hbar\left(-\cos\psi\cot\theta\dfrac{\partial}{\partial\psi} - \sin\psi\dfrac{\partial}{\partial\theta} + \dfrac{\cos\psi}{\sin\theta}\dfrac{\partial}{\partial\phi}\right) \\ J_y^{\mathrm{BF}} = i\hbar\left(\sin\psi\cot\theta\dfrac{\partial}{\partial\psi} - \cos\psi\dfrac{\partial}{\partial\theta} - \dfrac{\sin\psi}{\sin\theta}\dfrac{\partial}{\partial\phi}\right) \\ J_z^{\mathrm{BF}} = -i\hbar\dfrac{\partial}{\partial\psi} \end{cases} \quad \text{(A52)}$$

and the operators depending on the position of the atom defined as

$$\boldsymbol{l}^{\mathrm{BF}} = -i\hbar\boldsymbol{R} \times \boldsymbol{\nabla} \quad \text{and} \quad |\boldsymbol{p}_R|^2 = -\hbar^2\nabla^2 \quad \text{(A53)}$$

4. Two Rotors

We now consider the kinetic energy of the dimer A–B consisting of two rigid rotors. From classical mechanics we know that

$$T = T_A + T_B + T_{AB} \quad \text{(A54)}$$

where the kinetic energy of the "relative particle" is given by

$$2T_{AB} = \mu_{AB}\left|\frac{\mathrm{d}\vec{AB}}{\mathrm{d}t}\right|^2 \quad \text{and} \quad \mu_{AB} = \frac{m_A m_B}{m_A + m_B} \quad \text{(A55)}$$

The kinetic energies of the monomers X are indicated by T_X, $X = A, B$. In order to obtain quantum mechanical operators we describe the kinetic energies with respect to a frame. The most obvious frame is the space-fixed frame $\vec{e}$, with $\beta(t)$, $\alpha(t)$, and $R(t)$ being the spherical polar coordinates of $\vec{AB}$. Exactly as for the diatom, eq A15, we find

$$2T_{AB} = \frac{1}{\mu_{AB}R^2}\left[(\hat{l}^{\mathrm{SF}})^2 - \hbar^2\frac{\partial}{\partial R}R^2\frac{\partial}{\partial R}\right] \quad \text{(A56)}$$

with $(\hat{l}^{\mathrm{SF}})^2$ given by eq A22. The kinetic energies T_A and T_B are given by eq A32.

The main advantage of a space-fixed frame is that it yields a simple kinetic energy expression. However, the matrix elements of the anisotropic terms in the intermolecular potential are complicated when evaluated space-fixed and require much computer time. Furthermore, the Coriolis coupling between the motions of the monomers and the overall rotation of the dimer is often weak for low angular momentum quantum numbers. Since this coupling does not

appear explicitly in the space-fixed kinetic energy, it is difficult to take advantage of this fact and to simplify the computation by neglecting or approximating the Coriolis interaction. See ref 20 for a discussion of body- versus space-fixed axes in the framework of scattering theory.

For these reasons we consider an embedded frame $\vec{f}$, with its z axis along $\overrightarrow{AB}$, obtained from the space-fixed frame as in eq A17. Classically the kinetic energy is a rotational invariant, *i.e.* it can be written as,

$$2T = \frac{1}{\mu_{AB}R^2}[(l^{\mathrm{BF}})^2 + P^2] + \sum_X \boldsymbol{j}_X^T \mathrm{I}_X^{-1} \boldsymbol{j}_X \quad \text{(A57)}$$

where $P = \mu_{AB}\dot{R}$ is conjugate to R, $\boldsymbol{j}_X = \mathrm{R}(\alpha,\beta)^T \boldsymbol{j}_X^{\mathrm{SF}}$ (do not confuse $\boldsymbol{j}_X$ with $\boldsymbol{j}_X^{\mathrm{BF}}$ given in eq A36), $\boldsymbol{l}^{\mathrm{BF}}$ is given in eq A19, and

$$\mathrm{I}_X = \mathrm{R}(\alpha,\beta)^T \mathrm{I}_X^{\mathrm{SF}} \mathrm{R}(\alpha,\beta) \quad \text{(A58)}$$

Quantum mechanically we must proceed with care because the frame $\overrightarrow{\boldsymbol{g}_X}$ attached to the rotor X is expressed with respect to the embedded and space fixed frames as follows:

$$\overrightarrow{\boldsymbol{g}_X} = \vec{\boldsymbol{f}}\mathrm{R}(\zeta_X) = \vec{\boldsymbol{e}}\mathrm{R}(\alpha,\beta)\mathrm{R}(\zeta_X) \quad \text{(A59)}$$

and since $\vec{\boldsymbol{f}}$ is a noninertial frame, the kinetic energy expressions for the rigid rotors constituting the dimer must be revised. More specifically, for an arbitrary vector $\boldsymbol{r}$ we write

$$\dot{\mathrm{R}}(\alpha,\beta)\boldsymbol{r} = \mathrm{R}(\alpha,\beta)\begin{pmatrix} 0 & -\dot{\alpha}\cos\beta & \dot{\beta} \\ \dot{\alpha}\cos\beta & 0 & \dot{\alpha}\sin\beta \\ -\dot{\beta} & -\dot{\alpha}\sin\beta & 0 \end{pmatrix}\boldsymbol{r} \equiv \mathrm{R}(\alpha,\beta)\boldsymbol{\omega}_R \times \quad \text{(A60)}$$

where, with $\boldsymbol{\varrho} \equiv (\beta, \alpha)$

$$\boldsymbol{\omega}_R = \begin{pmatrix} -\dot{\alpha}\sin\beta \\ \dot{\beta} \\ \dot{\alpha}\cos\beta \end{pmatrix} = \mathrm{Y}\dot{\boldsymbol{\varrho}} \quad \text{and} \quad \mathrm{Y} = \begin{pmatrix} 0 & -\sin\beta \\ 1 & 0 \\ 0 & \cos\beta \end{pmatrix} \quad \text{(A61)}$$

So, we get an extra angular velocity component which must be added to the angular velocities $\boldsymbol{\omega}_X$ of the tops with respect to the frame $\vec{\boldsymbol{f}}$ obtained in the usual manner from $\dot{\mathrm{R}}(\zeta_X)$. Hence by an easy extension of the usual rigid rotor theory (ref 245, sections 4–9) the classical kinetic energy of X takes the form

$$2T_X = (\mathrm{M}_X\dot{\boldsymbol{\zeta}}_X + \mathrm{Y}\dot{\boldsymbol{\varrho}})^T \mathrm{I}_X(\mathrm{M}_X\dot{\boldsymbol{\zeta}}_X + \mathrm{Y}\dot{\boldsymbol{\varrho}}), \quad X = A, B \quad \text{(A62)}$$

The inertia tensor is defined in eq A58, *i.e.* it has the form of eq A25 with the particle coordinates expressed with respect to $\vec{\boldsymbol{f}}$. The matrix M_X is defined in eq A26, with the suffix X reminding us that it depends on ζ_X.

The kinetic energy T_{AB} has the diatom form, *cf.* eqs. A1 and A13:

$$2T_{AB} = \mu_{AB}\dot{R}^2 + \dot{\boldsymbol{\varrho}}^T \mathrm{K}\dot{\boldsymbol{\varrho}} \quad \text{where} \quad \mathrm{K} = \mu_{AB}\begin{pmatrix} R^2 & 0 \\ 0 & R^2\sin^2\beta \end{pmatrix} \quad \text{(A63)}$$

Combining eqs A54, A62, and A63 we obtain for the dimer

$$2T = \mu_{AB}\dot{R}^2 + (\dot{\boldsymbol{\varrho}}^T, \dot{\boldsymbol{\zeta}}_A^T, \dot{\boldsymbol{\zeta}}_B^T) \begin{pmatrix} \mathrm{K} + \mathrm{Y}^T(\mathrm{I}_A + \mathrm{I}_B)\mathrm{Y} & \mathrm{Y}^T\mathrm{I}_A\mathrm{M}_A & \mathrm{Y}^T\mathrm{I}_B\mathrm{M}_B \\ \mathrm{M}_A^T\mathrm{I}_A\mathrm{Y} & \mathrm{M}_A^T\mathrm{I}_A\mathrm{M}_A & \mathrm{O} \\ \mathrm{M}_B^T\mathrm{I}_B\mathrm{Y} & \mathrm{O} & \mathrm{M}_B^T\mathrm{I}_B\mathrm{M}_B \end{pmatrix} \begin{pmatrix} \dot{\boldsymbol{\varrho}} \\ \dot{\boldsymbol{\zeta}}_A \\ \dot{\boldsymbol{\zeta}}_B \end{pmatrix} \quad \text{(A64)}$$

which defines the angular part G of the metric tensor. According to the Beltrami expression A6 we must invert this tensor, which is most easily done by the Frobenius formula (ref 248, p 73) for the inverse of block matrices. Thus we find

$$\mathrm{G}^{-1} = \begin{pmatrix} \mathrm{E} & \mathrm{O} & \mathrm{O} \\ \mathrm{O} & \mathrm{M}_A^{-1} & \mathrm{O} \\ \mathrm{O} & \mathrm{O} & \mathrm{M}_B^{-1} \end{pmatrix} \begin{pmatrix} \mathrm{K}^{-1} & -\mathrm{K}^{-1}\mathrm{Y}^T & -\mathrm{K}^{-1}\mathrm{Y}^T \\ -\mathrm{Y}\mathrm{K}^{-1} & \mathrm{I}_A^{-1} + \mathrm{Y}\mathrm{K}^{-1}\mathrm{Y}^T & \mathrm{Y}\mathrm{K}^{-1}\mathrm{Y}^T \\ -\mathrm{Y}\mathrm{K}^{-1} & \mathrm{Y}\mathrm{K}^{-1}\mathrm{Y}^T & \mathrm{I}_B^{-1} + \mathrm{Y}\mathrm{K}^{-1}\mathrm{Y}^T \end{pmatrix} \begin{pmatrix} \mathrm{E} & \mathrm{O} & \mathrm{O} \\ \mathrm{O} & \mathrm{M}_A^{-1} & \mathrm{O} \\ \mathrm{O} & \mathrm{O} & \mathrm{M}_B^{-1} \end{pmatrix}^T \quad \text{(A65)}$$

The determinant of a block matrix can also be calculated (ref 248, p 71), we find that $\det(\mathrm{G}) = \det(\mathrm{M}_A)^2 \det(\mathrm{M}_B)^2 \det(\mathrm{K}) \propto R^4 \sin^2\theta_A \sin^2\theta_B \sin^2\beta$; the proportionality factor is a product of the inertia moments of the monomers and the reduced dimer mass. The classical kinetic energy in Hamilton form becomes:

$$2T = \frac{P^2}{\mu_{AB}} + \boldsymbol{p}_A^T\mathrm{M}_A^{-1}\mathrm{I}_A^{-1}(\mathrm{M}_A^{-1})^T\boldsymbol{p}_A + \boldsymbol{p}_B^T\mathrm{M}_B^{-1}\mathrm{I}_B^{-1}(\mathrm{M}_B^{-1})^T\boldsymbol{p}_B + [\boldsymbol{\pi}_\varrho^T - \boldsymbol{p}_A^T\mathrm{M}_A^{-1}\mathrm{Y} - \boldsymbol{p}_B^T\mathrm{M}_B^{-1}\mathrm{Y}]\mathrm{K}^{-1}[\boldsymbol{\pi}_\varrho - \mathrm{Y}^T(\mathrm{M}_A^{-1})^T\boldsymbol{p}_A - \mathrm{Y}^T(\mathrm{M}_B^{-1})^T\boldsymbol{p}_B] \quad \text{(A66)}$$

where $\boldsymbol{\pi}_\varrho$ is conjugate to $\boldsymbol{\varrho} \equiv (\beta, \alpha)$ and $\boldsymbol{p}_X$ to ζ_X.

In eq A57 we saw that the Hamiltonian becomes very simple when expressed in terms of angular momenta; we will see that the same is true for the corresponding quantum mechanical expression. In order to make the transition to quantum mechanics we must express the classical angular momenta in terms of linear momenta conjugate to the coordinates. It follows directly from eq A64 that

$$\boldsymbol{\pi}_\varrho = \mathrm{K}\dot{\boldsymbol{\varrho}} + \mathrm{Y}^T\sum_X \mathrm{I}_X(\mathrm{M}_X\dot{\boldsymbol{\zeta}}_X + \mathrm{Y}\dot{\boldsymbol{\varrho}}) \quad \text{(A67)}$$

$$\boldsymbol{p}_X = \mathbb{M}_X^T \mathbb{I}_X (\mathbb{M}_X \dot{\boldsymbol{\xi}}_X + \mathbb{Y}\dot{\boldsymbol{\varrho}}) \tag{A68}$$

It is not difficult to show with the use of eqs A26 and A61 that the angular momentum of X expressed with respect to the embedded frame is

$$\overrightarrow{j_X} = \vec{f}\, \mathbb{I}_X(\boldsymbol{\omega}_X + \boldsymbol{\omega}_R) = \vec{f}\, \mathbb{I}_X(\mathbb{M}_X \dot{\boldsymbol{\xi}}_X + \mathbb{Y}\dot{\boldsymbol{\varrho}}) \tag{A69}$$

from which follows by the use of eq A68 and the definition A28

$$\overrightarrow{j_X} = \vec{f}(\mathbb{M}_X^{-1})^T \boldsymbol{p}_X \equiv \vec{f}\, \boldsymbol{j}_X \tag{A70}$$

Incidentally, this proves that $\boldsymbol{j}_X$ indeed rotates as a vector, which we already used to arrive at eq A57. Substitution of eq A69 into eq A67 gives

$$\boldsymbol{\pi}_\varrho = \mathbb{K}\dot{\boldsymbol{\varrho}} + \mathbb{Y}^T(\boldsymbol{j}_A + \boldsymbol{j}_B) \tag{A71}$$

From eq A19, eq A14, and the definitions of $\mathbb{K}$ and $\mathbb{Y}$ we obtain

$$\mathbb{Y}^T \boldsymbol{l}^{\mathrm{BF}} = \begin{pmatrix} p_\beta \\ p_\alpha \end{pmatrix} = \mathbb{K}\dot{\boldsymbol{\varrho}} \tag{A72}$$

From $\vec{J} \equiv \vec{l} + \overrightarrow{j_A} + \overrightarrow{j_B}$, where $\vec{J}$ is a constant of the motion, we conclude that

$$\boldsymbol{\pi}_\varrho = \mathbb{Y}^T(\boldsymbol{l}^{\mathrm{BF}} + \boldsymbol{j}_A + \boldsymbol{j}_B) = \mathbb{Y}^T \boldsymbol{J} \tag{A73}$$

From the definition of $\mathbb{Y}$ and upon noting that $J_z = j_{Az} + j_{Bz}$, since $l_z^{\mathrm{BF}} = 0$, we find

$$\begin{cases} J_x = -\sin^{-1}\beta\, \pi_\alpha + \cot\beta(j_{Az} + j_{Bz}) \\ J_y = \pi_\beta \\ J_z = j_{Az} + j_{Bz} \end{cases} \tag{A74}$$

The quantum mechanical form of the operators $\boldsymbol{j}_X$ is obtained by replacing in eq A70 p_{X1} by $-i\hbar\, \partial/\partial\phi_X$, etc. This shows that these operators have the space-fixed form of eq A29, but with the Euler angles of the rotors referring to the embedded frame. The equations A74 give the quantum mechanical form of J_x, J_y, and J_z, the projections of the total angular momentum on the embedded axes. Just as in the diatom case in Appendix A.1, these projections do not satisfy the usual angular momentum commutation relations (eq A30), nor the anomalous ones (eq A37), which is why Brocks *et al.*[18] refer to them as pseudoangular momentum operators. Observe that $\boldsymbol{J}$ is the sum of the angular momentum of the "diatom" $A-B$ and the effective angular momentum $(\cot\beta(j_{Az} + j_{Bz}), 0, j_{Az} + j_{Bz})$, which arises from the motion of the rigid rotors. Because of the presence of $\sin\beta$ in the volume element, the operator J_y is not Hermitian. The quantum mechanical expression for the operator $\boldsymbol{l}^{\mathrm{BF}}$ follows from $\boldsymbol{l}^{\mathrm{BF}} = \boldsymbol{J} - \boldsymbol{j}_A - \boldsymbol{j}_B$.

The kinetic energy becomes by substitution of eqs A70 and A73 into eq A66 and remembering that $J_z - j_{Az} - j_{Bz} = 0$

$$2T = \frac{1}{\mu_{AB}}\left[P^2 + \frac{(J_x - j_{Ax} - j_{Bx})^2 + (J_y - j_{Ay} - j_{By})^2}{R^2}\right] + 2T_A + 2T_B$$

When evaluating the kinetic energy operator we can follow the route that led to this classical Hamiltonian with one modification: we must insert $[\det(\mathbb{G})]^{1/2}$ at two places in accordance with eq A6. Because of eq A31 the factors $\sin\theta_A$ and $\sin\theta_B$ drop out of the expressions, but $\sin\beta$ gives an extra term not present in the classical kinetic energy. Using

$$\sum_i [J_i, \sin\beta] = [J_y, \sin\beta] = [\pi_\beta, \sin\beta] = -i\hbar\cos\beta \tag{A75}$$

we find

$$2T = \frac{1}{\mu_{AB}R^2}\left[-\hbar^2 \frac{\partial}{\partial R} R^2 \frac{\partial}{\partial R} + (J_x - j_{Ax} - j_{Bx})^2 + (J_y - j_{Ay} - j_{By})^2 - i\hbar\cot\beta(J_y - j_{Ay} - j_{By})\right] + 2T_A + 2T_B \tag{A76}$$

By the definition of $\boldsymbol{J}$, eq A74, and the angular momentum commutation relations in eq A30 it is readily derived that

$$(J_x - j_{Ax} - j_{Bx})^2 + (J_y - j_{Ay} - j_{By})^2 = J^2 + (\boldsymbol{j}_A + \boldsymbol{j}_B)^2 - 2(\boldsymbol{j}_A + \boldsymbol{j}_B)\cdot\boldsymbol{J} - i\hbar\cot\beta(j_{Ay} + j_{By}) \tag{A77}$$

Note that $J^2 \equiv J_x^2 + J_y^2 + J_x^2$ is not the operator representing $|\vec{J}|^2$, since it gives the total angular momentum with respect to the embedded frame. Defining

$$\boldsymbol{J}^{\mathrm{SF}} \equiv \mathbb{R}(\alpha,\beta)\boldsymbol{J} \tag{A78}$$

we can show as for the orbital angular momentum, eq A22, that

$$(J^{\mathrm{SF}})^2 = J^2 - i\hbar\cot\beta J_y \tag{A79}$$

From eq A74 it follows then that $(J^{\mathrm{SF}})^2$ has the rigid rotor form

$$(J^{\mathrm{SF}})^2 = -\frac{\hbar^2}{\sin^2\beta}\left[\frac{\partial^2}{\partial\alpha^2} + \frac{\partial^2}{\partial\gamma^2} - 2\cos\beta\frac{\partial^2}{\partial\alpha\partial\gamma}\right] - \frac{\hbar^2}{\sin\beta}\frac{\partial}{\partial\beta}\sin\beta\frac{\partial}{\partial\beta} \tag{A80}$$

with $\gamma \equiv (\phi_A + \phi_B)/2$. The kinetic energy in the embedded frame can finally be written as

$$2T = \frac{1}{\mu_{AB}R^2}\left[-\hbar^2\frac{\partial}{\partial R}R^2\frac{\partial}{\partial R} + (J^{\mathrm{SF}})^2 + (\boldsymbol{j}_A + \boldsymbol{j}_B)^2 - 2(\boldsymbol{j}_A + \boldsymbol{j}_B)\cdot\boldsymbol{J}\right] + 2T_A + 2T_B \tag{A81}$$

We are free to write T_A and T_B in the principal axes form of eq A39, but notice that the angular momenta $\boldsymbol{j}_A^{\mathrm{BF}}$ and $\boldsymbol{j}_B^{\mathrm{BF}}$ in this expression are not the operators $\boldsymbol{j}_A$ and $\boldsymbol{j}_B$ appearing in eq A81. The latter are given by eq A70, that is, they have the space-fixed form of eq A29.

In the calculation of matrix elements of the Hamiltonian A81 it is convenient to introduce step operators. Writing $j_m = j_{Am} + j_{Bm}$, $(m = +, z, -)$, we define these by

$$j_\pm = j_x \pm ij_y \quad \text{and} \quad J_\pm = J_x \mp iJ_y \qquad \text{(A82)}$$

The Coriolis interaction then takes the form

$$2(\boldsymbol{j}_A + \boldsymbol{j}_B)\cdot\boldsymbol{J} = 2\boldsymbol{j}\cdot\boldsymbol{J} = 2j_zJ_z + j_+J_+ + j_-J_- \qquad \text{(A83)}$$

Notice that $J_z = j_z$ commutes with the whole Hamiltonian (eq A81), except with the last two terms of eq A83, the off-diagonal Coriolis interaction. The "pseudoshift" operators $J_\mp$ follow from eq A74. The usual body-fixed step operators $J_\pm$ follow from eq A52. Comparison of the pseudo- and body-fixed step operators shows the following relation, which we note for future reference

$$J_\pm = e^{\mp i\gamma}(J_x^{BF} \mp iJ_y^{BF}) \equiv e^{\mp i\gamma}J_\pm^{BF} \qquad \text{(A84)}$$

B. Angular Basis Functions

When using the irreducible matrices $\mathrm{D}^{(j)}(\alpha,\beta,\gamma)$, which represent the full rotation group $SO(3)$, one must be aware of different conventions used by different authors. In the first place, some authors rotate the reference frame (the "passive" convention) and others rotate the molecule (the "active" convention). Secondly, two Euler parametrizations are in common use: the *zxz* and the *zyz* convention. In the first case one rotates around the z, x', and z'' axes, successively, and in the second case around the z, y', and z'' axes. The third point to be noted is whether the three-dimensional rotations are mapped homomorphically ("Wigner's convention") or anti-homomorphically onto Hilbert space operators. A final point of concern is the phase of the kets carrying the irrep of $SO(3)$. Since we consider only integer quantum numbers in this work, this is tantamount to specifying the phases of the spherical harmonic functions. The physics literature seems to converge to the following convention: (i) active rotations, (ii) *zyz* Euler angles, (iii) Wigner's convention, and (iv) Condon and Shortley[249] phases for spherical harmonics. Making these choices, we define the Wigner rotation matrix depending on the Euler angles $0 \le \alpha < 2\pi$, $0 \le \beta \le \pi$, and $0 \le \gamma < 2\pi$ as follows

$$D^{(j)}_{m'm}(\alpha,\beta,\gamma) = \mathrm{e}^{-im'\alpha}d^{(j)}_{m'm}(\beta)\mathrm{e}^{-im\gamma} \qquad \text{(B1)}$$

The functions $d^{(j)}_{m'm}(\beta)$ were first derived by Wigner[250] by means of a simple group theoretical argument,

$$d^{(j)}_{m'm}(\beta) = [(j+m')!(j-m')!(j+m)!(j-m)!]^{1/2}\sum_s (-1)^{m'-m+s} \frac{\left(\cos\frac{\beta}{2}\right)^{2j+m-m'-2s}\left(\sin\frac{\beta}{2}\right)^{m'-m+2s}}{(j+m-s)!s!(m'-m+s)!(j-m'-s)!} \qquad \text{(B2)}$$

where s runs over all possible values such that the factorials are nonnegative. The complex conjugates of these functions satisfy the relations

$$j_z^{SF}D^{(j)}_{m'm}(\alpha,\beta,\gamma)^* = \hbar m' D^{(j)}_{m'm}(\alpha,\beta,\gamma)^* \qquad \text{(B3)}$$

$$(j_x^{SF} \pm ij_y^{SF})D^{(j)}_{m'm}(\alpha,\beta,\gamma)^* = \hbar\sqrt{j(j+1) - m'(m'\pm 1)}\,D^{(j)}_{m'\pm1,m}(\alpha,\beta,\gamma)^* \qquad \text{(B4)}$$

where the space-fixed angular momentum operators are defined in eq A29, with $\phi \leftrightarrow \alpha$, $\theta \leftrightarrow \beta$, and $\psi \leftrightarrow \gamma$. Note that the operators representing the components of the angular momentum along the space-fixed axes act on the first (row) index of the D matrix. The body-fixed operators of eq A52 act on the second (column) index

$$j_z^{BF}D^{(j)}_{m'm}(\alpha,\beta,\gamma)^* = \hbar m D^{(j)}_{m'm}(\alpha,\beta,\gamma)^* \qquad \text{(B5)}$$

$$(j_x^{BF} \mp ij_y^{BF})D^{(j)}_{m'm}(\alpha,\beta,\gamma)^* = \hbar\sqrt{j(j+1) - m(m\pm 1)}\,D^{(j)}_{m'm\pm1}(\alpha,\beta,\gamma)^* \qquad \text{(B6)}$$

where the role of the step-up and step-down operators is interchanged due to the anomalous commutation relation A37. From eqs B3 to B6 we find

$$(j^{BF})^2D^{(j)}_{m'm}(\alpha,\beta,\gamma)^* = (j^{SF})^2D^{(j)}_{m'm}(\alpha,\beta,\gamma)^* = \hbar^2 j(j+1)D^{(j)}_{m'm}(\alpha,\beta,\gamma)^* \qquad \text{(B7)}$$

i.e., the complex conjugates of the D matrices are simultaneous eigenfunctions of the commuting operators $(j^{SF})^2 = (j^{BF})^2$, j_z^{SF}, and j_z^{BF}. Since the symmetric top Hamiltonian can be written as $A(j^{BF})^2 + (C-A)(j_z^{BF})^2$ (*cf.* eq A39) it follows that the complex conjugate D matrices are eigenfunctions of this Hamiltonian, which is why they are often referred to as symmetric top functions.

The D matrices are orthogonal and normalizable:

$$\int_0^{2\pi}\int_0^{\pi}\int_0^{2\pi} \sin\beta\,\mathrm{d}\alpha\,\mathrm{d}\beta\,\mathrm{d}\gamma\; D^{(j)}_{m'm}(\alpha,\beta,\gamma)D^{(j')}_{\mu'\mu}(\alpha,\beta,\gamma)^* = \delta_{jj'}\,\delta_{m\mu}\,\delta_{m'\mu'}\frac{8\pi^2}{2j+1} \qquad \text{(B8)}$$

We recognize this as the great orthogonality relation applied to the full rotation group $SO(3)$. Furthermore, by the Peter–Weyl theorem (ref 251, section 7.2) the D matrices are complete on the Hilbert space $L^2[SO(3)]$.

From the completeness of the symmetric top functions follows by a simple argument (ref 251, p 160) the completeness of the functions $d^{(j)}_{m'm}(\beta)$ on the Hilbert space $L^2[0,\pi]$, [arbitrarily fixed m and m', j running: $j \ge \max(|m|, |m'|)$]. By the same argument it can be shown that the functions $D^{(j)}_{m'm}(\alpha,\beta,0)^*$ are complete with arbitrary fixed m and running j and m'. In particular it follows that the set

$$D^{(j)}_{m0}(\alpha,\beta,0)^* = C^j_m(\beta,\alpha) = \sqrt{\frac{4\pi}{2j+1}}Y^j_m(\beta,\alpha) \qquad \text{(B9)}$$

is complete.

Let us consider an angular basis for two rotors with Euler angles $\zeta_X \equiv (\phi_X,\theta_X,\psi_X)$, $X = A, B$, with respect to the two-angle embedded frame introduced in Appendix A.4. From the previous remarks it follows that

$$D^{(j_A)}_{m_Ak_A}(\zeta_A)^*\,D^{(j_B)}_{m_Bk_B}(\zeta_B)^*\,D^{(l)}_{mk}(\alpha,\beta,0)^* \qquad \text{(B10)}$$

forms a complete set, when all indices—except k—are running. The value of k may be chosen arbitrarily. This set is larger than necessary for use in variational calculations on the dimer, since it includes all different eigenfunctions of the total dimer angular momentum and its projection onto the space-fixed z axis. Because of the isotropy of space these two quantities are constants of the motion. To take advantage of this we first define, using Dirac's notation,

$$\langle\zeta_A,\zeta_B|j_A,k_A,j_B,k_B,j_{AB},m_{AB}\rangle \equiv \langle\zeta_A,\zeta_B|\{\Lambda\}m_{AB}\rangle \equiv \sum_{m_Am_B}\langle j_{AB}m_{AB}|j_Am_A;j_Bm_B\rangle D^{(j_A)}_{m_Ak_A}(\zeta_A)^* D^{(j_B)}_{m_Bk_B}(\zeta_B)^* \quad \text{(B11)}$$

where $\langle..|..;..\rangle$ is a Clebsch–Gordan coefficient and $\{\Lambda\} \equiv (j_A,k_A,j_B,k_B,j_{AB})$. Further we define space-fixed angles for the rotors

$$\mathbb{R}(\zeta_X^{SF}) = \mathbb{R}_z(\alpha)\mathbb{R}_y(\beta)\mathbb{R}(\zeta_X) \leftrightarrow |\zeta_X^{SF}\rangle = \mathscr{R}(\alpha,\beta)|\zeta_X\rangle \quad \text{(B12)}$$

where $\mathscr{R}(\alpha,\beta)$ is unitary. In Dirac notation

$$\langle\hat{\boldsymbol{R}}|lm\rangle \equiv C^l_m(\beta,\alpha) \quad \text{with} \quad \hat{\boldsymbol{R}} \equiv (\beta,\alpha) \quad \text{(B13)}$$

and

$$\langle\hat{\boldsymbol{R}}|\mathscr{R}(\alpha,\beta)|lm\rangle = \langle(0,0)|lm\rangle = C^l_m(0,0) = \delta_{m0} \quad \text{(B14)}$$

Let $|\{\Lambda\}JM\rangle$ be an eigenket of the total angular momentum $(J^{SF})^2$ and its projection J_z^{SF} on the space-fixed z axis obtained by vector coupling

$$|\{\Lambda\}JM\rangle = \sum_{m_{AB}m}|\{\Lambda\}m_{AB}\rangle|lm\rangle\langle j_{AB}m_{AB};lm|JM\rangle \quad \text{(B15)}$$

By the definition of vector coupling and the unitarity of the D matrix, we get

$$\mathscr{R}(\alpha,\beta)^{-1}|\{\Lambda\}JM\rangle = \sum_K|\{\Lambda\}JK\rangle D^{(J)}_{MK}(\alpha,\beta,0)^* \quad \text{(B16)}$$

We now transform from space-fixed to embedded coordinates as follows, where we use eqs B12, B16, and B14, respectively

$$\begin{aligned}\langle\zeta_A^{SF},\zeta_B^{SF},\hat{\boldsymbol{R}}|\{\Lambda\}JM\rangle &= \langle\zeta_A^{SF},\zeta_B^{SF},\hat{\boldsymbol{R}}|\mathscr{R}(\alpha,\beta)\mathscr{R}(\alpha,\beta)^{-1}|\{\Lambda\}JM\rangle \\ &= \sum_K\langle\zeta_A,\zeta_B,(0,0)|\{\Lambda\}JK\rangle D^{(J)}_{MK}(\alpha,\beta,0)^* \\ &= \sum_K\langle\zeta_A,\zeta_B|\{\Lambda\}K\rangle D^{(J)}_{MK}(\alpha,\beta,0)^*\langle j_{AB}K;l0|JK\rangle\end{aligned} \quad \text{(B17)}$$

This shows that the representations of the eigenket $|\{\Lambda\}JM\rangle$ in space-fixed and embedded coordinates are related linearly. In a variational calculation such a linear combination serves no purpose and one often uses the uncontracted basis functions, defined with respect to the embedded frame

$$D^{(J)}_{MK}(\alpha,\beta,0)^*\langle\zeta_A,\zeta_B|\{\Lambda\}K\rangle \equiv D^{(J)}_{MK}(\alpha,\beta,0)^* \times \sum_{m_Am_B}\langle j_{AB}K|j_Am_A;j_Bm_B\rangle D^{(j_A)}_{m_Ak_A}(\zeta_A)^*D^{(j_B)}_{m_Bk_B}(\zeta_B)^* \quad \text{(B18)}$$

which are also eigenstates of $(J^{SF})^2$ and J_z^{SF}. An advantage of these basis functions over the space-fixed basis in eq B17 is that they are simultaneously eigenstates of J_z, with eigenvalue K.

We end by saying a few words about the calculation of kinetic energy matrix elements between the basis functions B18. Since

$$m_A\phi_A + m_B\phi_B = (^1/_2)(\phi_A + \phi_B)(m_A + m_B) + (^1/_2)(\phi_A - \phi_B)(m_A - m_B) \quad \text{(B19)}$$

and $m_A + m_B = K$, by virtue of a selection rule on the Clebsch–Gordan coefficient in eq B18, we see that the basis functions contain the factor $\exp(iK\gamma)$ with $\gamma = (\phi_A + \phi_B)/2$. When operating with $(J^{SF})^2$, appearing in the Hamiltonian A81, it is convenient to transfer this factor to the first D matrix, writing it as $D^{(J)}_{MK}(\alpha,\beta,\gamma)^*$, after which eq B7 may be used. In order to act with the pseudoshift operators, defined in eq A82, we use their relation to the regular body-fixed step operators, eq A84, and find

$$J_\pm D^{(J)}_{MK}(\alpha,\beta,\gamma)^* = \hbar\sqrt{(J(J+1) - K(K\pm1)}e^{\mp i\gamma}D^{(J)}_{MK\pm1}(\alpha,\beta,\gamma)^* \quad \text{(B20)}$$

C. Symmetry

In this appendix we will discuss a few of the symmetry aspects that play a role in the study of van der Waals molecules. Let us first consider an atom–diatom system from a purely geometric point of view, *i.e.*, without introducing a coordinate frame. It consists of three atoms located at points A, B, and C, respectively. Let O be an arbitrary point and M be the center of mass of the diatom. The vector $\overrightarrow{OP}$, ($P = A$, B, C, or M) points from point O to point P. Obviously

$$\vec{r} \equiv \overrightarrow{AB} = \overrightarrow{OB} - \overrightarrow{OA} \quad \text{(C1)}$$

$$\vec{R} \equiv \overrightarrow{MC} = \overrightarrow{OC} - \overrightarrow{OM} \quad \text{(C2)}$$

Space inversion of an arbitrary point P with respect to the point O is defined by

$$E^*: \overrightarrow{OP} \rightarrow -\overrightarrow{OP} \quad \text{(C3)}$$

and so

$$E^*: \begin{cases}\vec{r} \rightarrow -\vec{r} \\ \vec{R} \rightarrow -\vec{R}\end{cases} \quad \text{(C4)}$$

Assume now that the atoms A and B are identical, so that the permutation P_{AB} of A and B is a symmetry operation and M is at the midpoint of the diatom A–B. Since neither M nor C are touched by P_{AB} the vector $\vec{R}$ is symmetric under P_{AB}. It follows directly from the definition of $\vec{r}$, eq C1, that this vector changes sign under P_{AB}.

Next we take the point O at the dimer center of mass and erect an arbitrarily oriented space-fixed frame at O

$$\vec{e} = (\vec{e_x}, \vec{e_y}, \vec{e_z}) \tag{C5}$$

What happens with the space-fixed coordinates of $\vec{R}$ and $\vec{r}$ ($\boldsymbol{R}^{SF}$ and $\boldsymbol{r}^{SF}$, respectively) under the two symmetry operations E^* and P_{AB}? To answer this question, we note that these operations, as defined above, are *active*, that is, the frame $\vec{e}$ does not change under these operations. The space-fixed Cartesian coordinates therefore transform as

$$E^*: \begin{cases} \boldsymbol{r}^{SF} \rightarrow -\boldsymbol{r}^{SF} \\ \boldsymbol{R}^{SF} \rightarrow -\boldsymbol{R}^{SF} \end{cases} \qquad P_{AB}: \begin{cases} \boldsymbol{r}^{SF} \rightarrow -\boldsymbol{r}^{SF} \\ \boldsymbol{R}^{SF} \rightarrow \boldsymbol{R}^{SF} \end{cases} \tag{C6}$$

Let $(r,\theta^{SF},\phi^{SF})$ be the polar coordinates of $\boldsymbol{r}^{SF}$ and let (R,β,α) be the same of $\boldsymbol{R}^{SF}$. The following symmetry properties are easily derived

$$E^*: \begin{cases} r \rightarrow r \\ \theta^{SF} \rightarrow \pi - \theta^{SF} \\ \phi^{SF} \rightarrow \pi + \phi^{SF} \end{cases} \qquad E^*: \begin{cases} R \rightarrow R \\ \beta \rightarrow \pi - \beta \\ \alpha \rightarrow \pi + \alpha \end{cases} \tag{C7}$$

The operation P_{AB} leaves β and α invariant and transforms θ^{SF} and ϕ^{SF} in the same way as E^*. In Table 1 we find the transformations of the angular functions under these substitutions.

So far the development is completely straightforward, but in the dimer-embedded frame more care is required, as this frame is not invariant under the two symmetry operations—in contrast to the space-fixed frame. In order to show this, we first recall the definition of the rotation matrices, *cf.* eqs A11, and the definition, eq A17, of the dimer frame

$$\vec{f} \equiv \vec{e}\ \mathbb{R}_z(\alpha)\mathbb{R}_y(\beta) \tag{C8}$$

By direct matrix multiplication the following useful rules are easily proved

$$\mathbb{R}_x(\pi)\mathbb{R}_y(\pi) = \mathbb{R}_z(\pi) \tag{C9a}$$

$$\mathbb{R}_x(\pi)\mathbb{R}_y(-\gamma) = \mathbb{R}_y(\gamma)\mathbb{R}_x(\pi) \tag{C9b}$$

$$\mathbb{R}_x(\gamma)\mathbb{R}_x(\gamma') = \mathbb{R}_x(\gamma + \gamma') \tag{C9c}$$

The same relations hold also with x, y, and z permuted.

Substitute now the angles (eq C7) transformed by E^* into eq C8 defining the dimer-embedded frame, and rewrite the ensuing matrix equation by the rules just stated:

$$\begin{aligned} \mathbb{R}_z(\pi + \alpha)\mathbb{R}_y(\pi - \beta) &= \mathbb{R}_z(\alpha)\mathbb{R}_z(\pi)\mathbb{R}_y(\pi)\mathbb{R}_y(-\beta) \\ &= \mathbb{R}_z(\alpha)\mathbb{R}_y(\beta)\mathbb{R}_x(\pi) \end{aligned} \tag{C10}$$

Hence we find that the dimer frame $\vec{f}$ transforms under E^* as

$$E^*: \vec{f} \rightarrow \vec{f}\ \mathbb{R}_x(\pi) \tag{C11}$$

Bunker[108] refers to $\mathbb{R}_x(\pi)$ as the equivalent rotation of E^*. Since β and α are invariant under P_{AB}, the dimer frame itself is also invariant under this permutation.

Consider next how the dimer-embedded coordinates transform

$$E^*: \vec{r} = \vec{f}\boldsymbol{r} \rightarrow -\vec{r} = \vec{f}\mathbb{R}_x(\pi)\boldsymbol{r}' \tag{C12}$$

so that

$$\boldsymbol{r}' = -\mathbb{R}_x(\pi)\boldsymbol{r} \quad \text{or} \quad E^*: \boldsymbol{r} \rightarrow -\mathbb{R}_x(\pi)\boldsymbol{r} \tag{C13}$$

For the elements x, y, z of $\boldsymbol{r}$ and its spherical polar coordinates this gives

$$\boldsymbol{r}' = \begin{pmatrix} -x \\ y \\ z \end{pmatrix} \quad \text{and} \quad E^*: \begin{cases} r \rightarrow r \\ \theta \rightarrow \theta \\ \phi \rightarrow \pi - \phi \end{cases} \tag{C14}$$

so that E^* is equivalent to a reflection of $\vec{r}$ in the yz plane of the dimer frame.

The dimer-frame coordinates

$$\boldsymbol{R} \equiv \begin{pmatrix} 0 \\ 0 \\ R \end{pmatrix}$$

of $\vec{R}$ are invariant under E^* as well as under P_{AB}. Since the frame $\vec{f}$ is invariant under P_{AB}, it follows straightforwardly for the dimer-frame coordinates of $\vec{r}$ that

$$P_{AB}: \begin{cases} r \rightarrow r \\ \theta \rightarrow \pi - \theta \\ \phi \rightarrow \pi + \phi \end{cases} \tag{C15}$$

Before leaving the atom−diatom case we wish to point out that E^* is a feasible operation of the first kind, because the intermolecular potential does not depend on ϕ and E^* only affects ϕ, *cf.* eq C14. However, P_{AB} gives a tunneling through a possible barrier in θ, see eq C15. Depending on the height of this barrier P_{AB} may, or may not, be feasible. Given the weakness of van der Waals forces, the barrier will in general be so low that the permutation is feasible and the symmetry group of the atom−homonuclear diatom system is of order 4 and isomorphic to C_{2v}.

In the case of a van der Waals molecule containing nonlinear monomers X, we must choose right-handed frames $\vec{g}_X$ attached to the monomers and specify the Euler angles of these frames with respect to another right-handed frame. This latter frame is in practice either a space-fixed frame $\vec{e}$ or a dimer-embedded frame $\vec{f}$. If a monomer is rigid, any body-fixed frame will do, because in that case the only feasible permutation inversions are of the first kind and equivalent to proper rotations. Recalling that a proper rotation conserves the handedness of a frame, this means that the feasible monomer permutation inversions transform the Euler angles of a rigid monomer in a well-defined way. If, however, the monomer is not (nearly) rigid, or in other words feasible operations of the second kind must be considered, then special care in defining the molecule frame must be taken. For instance, the well-known ammonia (umbrella) inversion transforms a right-handed monomer Eckart frame into a left-handed one, so that the effect of this inversion on the Euler angles of an Eckart frame cannot be defined. In such a case it is better to use the construction that is commonly applied to planar molecules, which consists

of choosing two orthonormal body-fixed vectors, say $\vec{g}_x$ and $\vec{g}_y$, and define the third as the vector product: $\vec{g}_z = \vec{g}_x \times \vec{g}_y$. In that case the frame is right-handed by definition, all the feasible permutation inversions are equivalent to rotations of the monomer and their effect on the Euler angles can be given.

We will now exemplify the procedure on the argon–ammonia van der Waals molecule[8] and start by reviewing briefly the symmetry of the free ammonia. Let M be the center of mass of NH_3 and let the protons be H_1, H_2, and H_3. The following is a body-fixed frame attached to ammonia:

$$\vec{g}_x = \sqrt{1/6}(2\vec{MH}_1 - \vec{MH}_2 - \vec{MH}_3) \quad \text{(C16a)}$$

$$\vec{g}_y = \sqrt{1/2}(\vec{MH}_2 - \vec{MH}_3) \quad \text{(C16b)}$$

$$\vec{g}_z = \vec{g}_x \times \vec{g}_y \quad \text{(C16c)}$$

This frame is not necessarily orthonormal, but if we impose the constraints that the N–H bond lengths and the HNH angles stay equal, then the frame becomes orthogonal and can be normalized. It is important to note that the normalization of $\vec{g}_x$ and $\vec{g}_y$ is equal, so that the frame as it stands can be used to derive the effects of the monomer permutation inversions. By some simple algebra it can be derived that

$$(123)\vec{\boldsymbol{g}} = \vec{\boldsymbol{g}}\, \mathbb{R}_z(-2\pi/3) \quad \text{(C17)}$$

$$(23)\vec{\boldsymbol{g}} = \vec{\boldsymbol{g}}\, \mathbb{R}_x(\pi) \quad \text{(C18)}$$

The vectors $\vec{g}_x$ and $\vec{g}_y$ change sign under E^* and the vector product $\vec{g}_z$ is invariant, so that

$$E^*\vec{\boldsymbol{g}} = \vec{\boldsymbol{g}}\, \mathbb{R}_z(\pi) \quad \text{(C19)}$$

We define the NH_3 inversion coordinate τ as the inner product of two collinear vectors:

$$\tau = \vec{MN}\cdot\vec{g}_z \quad \text{(C20)}$$

This coordinate is related to the umbrella angle ϱ defined in section III.C as $\tau = (^3/_2)r_0^3(1 - \zeta)\sin^2\varrho \times \cos\varrho$, where r_0 is the N–H bond length and $\zeta = m_N/(3m_H + m_N)$. Since $\vec{MN}$ is invariant under permutation of the protons, τ inherits its permutational properties from $\vec{g}_z$, or in other words, τ changes sign (and $\varrho \mapsto \pi - \varrho$) under the permutation (23) and both are invariant under (123). Because it does not affect the geometry of the molecule, (123) is a feasible permutation of the first kind. However, the permutation (23) is of the second kind, as it changes the internal coordinate τ. The operation E^* inverts $\vec{MN}$ and leaves $\vec{g}_z$ alone, so that τ changes sign under E^*, and E^* is also of the second kind. The operations of the second kind yield a tunneling through the umbrella barrier of NH_3 and give rise to an observable splitting of about 0.8 cm^{-1}. The group of operations of the first kind consists of {E,(123),(132),(12)*,(13)* (23)*} and is isomorphic to the point group C_{3v} of the nearly rigid molecule. The total molecular symmetry group, generated by (23), (123), and E^*, is of order 12 and is isomorphic to D_{3h}.

If we now assume that argon is at the point A, then we observe that the vector $\vec{MA}$ is invariant under the permutations of the protons, as the center of mass M of ammonia and the position of argon are not affected by the permutations. The operator E^* inverts the direction of $\vec{MA}$. We choose a dimer frame as in eq C8 and let the Euler angles of ammonia be given with respect to that frame

$$\vec{\boldsymbol{g}} = \vec{\boldsymbol{f}}\, \mathbb{R}_z(\phi)\mathbb{R}_y(\theta)\mathbb{R}_z(\psi) \quad \text{(C21)}$$

By using the rules in eq C9 we easily derive the effect of the operations on the coordinates and by the use of Table 1 we find how the angular functions behave.

The operations which are of the first kind in the free ammonia become of the second kind in the dimer, as ammonia no longer moves in an isotropic space, but experiences a θ- and ψ-dependent intermolecular potential. In the case of argon–ammonia the ψ-dependent barriers are so low that all first kind permutation inversions of the free ammonia remain feasible in the dimer. The permutation inversions of the second kind in the free ammonia are hindered by the intermolecular potential and for some time it was not clear whether these latter permutation inversions were feasible, that is, whether the umbrella inversion was quenched by the argon. Microwave experiments[138] and computations[9] have shown an umbrella splitting almost as large as in the free monomer, however, and hence the argon–ammonia dimer also has a group isomorphic to D_{3h}.

As a next example we will discuss briefly the ammonia dimer. Some early spectroscopic work[193] on this dimer did not show umbrella inversion splittings, and so it was assumed that the intermolecular potential quenches the inversions of both umbrellas. In this case of two identical monomers there are many permutations (the complete permutation inversion group is of the order $2 \times 6! = 2880$), and some of the *inter*monomer permutations may be feasible. And indeed, an analysis by Nelson and Klemperer[252] in the footsteps of earlier work[253] by Dyke on $(H_2O)_2$, revealed that a few intermolecular permutation inversions give rise to observable tunneling splittings. They found that the feasible operations constitute a group of order 36, which they refer to as G_{36}, following Bunker.[108] This group is a semidirect product,[109] designated by Ⓢ, of two outer products. Numbering the protons on monomer A by 1, 2, and 3 and those on B by 4, 5, and 6, and designating the respective nitrogens by 7 and 8, we can write the group as follows:

$$G_{36} = (C_3^A \otimes C_3^B)\ \text{Ⓢ}\ (C_2 \otimes C_s) \quad \text{(C22)}$$

where

$$C_3^A = \{E,(123),(132)\} \qquad C_3^B = \{E,(456),(465)\} \quad \text{(C23)}$$

$$C_2 = \{E,(14)(25)(36)(78)\} \qquad C_s = \{E,(23)(56)^*\} \quad \text{(C24)}$$

Recently the inversions of both monomer umbrellas have been observed[11] and hence (23) and (56) must now be considered to be feasible in the dimer. Adding these elements to the molecular symmetry group gives a group of order 144, designated by G_{144}. This group has the following structure

$$P_{72} \equiv (S_3^A \otimes S_3^B) \circledS C_2, \quad G_{144} \equiv P_{72} \otimes C_i \qquad \text{(C25)}$$

where S_3^X contains all six permutations of monomer X, ($X = A, B$), C_2 is defined in eq C24, and $C_i = \{E, E^*\}$. The effect of the generators of this group on the spherical polar components R, α, β of $\overrightarrow{M_AM_B}$ and the Euler angles, defined as in eq C21, of both monomers is given in Table 16. The umbrella coordinates ϱ_A and ϱ_B are defined as in section III.C, *cf.* also eq C20.

As a final example we will discuss the case of argon–benzene, where we choose to describe the motion of argon in a frame fixed to benzene, as introduced in Appendix A.3. We number the carbon atoms counterclockwise from 1 to 6 and choose $\vec{f}_x$ and $\vec{f}_y$ to be Eckart vectors.[254] Thus, we have the frame

$$\vec{f}_x = \frac{1}{\sqrt{3}}\left(\vec{C}_1 + \frac{1}{2}\vec{C}_2 - \frac{1}{2}\vec{C}_3 - \vec{C}_4 - \frac{1}{2}\vec{C}_5 + \frac{1}{2}\vec{C}_6\right) \qquad \text{(C26a)}$$

$$\vec{f}_y = {}^1/_2(\vec{C}_2 + \vec{C}_3 - \vec{C}_5 - \vec{C}_6) \qquad \text{(C26b)}$$

$$\vec{f}_z = \vec{f}_x \times \vec{f}_y \qquad \text{(C26c)}$$

The notation $\vec{C}_i$ is shorthand for $\overrightarrow{MC}_i$, where M is the mass center of the benzene. When the molecule is a regular hexagon, the vector $\vec{f}_x$ lies on the line from atom 4 to 1 and $\vec{f}_y$ is perpendicular to it. When the molecule does not have 6-fold symmetry, the vectors are not necessarily orthogonal, and an orthogonalization must be performed in order to be able to define Euler angles. A symmetric (Löwdin) orthogonalization leads to an Eckart frame.[254]

The permutation inversion group of the free benzene is isomorphic to its point group D_{6h} and is referred to as $PI(D_{6h})$. This isomorphism arises by virtue of the fact that benzene is nearly rigid, *i.e.* it does not show observable torsional or inversional splittings. All feasible permutation inversions are of the first kind. The group has the following structure:

$$PI(C_{6v}) = C_6 \circledS \{E,(35)(26)^*\} \qquad \text{(C27)}$$

$$PI(D_{6h}) = PI(C_{6v}) \otimes \{E,E^*\} \qquad \text{(C28)}$$

where C_6 is the cyclic group generated by (1 2 3 4 5 6). By acting with the generators on the basis (C26), we easily derive

$$(1\,2\,3\,4\,5\,6)\,\vec{f} = \vec{f}\,\mathbb{R}_z\left(\frac{\pi}{3}\right) \qquad \text{(C29)}$$

$$(3\,5)(2\,6)^*\,\vec{f} = \vec{f}\,\mathbb{R}_x(\pi) \qquad \text{(C30)}$$

$$E^*\,\vec{f} = \vec{f}\,\mathbb{R}_z(\pi) \qquad \text{(C31)}$$

Let us now add argon with position vector $\overrightarrow{MA} = \vec{f}\boldsymbol{A}$ to the system. Since both M and A are invariant under pure permutations, $\overrightarrow{MA}$ is also. So we find

$$(1\,2\,3\,4\,5\,6)\,\overrightarrow{MA} = (1\,2\,3\,4\,5\,6)\,\vec{f}\,\boldsymbol{A} = \vec{f}'\,\boldsymbol{A}' = \vec{f}\,\mathbb{R}_z\left(\frac{\pi}{3}\right)\boldsymbol{A}' = \overrightarrow{MA} = \vec{f}\,\boldsymbol{A} \qquad \text{(C32)}$$

By this, and similar reasoning for the other generators, while remembering that $\overrightarrow{MA}$ changes sign under E^*, we find for the argon coordinate vector

$$(1\,2\,3\,4\,5\,6)\,\boldsymbol{A} \rightarrow \mathbb{R}_z\left(-\frac{\pi}{3}\right)\boldsymbol{A} \qquad \text{(C33)}$$

$$(3\,5)(2\,6)^*\boldsymbol{A} \rightarrow -\mathbb{R}_x(\pi)\boldsymbol{A} \qquad \text{(C34)}$$

$$E^*\boldsymbol{A} \rightarrow -\mathbb{R}_z(\pi)\boldsymbol{A} \qquad \text{(C35)}$$

In order to study the feasibility of the operations, we designate the spherical polar coordinates of $\boldsymbol{A}$ by R, θ, and ϕ. Obviously the length R is invariant and the angles transform as

$$(1\,2\,3\,4\,5\,6): \begin{cases} \theta \rightarrow \theta \\ \phi \rightarrow \phi - \dfrac{\pi}{3} \end{cases}$$

$$(3\,5)(2\,6)^*: \begin{cases} \theta \rightarrow \theta \\ \phi \rightarrow \pi - \phi \end{cases} \qquad E^*: \begin{cases} \theta \rightarrow \pi - \theta \\ \phi \rightarrow \phi \end{cases} \qquad \text{(36)}$$

The interaction between the benzene and the argon is not strongly ϕ dependent. But it is very θ dependent, since the plane $\theta = 90°$ is the plane of the benzene and the barrier for the tunneling of argon through this plane is high. We can expect, therefore, that E^* will not be feasible, whereas (1 2 3 4 5 6) and (3 5)(2 6)* will very likely be feasible. Indeed, this has been found, both in the spectra[169,171] and in calculations.[51] Consequently, the appropriate permutation inversion group for the system argon–benzene is $PI(C_{6v})$. We wish to emphasize that this symmetry does not imply that argon is restricted to move on the 6-fold axis of the rigid benzene; the atom moves above (or under) the plane of the molecule, hindered only by the weak van der Waals potential. The wave functions of argon below and above the plane are degenerate to all practical purposes.

References

(1) Wilson, E. B.; Decius, J. C.; Cross, P. C. *Molecular Vibrations*. McGraw-Hill: New York, 1955.
(2) Califano, S. *Vibrational States*; Wiley: London, 1976.
(3) Papoušek, D.; Aliev, M. W. *Molecular Vibration-Rotational Spectra*; Elsevier: Amsterdam, 1982.
(4) Bunker, P. R.; Jensen, P.; Karpfen, A.; Kofranek, M.; Lischka, H. *J. Chem. Phys.* **1990**, *92*, 7432.
(5) Coudert, L. H.; Hougen, J. T. *J. Mol. Spectrosc.* **1988**, *130*, 86.
(6) Fraser, G. T. *Int. Rev. Phys. Chem.* **1991**, *10*, 189.
(7) van Bladel, J. W. I.; van der Avoird, A.; Wormer, P. E. S. *J. Chem. Phys.* **1991**, *94*, 501.
(8) van Bladel, J. W. I.; van der Avoird, A.; Wormer, P. E. S. *J. Phys. Chem.* **1991**, *95*, 5414.
(9) van Bladel, J. W. I.; van der Avoird, A.; Wormer, P. E. S. *Chem. Phys.* **1992**, *165*, 47.
(10) van Bladel, J. W. I.; van der Avoird, A.; Wormer, P. E. S.; Saykally, R. J. *J. Chem. Phys.* **1992**, *97*, 4750.

(11) Loeser, J. G.; Schmuttenmaer, C. A.; Cohen, R. C.; Elrod, M. J.; Steyert, D. W.; Saykally, R. J.; Bumgarner, R. E.; Blake, G. A. *J. Chem. Phys.* **1992**, *97*, 4727.
(12) Havenith, M.; Linnartz, H.; Zwart, E.; Kips, A.; ter Meulen, J. J.; Meerts, W. L. *Chem. Phys. Lett.* **1992**, *193*, 261.
(13) Watson, J. K. *Mol. Phys.* **1968**, *15*, 479.
(14) Podolsky, B. *Phys. Rev.* **1928**, *32*, 812.
(15) Essén, H. *Am. J. Phys.* **1978**, *46*, 983.
(16) Bratoz, S.; Martin, M. L. *J. Chem. Phys.* **1965**, *42*, 1051.
(17) Hutson, J. M. *Adv. Mol. Vib. Collision Dyn.* **1991**, *1*, 1.
(18) Brocks, G.; van der Avoird, A.; Sutcliffe, B. T.; Tennyson, J. *Mol. Phys.* **1983**, *50*, 1025.
(19) Le Roy, R. J.; Carley, J. S. *Adv. Chem. Phys.* **1980**, *42*, 353.
(20) Pack, R. T. *J. Chem. Phys.* **1974**, *60*, 633.
(21) Cooper, A. R.; Hutson, J. M. *J. Chem. Phys.* **1993**, *98*, 5337.
(22) Biedenharn, L. C.; Louck, J. D. *Angular Momentum in Quantum Physics*; Addison-Wesley: London, 1981.
(23) Brocks, G.; van Koeven, D. *Mol. Phys.* **1988**, *63*, 999.
(24) van der Avoird, A. *J. Chem. Phys.* **1993**, *98*, 5327.
(25) Jeziorski, B.; Moszynski, R.; Szalewicz, K. *Chem. Rev.* **1994**, this issue.
(26) Chałasinski, G.; Szczesniak, M. M. *Chem. Rev.* **1994**, this issue.
(27) van Duijneveldt, F. B.; van Duijneveldt-van de Rijdt, J. G. C. M.; van Lenthe, J. *Chem. Rev.* **1994**, this issue.
(28) Hobza, P.; Selzle, H. L.; Schlag, E. W. *Chem. Rev.* **1994**, this issue.
(29) Jeziorski, B.; Kołos, W. In *Molecular Interactions*; Ratajczak, H., Orville-Thomas, W. J., Eds.; Wiley: New York, 1982; Vol. 3, p 1.
(30) Cwiok, T.; Jeziorski, B.; Kołos, W.; Moszynski, R.; Szalewicz, K. *J. Mol. Struct. (Theochem)* **1994**, *307*, 135.
(31) Williams, H. L.; Szalewicz, K.; Jeziorski, B.; Moszynski, R.; Rybak, S. *J. Chem. Phys.* **1993**, *98*, 1279.
(32) Moszynski, R.; Jeziorski, B.; Wormer, P. E. S.; van der Avoird, A. *Chem. Phys. Lett.* **1994**, *221*, 161.
(33) Moszynski, R.; Wormer, P. E. S.; Jeziorski, B.; van der Avoird, A. *J. Chem. Phys.* **1994**, *101*, 2811.
(34) Moszynski, R.; Jeziorski, B.; van der Avoird, A.; Wormer, P. E. S. *J. Chem. Phys.* **1994**, *101*, 2825.
(35) van der Avoird, A.; Wormer, P. E. S.; Mulder, F.; Berns, R. M. *Top. Curr. Chem.* **1980**, *93*, 1.
(36) Brink, D. M.; Satchler, G. R. *Angular Momentum*; Clarendon: Oxford, 1975.
(37) Abramowitz, M., Stegun, I. A., Eds. *Handbook of Mathematical Functions*; Natl. Bur. Standards: Washington, D.C., 1964.
(38) Choi, S. E.; Light, J. C. *J. Chem. Phys.* **1990**, *92*, 2129.
(39) Kitaigorodski, A. I. *Molecular Crystals and Molecules*; Academic: New York, 1973.
(40) Stone, A. J.; Price, S. L. *J. Phys. Chem.* **1988**, *92*, 3325.
(41) Pack, R. T. *Chem. Phys. Lett.* **1978**, *55*, 197.
(42) Hutson, J. M. *J. Chem. Phys.* **1992**, *96*, 6752.
(43) Cohen, R. C.; Saykally, R. J. *J. Phys. Chem.* **1990**, *94*, 7991.
(44) Cohen, R. C.; Saykally, R. J. *J. Chem. Phys.* **1993**, *98*, 6007.
(45) Ahlrichs, R.; Penco, R.; Scoles, G. *Chem. Phys.* **1977**, *19*, 119.
(46) Tang, K. T.; Toennies, J. P. *J. Chem. Phys.* **1984**, *80*, 3726.
(47) Tennyson, J.; Sutcliffe, B. T. *J. Chem. Phys.* **1982**, *77*, 4061.
(48) Bačić, Z.; Light, J. C. *J. Chem. Phys.* **1986**, *85*, 4594.
(49) Clary, D. C.; Nesbitt, D. J. *J. Chem. Phys.* **1989**, *90*, 7000.
(50) Cooley, J. W. *Math. Comput.* **1961**, *15*, 363.
(51) Brocks, G.; Huygen, T. *J. Chem. Phys.* **1986**, *85*, 3411.
(52) Mandziuk, M.; Bačić, Z. *J. Chem. Phys.* **1993**, *98*, 7165.
(53) Messiah, A. *Quantum Mechanics*; North-Holland: Amsterdam, 1969.
(54) Huber, D. *Int. J. Quantum Chem.* **1985**, *28*, 245.
(55) Arthurs, A. M.; Dalgarno, A. *Proc. R. Soc. (London) A* **1960**, *256*, 540.
(56) Child, M. S. *Molecular Collision Theory*; Academic: New York, 1974.
(57) Johnson, B. R. *J. Comput. Phys.* **1973**, *13*, 445.
(58) Manolopoulos, D. E. *J. Chem. Phys.* **1986**, *85*, 6425.
(59) Dunker, A. M.; Gordon, R. G. *J. Chem. Phys.* **1976**, *64*, 4984.
(60) Johnson, B. R. *J. Chem. Phys.* **1978**, *69*, 4678.
(61) Shapiro, M.; Balint-Kurti, G. G. *J. Chem. Phys.* **1979**, *71*, 1461.
(62) Danby, G. *J. Phys. B* **1983**, *16*, 3393.
(63) Hutson, J. M.; Le Roy, R. J. *J. Chem. Phys.* **1985**, *83*, 1197.
(64) Slee, T.; Le Roy, R. J. *J. Chem. Phys.* **1993**, *99*, 360.
(65) Mladenović, M.; Bačić, Z. *J. Chem. Phys.* **1991**, *94*, 4988.
(66) Peet, A. C.; Yang, W. *J. Chem. Phys.* **1989**, *91*, 6598.
(67) Peet, A. C.; Yang, W. *J. Chem. Phys.* **1989**, *90*, 1746.
(68) Yang, W.; Peet, A. C.; Miller, W. H. *J. Chem. Phys.* **1989**, *91*, 7537.
(69) Brezinski, C. *Padé-type Approximation and General Orthogonal Polynomials*; Birkhäuser: Boston, 1980.
(70) Stoer, J.; Bulirsch, R. *Introduction to Numerical Analysis*; Springer: New York, 1980.
(71) Muckerman, J. T. *Chem. Phys. Lett.* **1990**, *173*, 200.
(72) Friesner, R. A.; Bentley, J. A.; Menou, M.; Leforestier, C. *J. Chem. Phys.* **1993**, *99*, 324.
(73) Henderson, J. R.; Tennyson, J. *Comput. Phys. Commun.* **1993**, *75*, 365.
(74) Block, P. A.; Pedersen, L. G.; Miller, R. E. *J. Chem. Phys.* **1993**, *98*, 3754.
(75) Parlett, B. N. *The Symmetric Eigenvalue Problem*; Prentice-Hall: Englewood Cliffs, 1980.
(76) Cullum, J. K.; Willoughby, R. A. *Lanczos Algorithms for Large Symmetric Eigenvalue Computations*; Birkhäuser: Boston, 1985.
(77) Davidson, E. R. *J. Comput. Phys.* **1975**, *17*, 87.
(78) Holmgren, S. L.; Waldman, M.; Klemperer, W. *J. Chem. Phys.* **1977**, *67*, 4414.
(79) Rick, S. W.; Lynch, D. L.; Doll, J. D. *J. Chem. Phys.* **1991**, *95*, 3505.
(80) Bačić, Z.; Kennedy-Mandziuk, M.; Moskowitz, J. W. *J. Chem. Phys.* **1992**, *97*, 6472.
(81) Quack, M.; Suhm, M. A. *J. Chem. Phys.* **1991**, *95*, 28.
(82) Quack, M.; Stohner, J.; Suhm, M. A. *J. Mol. Struct.*, in press (EUCMOS21 Proceedings).
(83) Bernu, B.; Ceperley, D. M.; Lester, W. A. *J. Chem. Phys.* **1990**, *93*, 552.
(84) McQuarrie, D. *Statistical Mechanics*; Harper & Row: New York, 1976.
(85) Dunker, A. M.; Gordon, R. G. *J. Chem. Phys.* **1978**, *68*, 700.
(86) Brocks, G.; Tennyson, J.; van der Avoird, A. *J. Chem. Phys.* **1984**, *80*, 3223.
(87) Poll, J. D.; Hunt, J. L. *Can. J. Phys.* **1976**, *54*, 461.
(88) Brocks, G.; van der Avoird, A. *Mol. Phys.* **1985**, *55*, 11 (Note that the coefficient $M_{2,2,3,1}$ in this paper is too large by a factor of $\sqrt{2}$.)
(89) Nelson, D. D.; Fraser, G. T.; Klemperer, W. *Science* **1987**, *238*, 1670.
(90) Novick, S. E.; Leopold, K. R.; Klemperer, W. In *Atomic and Molecular Clusters*; Bernstein, E. R., Ed.; Elsevier: Amsterdam, 1990.
(91) Klemperer, W. *Science* **1992**, *257*, 887.
(92) Saykally, R. J. *Acc. Chem. Res.* **1989**, *22*, 295.
(93) Cohen, R. C.; Saykally, R. J. *J. Phys. Chem.* **1992**, *96*, 1024.
(94) Saykally, R. J.; Blake, G. A. *Science* **1993**, *259*, 1570.
(95) Meerts, W. L.; Majewski, W. A.; van Herpen, W. M. *Can. J. Phys.* **1984**, *62*, 1293.
(96) Champagne, B. B.; Plusquellic, D. F.; Pfanstiel, J. F.; Pratt, D. W.; van Herpen, W. M.; Meerts, W. L. *Chem. Phys.* **1991**, *156*, 251.
(97) Nesbitt, D. J. *Chem. Rev.* **1988**, *88*, 843.
(98) Miller, R. E. *Science* **1988**, *240*, 447.
(99) Henderson, G.; Ewing, G. E. *Mol. Phys.* **1974**, *27*, 903.
(100) Long, C. A.; Henderson, G.; Ewing, G. E. *Chem. Phys.* **1973**, *2*, 485.
(101) Henderson, G.; Ewing, G. E. *J. Chem. Phys.* **1973**, *59*, 2280.
(102) Long, C. A.; Ewing, G. E. *J. Chem. Phys.* **1973**, *58*, 4824.
(103) McKellar, A. R. W. *J. Chem. Phys.* **1988**, *88*, 4190.
(104) Brocks, G. *J. Chem. Phys.* **1988**, *88*, 578.
(105) Garcia Ayllon, A.; Santamaria, J.; Miller, S.; Tennyson, J. *Mol. Phys.* **1990**, *71*, 1043.
(106) Hougen, J. T. *J. Chem. Phys.* **1962**, *37*, 1433.
(107) Longuet-Higgins, H. C. *Mol. Phys.* **1963**, *6*, 445.
(108) Bunker, P. R. *Molecular Symmetry and Spectroscopy*; Academic: New York, 1979.
(109) Ezra, G. S. *Symmetry Properties of Molecules*; Springer: Berlin, 1982.
(110) Maitland, G. C.; Rigby, M.; Smith, E. B.; Wakeham, W. A. *Intermolecular Forces*; Oxford University Press: Oxford, 1981.
(111) Luo, F.; McBane, G. C.; Kim, G.; Giese, C. F.; Gentry, W. R. *J. Chem. Phys.* **1993**, *98*, 3564.
(112) Aziz, R. A. In *Inert Gases*; Klein, M. L., Ed.; Springer: Berlin, 1984.
(113) Hutson, J. M. *Annu. Rev. Phys. Chem.* **1990**, *41*, 123.
(114) Marshall, M. D.; Jensen, P.; Bunker, P. R. *Chem. Phys. Lett.* **1991**, *176*, 255.
(115) Le Roy, R. J.; van Kranendonk, J. *J. Chem. Phys.* **1974**, *61*, 4750.
(116) McKellar, A. R. W.; Welsh, H. L. *J. Chem. Phys.* **1971**, *55*, 595.
(117) McKellar, A. R. W. *Faraday Discuss. Chem. Soc.* **1982**, *73*, 89.
(118) Waaijer, M.; Reuss, J. *Chem. Phys.* **1981**, *63*, 263.
(119) Buck, U.; Meyer, A.; Le Roy, R. J. *J. Chem. Phys.* **1984**, *80*, 5589.
(120) Le Roy, R. J.; Hutson, J. M. *J. Chem. Phys.* **1987**, *86*, 837.
(121) McKellar, A. R. W. Unpublished results.
(122) McKellar, A. R. W. In *Spectral Line Shapes*; edited by Frommhold, L., Keto, J. W., Eds.; AIP Conference Proceedings 216; American Institute of Physics: New York, 1990; Vol. 6, p 369. McKellar, A. R. W. *Faraday Discuss. Chem. Soc.* **1994**, *97*, 000.
(123) Le Roy, R. J.; Corey, G. C.; Hutson, J. M. *Faraday Discuss. Chem. Soc.* **1982**, *73*, 339.
(124) Le Roy, R. J. In *Resonances in Electron-Molecule Scattering, van der Waals Complexes and Reactive Chemical Dynamics*, ACS Symp. Ser. No. 263, Truhlar, D. G., Ed.; American Chemical Society: Washington, 1984; p 231.
(125) Le Roy, R. J.; Hutson, J. M. University of Waterloo Chemical Physics Research Report CP-287, 1986.
(126) Frick, J. *Thesis*, MPI Strömungsforschung, Bericht 9, Göttingen, 1984.

(127) Boughton, C. V.; Miller, R. E.; Vohralik, P. F.; Watts, R. O. *Mol. Phys.* **1986**, *58*, 827.
(128) Lovejoy, C. M.; Nesbitt, D. J. *J. Chem. Phys.* **1990**, *93*, 5387.
(129) Tennyson, J.; Sutcliffe, B. T. *J. Chem. Phys.* **1983**, *79*, 43.
(130) Gianturco, F. A.; Palma, A.; Villarreal, P.; Delgado-Barrio, G. *Chem. Phys. Lett.* **1984**, *111*, 399.
(131) Rodwell, W. R.; Sim Fai Lam, L. T.; Watts, R. O. *Mol. Phys.* **1981**, *44*, 225.
(132) Rijks, W.; Wormer, P. E. S. *J. Chem. Phys.* **1988**, *88*, 5704.
(133) Wormer, P. E. S.; Hettema, H. *J. Chem. Phys.* **1992**, *97*, 5592.
(134) Wormer, P. E. S.; Hettema, H. *Polcor Package*; Nijmegen, 1992.
(135) Brown, J. M.; Hougen, J. T.; Huber, K.-P.; Johns, J. W. C.; Kopp, I.; Lefebvre-Brion, H.; Merer, A. J.; Ramsay, D. A.; Rostas, J.; Zare, R. N. *J. Mol. Spectrosc.* **1975**, *55*, 500.
(136) Ashton, C. J.; Child, M. S.; Hutson, J. M. *J. Chem. Phys.* **1983**, *78*, 4025.
(137) Tucker, S. C.; Truhlar, D. G. *J. Chem. Phys.* **1986**, *86*, 6251.
(138) Fraser, G. T.; Nelson, D. D.; Charo, A.; Klemperer, W. *J. Chem. Phys.* **1985**, *82*, 2535.
(139) Nelson, D. D.; Fraser, G. T.; Peterson, K. I.; Klemperer, W.; Lovas, F. J.; Suenram, R. D. *J. Chem. Phys.* **1986**, *85*, 5512.
(140) Bizarri, A.; Heijmen, B.; Stolte, S.; Reuss, J. *Z. Phys. D* **1988**, *10*, 291.
(141) Gwo, J.; Havenith, M.; Busarow, K. L.; Cohen, R. C.; Schmuttenmaer, C. A.; Saykally, R. J. *Mol. Phys.* **1990**, *71*, 453.
(142) Zwart, E.; Linnartz, H.; Meerts, W. L.; Fraser, G. T.; Nelson, D. D.; Klemperer, W. *J. Chem. Phys.* **1991**, *96*, 793.
(143) Fraser, G. T.; Pine, A. S.; Kreiner, W. A. *J. Chem. Phys.* **1991**, *94*, 7061.
(144) Schmuttenmaer, C. A.; Cohen, R. C.; Loeser, J. G.; Saykally, R. J. *J. Chem. Phys.* **1991**, *95*, 9.
(145) Schmuttenmaer, C. A.; Cohen, R. C.; Saykally, R. J. *J. Chem. Phys.* **1994**, *101*, 146.
(146) Zwart, E.; Meerts, W. L. *Chem. Phys.* **1991**, *151*, 407.
(147) Fraser, G. T.; Lovas, F. J.; Suenram, R. D.; Matsumura, K. *J. Mol. Spectrosc.* **1990**, *144*, 97.
(148) Suzuki, S.; Bumgarner, R. E.; Stockman, P. A.; Green, P. G.; Blake, G. A. *J. Chem. Phys.* **1991**, *94*, 824.
(149) Cohen, R. C.; Saykally, R. J. *J. Chem. Phys.* **1991**, *95*, 7891.
(150) Lascola, R.; Nesbitt, D. J. *J. Chem. Phys.* **1991**, *95*, 7917.
(151) Chałasinski, G.; Cybulski, S. M.; Szczesniak, M. M.; Scheiner, S. *J. Chem. Phys.* **1989**, *91*, 7809.
(152) Chałasinski, G.; Szczesniak, M. M.; Scheiner, S. *J. Chem. Phys.* **1991**, *94*, 2807.
(153) Bulski, M.; Wormer, P. E. S.; van der Avoird, A. *J. Chem. Phys.* **1991**, *94*, 491.
(154) Bulski, M.; Wormer, P. E. S.; van der Avoird, A. *J. Chem. Phys.* **1991**, *94*, 8096.
(155) Rijks, W.; Wormer, P. E. S. *J. Chem. Phys.* **1989**, *90*, 6507; **1990**, *92*, 5754 (E).
(156) Bulski, M.; Wormer, P. E. S.; van der Avoird, A. Unpublished results.
(157) Herzberg, G. *Molecular Spectra and Molecular Structure*; Van Nostrand Reinhold: New York, 1945; Vol. II, p 426.
(158) van Bladel, J. W. I.; van der Avoird, A.; Wormer, P. E. S. Unpublished results.
(159) Wormer, P. E. S.; Olthof, E. H. T.; Engeln, R. A. H.; Reuss, J. *Chem. Phys.* **1993**, *178*, 189.
(160) Papoušek, D.; Stone, J. M. R.; Špirko, V. *J. Mol. Spectrosc.* **1973**, *48*, 17.
(161) Chang, H.-C.; Tao, F.-M.; Klemperer, W.; Healy, C.; Hutson, J. M. *J. Chem. Phys.* **1993**, *99*, 9337.
(162) Hutson, J. M. *J. Chem. Phys.* **1990**, *92*, 157.
(163) Schleipen, J.; ter Meulen, J. J.; van der Sanden, G. C. M.; Wormer, P. E. S.; van der Avoird, A. *Chem. Phys.* **1992**, *163*, 161.
(164) van der Sanden, G. C. M.; Wormer, P. E. S.; van der Avoird, A.; Schleipen, J.; ter Meulen, J. J. *J. Chem. Phys.* **1992**, *97*, 6460; **1994**, *100*, 5393(E).
(165) Faeder, J. *J. Chem. Phys.* **1993**, *99*, 7664.
(166) Parneix, P.; Halberstadt, N.; Bréchignac, Ph.; Amar, F. G.; van der Avoird, A.; van Bladel, J. W. I. *J. Chem. Phys.* **1993**, *98*, 2709.
(167) Consalvo, D.; van der Avoird, A.; Piccirillo, S.; Coreno, M.; Giardini-Guidoni, A.; Mele, A.; Snels, M. *J. Chem. Phys.* **1993**, *99*, 8398.
(168) Mandziuk, M.; Bačić, Z.; Droz, T.; Leutwyler, S. *J. Chem. Phys.* **1994**, *100*, 52.
(169) Weber, Th.; von Bargen, A.; Riedle, E.; Neusser, H. J. *J. Chem. Phys.* **1990**, *92*, 90.
(170) Weber, Th. Thesis, Institut für Physikalische und Theoretische Chemie, Technische Universität München, 1991.
(171) Neusser, H. J.; Sussmann, R.; Smith, A. M.; Riedle, E.; Weber, Th. *Ber. Bunsen-ges. Phys. Chem.* **1992**, *96*, 1252.
(172) Brupbacher, Th.; Bauder, A. *Chem. Phys. Lett.* **1990**, *173*, 435.
(173) Venturo, V. A.; Felker, P. M. *J. Phys. Chem.* **1993**, *97*, 4882.
(174) Hobza, P.; Selzle, H. L.; Schlag, E. W. *J. Chem. Phys.* **1991**, *95*, 391.
(175) Bludský, O.; Špirko, V.; Hrouda, V.; Hobza, P. *Chem. Phys. Lett.* **1992**, *196*, 410.
(176) Herzberg, G. *Molecular Spectra and Molecular Structure*; Van Nostrand: New York, 1966; Vol. III.
(177) van der Avoird, A.; Riedle, E. Manuscript in preparation.
(178) Brupbacher, Th.; Makarewicz, J.; Bauder, A., XIIIth Colloquium on high resolution molecular spectroscopy, Book of abstracts, Riccione, 1993. Brupbacher, Th.; Makarewicz, J.; Bauder, A. *J. Chem. Phys.*, submitted for publication.
(179) Brobjer, J. T.; Murrell, J. N. *Mol. Phys.* **1983**, *50*, 885.
(180) Hancock, G. C.; Truhlar, D. G.; Dykstra, C. E. *J. Chem. Phys.* **1988**, *88*, 1786.
(181) Kofranek, M.; Lischka, H.; Karpfen, A. *Chem. Phys.* **1988**, *121*, 137.
(182) Bunker, P. R.; Kofranek, M.; Lischka, H.; Karpfen, A. *J. Chem. Phys.* **1988**, *89*, 3002.
(183) Kistenmacher, H.; Popkie, H.; Clementi, E.; Watts, R. O. *J. Chem. Phys.* **1974**, *60*, 4455.
(184) Jeziorski, B.; van Hemert, M. C. *Mol. Phys.* **1976**, *31*, 713.
(185) Coker, D. F.; Watts, R. O. *J. Phys. Chem.* **1987**, *91*, 2513.
(186) Szalewicz, K.; Cole, S. J.; Kołos, W.; Bartlett, R. J. *J. Chem. Phys.* **1988**, *89*, 3662.
(187) Rybak, S.; Jeziorski, B.; Szalewicz, K. *J. Chem. Phys.* **1991**, *95*, 6576.
(188) Howard, B. J.; Dyke, Th. R.; Klemperer, W. *J. Chem. Phys.* **1984**, *81*, 5417.
(189) Gutowsky, H. S.; Chuang, C.; Keen, J. D.; Klots, T. D.; Emilsson, T. *J. Chem. Phys.* **1985**, *83*, 2070.
(190) Pine, A. S.; Howard, B. J. *J. Chem. Phys.* **1986**, *84*, 590.
(191) Zwart, E.; ter Meulen, J. J.; Meerts, W. L. *J. Mol. Spectrosc.* **1991**, *147*, 27.
(192) Pugliano, N.; Cruzan, J. D.; Loeser, J. G.; Saykally, R. J. *J. Chem. Phys.* **1993**, *98*, 6600.
(193) Nelson, D. D.; Fraser, G. T.; Klemperer, W. *J. Chem. Phys.* **1985**, *83*, 6201.
(194) Liu, S.; Dykstra, C. E.; Kolenbrander, K.; Lisy, J. M. *J. Chem. Phys.* **1986**, *85*, 2077.
(195) Frisch, M. J.; Del Bene, J. E.; Binkley, J. S.; Schaefer, H. F. *J. Chem. Phys.* **1986**, *84*, 2279.
(196) Sagarik, K. P.; Ahlrichs, R.; Brode, S. *Mol. Phys.* **1986**, *57*, 1247.
(197) Hassett, D. M.; Marsden, C. J.; Smith, B. J. *Chem. Phys. Lett.* **1991**, *183*, 449.
(198) Tao, F.-M.; Klemperer, W. *J. Chem. Phys.* **1993**, *99*, 5976.
(199) Nelson, D. D.; Klemperer, W.; Fraser, G. T.; Lovas, F. J.; Suenram, R. D. *J. Chem. Phys.* **1987**, *87*, 6364.
(200) Havenith, M.; Cohen, R. C.; Busarow, K. L.; Gwo, D-H.; Lee, Y. T.; Saykally, R. J. *J. Chem. Phys.* **1991**, *94*, 4776.
(201) Linnartz, H.; Kips, A.; Meerts, W. L.; Havenith, M. *J. Chem. Phys.* **1993**, *99*, 2449.
(202) Baum, R. M. *Chem. Eng. News* **1992**, 19 October, 20.
(203) Olthof, E. H. T.; van der Avoird, A.; Wormer, P. E. S. *J. Mol. Struct. (Theochem)* **1994**, *307*, 201.
(204) van der Avoird, A.; Olthof, E. H. T.; Wormer, P. E. S. *Faraday Discuss. Chem. Soc.* **1994**, *97*, in press.
(205) Olthof, E. H. T.; van der Avoird, A.; Wormer, P. E. S. *J. Chem. Phys.* **1994**, in press.
(206) Olthof, E. H. T.; van der Avoird, A.; Wormer, P. E. S.; Loeser, J.; Saykally, R. J. *J. Chem. Phys.* **1994**, in press.
(207) Dykstra, C. E.; Andrews, L. *J. Chem. Phys.* **1990**, *92*, 6043.
(208) Chakravarty, C.; Clary, D. C.; Degli Esposti, A.; Werner, H.-J. *J. Chem. Phys.* **1991**, *95*, 8149.
(209) van der Avoird, A. *J. Chem. Phys.* **1983**, *79*, 1170.
(210) Tennyson, J.; Mettes, J. *Chem. Phys.* **1983**, *76*, 195.
(211) Mettes, J.; Heijmen, B.; Verhoeve, P.; Reuss, J.; Lainé, D.; Brocks, G. *Chem. Phys.* **1985**, *92*, 9.
(212) Jansen, G.; Hess, B. A.; Wormer, P. E. S. *Chem. Phys. Lett.* **1993**, *214*, 103.
(213) van der Avoird, A.; Brocks, G. *J. Chem. Phys.* **1987**, *87*, 5346.
(214) Dubernet, M.-L.; Flower, D.; Hutson, J. M. *J. Chem. Phys.* **1991**, *94*, 7602.
(215) Cooper, A. R.; Jain, S.; Hutson, J. M. *J. Chem. Phys.* **1993**, *98*, 2160.
(216) Hutson, J. M.; Beswick, J. A.; Halberstadt, N. *J. Chem. Phys.* **1989**, *90*, 1337.
(217) Elrod, M. J.; Steyert, D. W.; Saykally, R. J. *J. Chem. Phys.* **1991**, *95*, 3182.
(218) Rick, S. W.; Leitner, D. M.; Doll, J. D.; Freeman, D. L.; Frantz, D. D. *J. Chem. Phys.* **1991**, *95*, 6658.
(219) Jortner, J. *Z. Phys.* **1992**, *D24*, 247.
(220) Leutwyler, S.; Bösiger, J. *Chem. Rev.* **1990**, *90*, 489.
(221) Shalev, E.; Ben-Horin, N.; Even, U.; Jortner, J. *J. Chem. Phys.* **1991**, *95*, 3147.
(222) Shelly, J. C.; Le Roy, R. J.; Amar, F. G. *Chem. Phys. Lett.* **1988**, *152*, 14.
(223) Eichenauer, D.; Le Roy, R. J. *J. Chem. Phys.* **1988**, *88*, 2898.
(224) Amar, F. G.; Weerasinghe, S. In *Mode Selective Chemistry*, Proc. 24th Jerusalem Quantum Chemistry Symposium; Pullman, B., Jortner, J., Eds.; Kluwer: Dordrecht, 1991.
(225) Bréchignac, P.; Coutant, B. *Z. Phys. D* **1989**, *14*, 87.
(226) Hinde, R. J.; Berry, R. S.; Wales, D. J. *J. Chem. Phys.* **1992**, *96*, 1376.
(227) Stephenson, T. A.; Rice, S. A. *J. Chem. Phys.* **1984**, *81*, 1083.

(228) Gutmann, M.; Willberg, D. M.; Zewail, A. H. *J. Chem. Phys.* **1992**, *97*, 8037; 8048.
(229) Beswick, J. A.; Shapiro, M. *Chem. Phys.* **1982**, *64*, 333.
(230) Halberstadt, N.; Bréchignac, Ph.; Beswick, J. A.; Shapiro, M. *J. Chem. Phys.* **1986**, *84*, 170.
(231) Halberstadt, N.; Beswick, J. A.; Janda, K. C. *J. Chem. Phys.* **1987**, *87*, 3966.
(232) Roncero, O.; Beswick, J. A.; Halberstadt, N.; Villarreal, P.; Delgado-Barrio, G. *J. Chem. Phys.* **1990**, *92*, 3348.
(233) García-Vela, A.; Villarreal, P.; Delgado-Barrio, G. *J. Chem. Phys.* **1991**, *94*, 7868.
(234) Zhang, D. H.; Zhang, J. Z. H.; Bačić, Z. *Chem. Phys. Lett.* **1992**, *194*, 313.
(235) Schinke, R. *Photodissociation Dynamics*; Cambridge University Press: Cambridge, 1993.
(236) Soep, B.; Whitham, C. J.; Keller, A.; Visticot, J. P. *Faraday Discuss. Chem. Soc.* **1991**, *91*, 191.
(237) Soep, B.; Abbés, S.; Keller, A.; Visticot, J. P. *J. Chem. Phys.* **1992**, *96*, 440.
(238) Shin, S. K.; Chan, Y.; Nickolaiser, S.; Sharpe, S. W.; Baudot, R. A.; Wittig, C. *Adv. Photochem.* **1991**, *16*, 249.
(239) Special Issue on van der Waals Molecules. *Chem. Rev.* **1988**, *88*.
(240) Hobza, P.; Zahradnik, R. *Intermolecular Complexes*; Elsevier: Amsterdam, 1988.
(241) *Structure and Dynamics of Weakly Bound Molecular Complexes*; Weber, A., Ed.; NATO ASI Series C: 212, Reidel: Dordrecht, 1987.
(242) *Dynamics of Polyatomic Van der Waals Complexes*; Halberstadt, N., Janda, K. C., Eds.; NATO ASI Series B 227, Plenum: New York, 1990.
(243) *Atomic and Molecular Clusters*; Bernstein, E. R., Ed., Elsevier: Amsterdam, 1990.
(244) Beswick, J. A.; Halberstadt, N. *Dynamics of Weakly Bound Complexes*; Kluwer: Dordrecht, 1993.
(245) Goldstein, H. *Classical Mechanics*, 2nd ed.; Addison-Wesley: Reading, 1980.
(246) Margenau, H.; Murphy, G. M. *The Mathematics of Physics and Chemistry*, 2nd ed.; Van Nostrand, Inc.: Princeton, 1956.
(247) Whittaker, E. T. *A Treatise on the Analytical Dynamics of Particles and Rigid Bodies*, 4th ed.; Cambridge University Press: Cambridge, 1965.
(248) Gantmacher, F. R. *Matrizentheorie*; Springer: Berlin, 1986.
(249) Condon, E. U.; Shortley, G. H. *Theory of Atomic Spectra*; Cambridge University Press: Cambridge, 1935.
(250) Wigner, E. P. *Group Theory and Its Application to the Quantum Mechanics of Atomic Spectra*; Academic: New York, 1959 (translation of the 1931 German edition).
(251) Talman, J. D. *Special Functions*; Benjamin: New York, 1968.
(252) Nelson, D. D.; Klemperer, W. *J. Chem. Phys.* **1987**, *87*, 139.
(253) Dyke, T. R. *J. Chem. Phys.* **1977**, *66*, 492.
(254) Louck, J. D.; Galbraith, H. W. *Rev. Mod. Phys.* **1976**, *48*, 69.